Protein Quality Control Systems of the Thick Filament Protein Myosin in Zebrafish Skeletal Muscle Assembly and Maintenance

by

Casey Michelle Carlisle

A thesis submitted in partial fulfillment of the requirements for the degree of

Master of Science
in
Physiology, Cell, and Developmental Biology

Department of Biological Sciences
University of Alberta

ABSTRACT:

Skeletal and cardiac muscle function is dependent on the proper assembly and maintenance of the smallest contractile unit of striated muscle, the sarcomere. The sarcomere is composed of hundreds of proteins and associated factors, each of which must be properly folded, inserted into the sarcomere, and monitored for damage. Systems that perform each of these roles are critical for muscle homeostasis are called protein quality control systems. Although protein quality control systems have been widely studied in neurogenerative diseases, they are understudied in muscle. Here I hypothesize that different protein quality control systems respond to the thick filament protein, myosin, when it is damaged before the sarcomere has assembled, or after sarcomere assembly is complete. Using zebrafish as a model system, I show that the mutant *steif* fails to assemble myosin thick filaments, while the mutant *herzschlag* assembles thick filaments that degenerate due to contraction induced damage. Using immunofluorescence, hematoxylin and eosin staining, and transmission electron microscopy, I show that *herzschlag* mutants have a specific loss of slow muscle tissue. By pharmacologically inhibiting the proteasome, I show that this loss is dependant on the ubiquitin proteasome system. Similar analysis in *steif* mutants reveals that these fish differ in their ability to tolerate proteasome inhibition, and qPCR of protein quality control factors shows different expression profiles in these fish. Together, this work suggests that different protein quality control mechanisms respond to myosin damage depending on the developmental stage in which it occurs. This work has implications in the treatment of striated muscle myopathies, specifically in the identification of druggable therapeutic targets.

PREFACE:

The research conducted for this thesis was performed in agreement with the guidelines set by the Canadian Council for Animal Care and procedures approved by the Animal Care and Use Committee of the University of Alberta. (AUP: 14-0101 FR).

Portions of Chapter 1 (Section 1.2; 1.2.1; 1.2.1.1; 1.2.1.2; 1.2.1.3 and Section 1.3; 1.3.1) were published as C. Carlisle, K. Prill, D. Pilgrim "Chaperones and the Proteasome System: Regulating the Construction and Demolition of Striated Muscle" 2018. *International Journal of Molecular Sciences*, vol. 19, 1-22. I wrote the second half of the manuscript and produced manuscript figures 5 and 6, while Dr. Prill wrote the first half and produced manuscript figures 1-4. Dr. Pilgrim was the supervisory author and contributed to manuscript edits.

Chapters 2 through 5 are modified from a manuscript submission "Slow muscle atrophy in the zebrafish titin 2 mutant, *herzschlag*, is dependent on the Ubiquitin Proteasome System" *Mechanisms of Development*: MOD_2019_35. I wrote the manuscript and performed the majority of the data collection and analysis. Dr. Prill assisted with data collection for Figure 17, data interpretation, experimental design, and manuscript edits. Dr. Pilgrim was the supervisory author and contributed to manuscript edits.

Data collection in Figure 25 was assisted by Emily Harvey, who performed one biological replicate of *trim55b* and *trim63b* in *steif* embryos, and two biological replicates of *trim63a*, *trim55b*, and *trim63b* in *steif* embryos. Images in Figure 13C and Figure 13D were taken by Dr. Kendal Prill.

All work, with the exception of the contributions mentioned above, in this thesis is original work by Casey Carlisle.

It would seem that I must go forward where I have never been, instead of backwards where I have.

-Winnie the Pooh

ACKNOWLEDGEMENTS:

This thesis could not have been completed without the help and support of many amazing people. First, I would like to thank my fantastic committee members: Dr. David Pilgrim, Dr. Richard Schulz, and Dr. Ted Allison. To Dr. Pilgrim, thank you for supervising me for three years, allowing me to take my project in the direction I wanted to go and always pushing me to learn more and become a better scientist. To my co-supervisor, Dr. Schulz, thank you for always being there for support and guidance, inviting me to talks and opportunities both on and off campus, and making me feel like a welcome part of your lab. Dr. Allison, thank you for making time to discuss career options with me and introducing me to faculty members. Your support throughout my degree, both inside and outside of class, was greatly appreciated.

Without the support and patience of Dr. Andrew Waskiewicz, none of our zebrafish work could have been accomplished. Thank you for access to your fish facilities, your guidance and career advice, and for offering to chair my exam. I would also like to thank Auriana Engler and SASS for keeping our fish healthy and happy, and the fish for continuing to lay embryos despite my singing.

To Dr. Keith Tierney and Dr. Danielle Philbert, thank you for taking a chance on an undergraduate student, introducing me to research and sparking my interest in zebrafish muscle development. To Arlene Oatway and James MacLagan, thank you for your extensive knowledge, reagents-for-coffee trades, troubleshooting advice, and gossip. My experiments would not have worked without your help and you made my time at the University of Alberta much brighter.

To Jade Pyo, Qelsey Fraser, George Kinley, and Gavin Neil, thank you for always being a little nerdier than me, even if it was just pretend. I would not have survived this degree without

our coffee and subway runs, Disney singing, Destiny playing, and our Dungeons & Dragons group. Thank you for supporting me through laughter and tears, both separate and when simultaneous. To Dr. Paul Chrystal, thank you for being the weirder of the two of us, for your troubleshooting tips, and for your patience when I ignored them. Thank you for making me dinner, introducing me to your favourite things, and for letting me use the brain every once and a while. Your help, support, and motivation has made me a better scientist and I am thankful to have met you.

Dr. Kendal Prill, you are my mentor, role model, fellow Gryffindor, and friend. Your enthusiasm is infectious and you inspire me to be a better scientist. I would not be where I am without you. Thank you for always understanding my jokes, or laughing and pretending you did. Thank you for excitedly listening to my science rants at all hours of the day, for always being down to get ice caps, your extensive knowledge of office quotes, and your unwavering support and friendship.

Finally, to mom and dad, thank you for answering the phone day or night and sympathetically listening to my good news, bad news, or news so jargon heavy that it was unintelligible. Grad school is challenging, but having parents who support and love you unconditionally makes all the difference. You taught me to work hard, but most importantly, to love what you do and I know that wherever my career takes me that you will be there, ridiculously proud.

TABLE OF CONTENTS:

LIST OF TABLES:

LIST OF FIGURES:

LIST OF ABBREVIATIONS:

Abbreviation	Full name
3D	three dimensional
bp	base pairs
cDNA	complementary deoxyribonucleic acid
DCM	dilated cardiomyopathy
DMSO	dimethyl sulfoxide
H&E	hematoxalin and eosin
HCM	hypertrophic cardiomyopathy
hel	*herzschlag*
hpf	hours post fertilization
LB	Lysogeny Broth
LGMD2J	limb-girdle muscular dystrophy type 2J
M	molarity
ml	millilitres
MMP	matrix metalloproteinase
MuRF	muscle Ring Finger
ng	nanogram
PBST	phosphate buffered saline with Tween-20
qPCR	quantitative polymerase chain reaction
RPM	revolutions per minute
stf	*steif*
TEM	transmission electron micropscopy
Ub	ubiquitin
UPS	ubiquitin proteasome system
WT	wild-type

CHAPTER 1. INTRODUCTION:

Striated muscle includes both cardiac and skeletal muscle and is defined by its striated appearance, caused by repeating units called sarcomeres. Muscle tissue is highly organized, with bundles of fascicles forming muscle tissue (Figure 1A), bundles of muscle fibers forming fascicles (Figure 1B), and bundles of myofibrils forming muscle fibers (Figure 1C). Sarcomeres, the basic unit of striated muscle, are organized end to end to form myofibrils (Figure 1D). The precise alignment of the sarcomere has been studied since the early 1900s (Heidenhain, 1913) but despite over a century of ongoing muscle research, we still know remarkably little about sarcomere development. This is largely due to the complexity of the sarcomere (Figure 1E), with hundreds of proteins and associated factors (eg. miRNA) required for proper assembly and maintenance of the structure. These proteins and factors fall into three broad categories: structural, assembly, and maintenance.

Structural factors of the sarcomere are the proteins that compose the sarcomere and are required for contraction and stability. Examples of structural sarcomere components include, but are not limited to, actin, myosin, titin, nebulin, myomesin, α-actinin, and obscurin. While structural factors are the physical parts of the sarcomere, assembly factors are proteins associated with the sarcomere. These proteins may fold or assemble structural proteins, or act as transcription factors associated with the regulation of structural, maintenance, or other assembly proteins. Examples of assembly factors include UNC45B, HSP90α1, SMYD1B, and HSF-1 (Carlisle et al., 2018). Lastly, maintenance factors are those proteins that are required to recognize, remove, and replace structural components of the sarcomere. Maintenance factors include muscle E3 ligases like MuRF1, and co-chaperones like Bag-1 and Bag-3 (Carlisle et al., 2018).

Identification of the sarcomere components required for the assembly and maintenance of the sarcomere and how they interact with one another has been a limiting step in understanding muscle development as the loss or interruption in the function of these components is often lethal. However, with the development of genetic techniques and characterization of tractable model systems, we are better able to isolate and identify novel proteins required for sarcomere health and to determine their function in sarcomere assembly and maintenance.

1.1 Early Muscle Development

In skeletal muscle, the process of muscle development begins with the commitment of cell types to muscle fate. Paraxial mesoderm on either side of the neural tube segments to form somites, which are patterned by wnt signalling from the neural tube, sonic hedgehog signalling from the notochord, delta-notch signalling from migrating neural crest cells, and inhibited by bone morphogenic protein signalling from the lateral plate mesoderm (reviewed in Chal and Pourquié, 2017). Cells from the dermomyotome (dorsal somite), delaminate to form myocytes and the primary myotome (Chal and Pourquié, 2017). These cells express a network of transcription factors required to initiate and maintain myogenesis, called Myogenic Regulatory Factors (Buckingham and Rigby, 2014). Knockouts of members of the MyoD family of Myogenic Regulatory Factors, including MyoD, Myf5, Mrf4, and myogenin dramatically affect the development of skeletal muscle (reviewed in Natalia et al., 2013). Myocytes align anterior to posterior and fuse, elongating to form myofibers which express myosin heavy chains (Sieiro-Mosti et al., 2014). These fibers are supplemented by a second pool of muscle progenitors, which delaminate from the central dermomyotome and also contribute to fast muscle before eventually becoming satellite cells (Chal and Pourquié, 2017).

1.1.1 Skeletal Muscle Development in the Zebrafish

While zebrafish muscle development is comparable to human muscle development, it occurs *ex utero*, transparently, and under a much shorter time span. Like humans, zebrafish also have fast (anaerobic) twitch muscle fibers and slow (aerobic) twitch muscle fibers, which are distinct based on mitochondrial count and the myosin heavy chains they express. Unlike humans who have mixed fast and slow fibers in their muscle tissue, zebrafish fast and slow muscle is spatially segregated and both fiber types are formed and functional by 24 hours post fertilization (hpf). The high fecundity, developmental transparency, and rapid development of the zebrafish has made it a popular model to study skeletal muscle development.

Muscle development in the zebrafish begins with segmentation of the paraxial mesoderm shortly after gastrulation. By 10.3 hpf, the first somite is formed (Figure 2A) and an additional somite forms every 30 minutes after until 24 hpf, or 30 somites (Figure 2E; Hanneman and Westerfield, 1989; Stickney et al., 2000). Before the appearance of the first somite, the cells that will give rise to slow muscle have already been specified, and strongly express *myoD* as well as other muscle-related transcription factors (Devoto et al., 1996). These cells, which are known as adaxial cells due to their positioning next to the notochord (Figure 2B), will begin to migrate away from the notochord to the periphery of the somite where they differentiate into slow muscle cells (Figure 2D; Devoto et al., 1996). A subset of the adaxial cells migrate to what will become the horizontal myosepta (Felsenfeld et al., 1990), where they will differentiate to muscle pioneer cells (Devoto et al., 1996). While the function of muscle pioneer cells is not fully understood (Stickney et al., 2000), they may be responsible for proper myosepta development (Halpern et al., 1993).

The population of cells surrounding the adaxial cells, called lateral presomitic cells (Figure 2B), are the precursors to fast muscle (Devoto et al., 1996). Unlike the adaxial cells, the lateral presomitic cells will not migrate and stay located deep within the embryo. At approximately 10.5 hpf, lateral presomitic cells begin to express *myoD* and *myogenin* (Stickney et al., 2000), at which they begin to differentiate. The patterning of the somite into fast and slow muscle is believed to be controlled by signals from the notochord (Stickney et al., 2000). Lying central in the somite, the notochord secretes sonic hedgehog, a glycoprotein that, when overexpressed, causes ectopic slow muscle at the expense of fast muscle (Blagden et al., 1997; Stickney et al., 2000). While it was originally thought that fast muscle was the 'default state' as muscle tissues expressing fast myosin heavy chain form in the absence of sonic hedgehog and the notochord (Blagden et al., 1997), more recent work has shown that certain fast muscle cell types also require sonic hedgehog (Wolff et al., 2003). Currently, it is believed that temporal and dose differences in sonic hedgehog activates a host of transcription factors that regulate muscle fiber fate, and maintains it over the life of the animal (reviewed in Jackson and Ingham, 2013).

After tissue has been specified to become muscle, muscle proteins and associated factors are produced and must assemble into sarcomeres. By 15 somites (~16 hpf), slow muscle sarcomeres have begun to form, as deduced by the presence of slow myosin heavy chain (Blagden et al., 1997). Fast muscle sarcomeres are slower to develop, with fast myosin heavy chain first detected at 21 somites (~19 hpf; Blagden et al., 1997). At 24 hpf, muscle development is largely complete and the embryos are motile.

1.2 Sarcomere Assembly

Many models have been proposed for how sarcomeres assemble (reviewed in Carlisle et al., 2018; Sanger et al., 2005) with increasing complexity, ranging from spontaneous assembly (Costa et al., 2002), template models (Holtzer et al., 1997; Lu et al., 1992), and the premyofibril model (Rhee et al., 1994; Sanger et al., 2009). While the exact mechanism of sarcomere assembly is still being uncovered, the pre-myofibril model (Figure 3) has the most supporting (and the least refuting) evidence. First proposed from observations in developing avian heart cells (Rhee et al., 1994), the premyofibril model of sarcomere assembly suggests that α-actinin Z-bodies, actin filaments, and non-muscle myosin align to form a structure called a premyofibril. Premyofibrils mature into nascent myofibrils as the Z-bodies align into punctate Z-bands, and incorporate titin filaments and muscle myosin. The transition of the Z-bands from punctate to linear along with the alignment of thick filaments and incorporation of M-band proteins marks the transition from nascent myofibrils to mature myofibrils (reviewed in Sanger et al., 2005). Since their discovery in cardiac avian cell culture, premyofibrils have since been observed in zebrafish embryos (Sanger et al., 2009), making the premyofibril model one of the few models of sarcomere assembly that is supported by both *in vitro* and *in vivo* evidence. However, gaps in our knowledge still remain regarding sarcomere assembly, and it is likely that proteins additional to those outlined in the premyofibril model are required for successful assembly of the sarcomere. This is supported by various genetic screens uncovering animals with sarcomere assembly defects whose cognate mutations are not in known sarcomere structural genes (Felsenfeld et al., 1990; Granato et al., 1996). Uncovering the roles of these genes in sarcomere assembly will be important in completing our understanding of muscle development.

1.2.1 Protein Quality Control During Sarcomere Assembly

As the sarcomere matures, protein quality control systems are important to fold and recognize improperly folded sarcomere proteins, as well as to replace components of the nascent sarcomere with those of the complete sarcomere. Although it is unclear how protein quality control systems are initiated, possible triggers are the presence of protein aggregates, or exposure of hydrophobic domains in misfolded proteins. In cases like the unfolded protein response or the misfolded myosin response, progress is being made on the elucidation of a molecular mechanism, which will be discussed below. It is also unclear how components of the nascent sarcomere, like non-muscle myosin, are replaced by components of the mature sarcomere, like muscle myosin (Sanger et al., 2005). The myosin chaperone, Unc45b, has been implicated in this process (Myhre et al., 2014a), but the mechanism of non-muscle myosin replacement by muscle myosin has yet to be determined. While each sarcomere component must be monitored for proper folding and assembly, only protein quality control systems that regulate muscle myosin will be discussed in this thesis.

1.2.1.1 Myosin Chaperones and the Misfolded Myosin Response

Thick filaments in the sarcomere are composed primarily of myosin. While non-muscle myosin isoforms exist, and are important for cell division and transport Hartman and Spudich, 2012, they are outside the scope of this thesis and will not be discussed. Muscle myosin (Figure 4) is composed of two heavy chains and two light chains. Each heavy chain consists of a globular head domain and an α-helical tail domain, which wind around each other to form a dimer (Cooper, 2000). Myosin head domains are responsible for binding and releasing actin in an ATP dependent process to facilitate muscle contraction. Each heavy chain has two associated light

chains, an essential light chain and a regulatory light chain, attached to the neck region which is believed to increase the speed and efficiency of actin/myosin binding and release (Trybus, 1994).

To reach their 3D conformation, myosins rely on other proteins, called myosin chaperones. Hsp90, Hsp70, Hsp40, Smyd1b, Unc45, CCT chaperonin, and their co-factors, have all been characterized as myosin chaperones (reviewed in Carlisle et al., 2018; Hellerschmied and Clausen, 2014), but genetic screens in *Drosophila* suggest there may be many more (Schnorrer et al., 2010). The evidence that myosin chaperones are essential for proper myosin folding and thick filament assembly is overwhelming, both *in vitro* (Just et al., 2011b; Liu et al., 2008) and *in vivo* (Bernick et al., 2010; Du et al., 2008; Etard et al., 2007; Hawkins et al., 2008; Just et al., 2011b; Li et al., 2013; Prill et al., 2015; Wohlgemuth et al., 2007). More recently, a mechanism of response has been uncovered when one or more myosin chaperones are missing or unable to properly fold myosin (Etard et al., 2015). This response, dubbed the misfolded myosin response (Figure 5), has similarities to the previously characterized Unfolded Protein Response (Liu and Kaufman, 2003) but describes the transcriptional and translational changes that occur specifically when myosin is misfolded. Both the Unfolded Protein Response and myosin specific misfolded myosin response are triggered by recognition of a misfolded/unfolded protein, although the unfolded protein response signalling cascade appears to start with Binding Imunoglobulin Protein (Carrara et al., 2015), while the misfolded myosin response is initiated through myosin chaperones and HSF-1 (Etard et al., 2015).

1.2.1.2 Myosin Chaperone Homeostasis

While specific chaperones are required for proper sarcomere assembly, chaperone expression must be tightly regulated, as an overabundance of a particular chaperone can cause equally severe muscle defects as a loss of function. *C. elegans* UNC-45, zebrafish Unc45b and

human skeletal muscle Unc45 have been shown to cause muscle disorganization when overexpressed either transgenically or by blocking its degradation (Bernick et al., 2010; Hoppe et al., 2004; Janeisch et al., 2007). This suggests a model where chaperone homeostasis is a highly regulated process. In invertebrates, a mechanism for Unc45 removal has been elucidated by which Unc45, UFD2, CDC-48 and CHN-1 (*C. elegans* orthologue of CHIP [carboxyl terminus of Hsc70 interacting protein]) form a complex that is able to polyubiquitinate Unc45 (Hoppe et al., 2004; Janeisch et al., 2007; see Figure 6). The integrity of this system is important in humans as well, as mutations in p97 (human CDC-48), cause inclusion body myopathy, which is associated with Paget disease of bone and frontotemporal dementia. Paget disease of bone and frontotemporal dementia results in sarcomere assembly defects, which is attributed to excess skeletal muscle Unc45 (Janeisch et al., 2007). While the mechanisms behind the sarcomere defects in Unc45/Unc45b/Skeletal Muscle Unc45 overexpression models are still being uncovered, some suggestions have been put forth. Willis and colleagues (2009) suggest that these defects result from too many Unc45 molecules attached to myosin, which: (a) impedes sarcomere assembly, and (b) causes the formation of aggregates (Figure 6C). Other models suggest that Unc45 overexpression may cause the sarcomere to assemble incorrectly, which is later recognized and disassembled (Kim et al., 2008).

Although Unc45 is known to work with Hsp90 and Smyd1b to fold myosin (Barral et al., 2002; Li et al., 2013; Prill et al., 2015), no similar complexes have yet been reported for control of Hsp90 or Smyd1b turnover. As no data yet exists for Smyd1b overexpression, it is unsurprising that no complex regulating Smyd1b expression has yet been discovered. Importantly, the sarcomere defects associated with excess Unc45/Unc45b/SM-Unc45 also appear to proceed through an Hsp90 independent pathway (Bernick et al., 2010). While it does appear

that Hsp90a/b isoform homeostasis is important for proper muscle specification (Echeverría et al., 2016), no consequences to sarcomere assembly have been described to date when Hsp90 is overexpressed in muscle (Bernick et al., 2010). This could be due to the general expression of Hsp90 such that it requires Unc45 cooperation in striated muscle, or it may indicate that the myosin chaperone actions of Hsp90 and Unc45 differ enough that overexpression of one is detrimental but the other is benign, such that only homeostasis of Unc45 is tightly regulated.

1.3 Sarcomere Maintenance

1.3.1 Protein Quality Control During Sarcomere Maintenance

Even after the sarcomere is fully assembled, protein quality control systems are essential for sarcomere health. As filament systems contract, sarcomere protein damage is inevitable, ensuring a constant need for protein turnover. As such, multiple systems are implicated in protein turnover including calpains and other proteases, chaperone systems, the ubiquitin proteasome system (UPS), and autophagy.

1.3.1.1 The Ubiquitin Proteasome System

The components of the ubiquitin proteasome system (Figure 7) were first discovered in 1979 in reticulocytes (Hershko et al., 1979), and over the next decade their functions characterized (reviewed in Hershko, 1996; Hershko and Ciechanover, 1998). The UPS works through the actions of three enzymes. E1, or the ubiquitin activating enzyme, activates ubiquitin (Ub) in an ATP dependent process and transfers it to E2, the ubiquitin carrier protein. After accepting the activated Ub from the E1 enzyme, E2 enzymes carry Ub to E3 enzymes. E3 enzymes, or ubiquitin ligases, provide the UPS with substrate specificity as they are responsible for ligating Ub to the target protein, usually conjugated to a lysine residue (Hershko, 1996). In yeast, three E1-like enzymes have been characterized, and thirteen E2 enzymes (reviewed in

Hochstrasser, 1996). It is believed that more than 1000 E3 enzymes are encoded in the mammalian genome (Varshavsky, 2017).

One particular family of E3 enzymes involved in striated muscle turnover are the MuRFs (Muscle Ring Finger) proteins. MuRF1 (Trim63) was first identified as being upregulated in atrophying muscle (Bodine et al., 2001). Using MuRF1 as bait in a yeast two hybrid screen, two homologues of MuRF1, MuRF2 (Trim55) and MuRF3 (Trim54) were identified (Centner et al., 2001). While all three MuRFs are expressed in striated muscle, MuRF1 and MuRF2 have been implicated in sarcomere protein turnover (Clarke et al., 2007; Cohen et al., 2009; Lodka et al., 2016; Moriscot et al., 2010; Witt et al., 2005), while MuRF3 appears to be involved mainly in cell differentiation during myofibrillogenesis and microtubule stability (Spencer et al., 2000). A fourth member of the MuRF family was identified in teleosts, MuRF4 (Trim101), although its function remains uncharacterized (Macqueen et al., 2014).

While most substrates can be recognized and polyubiquitinated by E1, E2, and E3 enzymes, a subset of these proteins require an additional factor for UPS mediated degradation (reviewed in Hoppe, 2005). These factors, called E4 enzymes, appear to be responsible for the generation of polyubiquitin chains, and in their absence, substrates can only be monoubiquitinated (Koegl et al., 1999). E4 enzymes do not appear to interact with E2 enzymes, and they are not able to ubiquitinate substrates in the absence of an E3 enzyme, suggesting that the functions of E3 and E4 enzymes are different (Matsumoto et al., 2004). The role of E4 enzymes has still not been fully elucidated, but it has been proposed that they add an additional level of regulation to substrates that have active signalling roles when only monoubiquitinated (Hoppe, 2005).

Whether an E4 enzyme is involved or not, a damaged protein is marked for degradation by serial addition of Ub to the Lysine^{48} of the previous Ub to form a polyubiquitin chain (Chau et al., 1989). The targeted protein is then moved to a protein complex known as the proteasome, composed of three sub-complexes: CF-1, CF-2, and CF-3 (Ganoth et al., 1988). The catalytic core, also known as the 20S proteasome, corresponds to CF-3 (Eytan et al., 1989), and is capped by two 19S regulatory complexes to form the 26S proteasome (reviewed in Coux et al., 1996). It is possible that CF-1 and CF-2 constitute these 19S regulatory caps, as CF-1 and CF-2 form complexes with CF-3 in an ATP dependent process (Eytan et al., 1989). Unfolded proteins are fed through the proteasome for ATP-dependent degradation and recycling of Ub and amino acids (Hershko, 1996; Hough et al., 1986). However, ubiquitination does not only destine a protein for degradation, as ubiquitination is reversible through deubiquitinating enzymes (Amerik and Hochstrasser, 2004; Hanpude et al., 2015), and ubiquitin is also implicated in signalling networks (reviewed in Ciechanover, 1994).

One such signalling mechanism, the N-end rule (reviewed in Varshavsky, 2011), was initially discovered as a method of regulating the half-life of a cellular protein (Bachmair et al., 1986). Although in prokaryotes this process can be ubiquitin-independent, in eukaryotes the N-end rule is linked to the UPS (Varshavsky, 2011). The N-end rule describes a phenomenon by which the N-terminal amino acid of a protein (methionine) is cleaved by methionyl aminopeptidase, exposing a ‘new’ N-terminal amino acid, called a ‘degron’, which destabilizes the protein (Bachmair et al., 1986). The half-life and fate of the protein depends on which amino acid is exposed as the new N-terminus, with residues like methionine, lysine, and valine conferring stability, leucine, tryptophan, and phenylalanine highly unstable, and cysteine, aspartic acid, and glutamic acid, marking proteins for UPS degradation (for a full list, see Eldeeb

et al., 2017). This method of regulation is not only useful for protein turnover, but also has broad biological applications, as the N-end rule is a method of spatially regulating how far a diffusible molecule can travel, and temporally by regulating how long a signalling molecule can persist (Eldeeb et al., 2017; Varshavsky, 2011). As such, the N-end rule has been implicated in a wide variety of biological processes, such as development, oxygen sensing, genome repair, gluconeogenesis, apoptosis, immunity, autophagy, and others (reviewed in Varshavsky, 2017).

Beyond its connections to signalling roles, the UPS is critical for proper development, homeostasis, and survival (Ciechanover, 1994; Coux et al., 1996), and the UPS is implicated in many neurodegenerative diseases (reviewed in Aguzzi and O'Connor, 2010; Subhankar, 2008), and recently become a pharmaceutical target to treat certain cancers (reviewed in Goldberg, 2012). However, UPS function in striated muscle is understudied in comparison to its role in other systems (reviewed in Carlisle et al., 2018).

1.3.1.2 Chaperones Beyond Assembly

Molecular chaperones were initially recognized only as aids for certain proteins that required additional factors to facilitate proper folding and prevent precipitation (Laskey et al., 1978). The role of chaperones was later extended to include binding and folding client proteins after their synthesis, preventing the aggregation of misfolded proteins and aiding in the formation of macromolecular structures (Ellis, 2006). Recently, connections between chaperones and protein degradation have been established (Kettern et al., 2010), linking chaperones with both autophagy and the UPS. Chaperone-mediated autophagy and Chaperone-assisted selective autophagy connect the chaperone system to protein quality control.

Chaperone-mediated autophagy involves the delivery of a chaperone substrate across a lysosomal membrane in a ubiquitin-independent manner (Kaushik and Cuervo, 2012a). Although Hsp70 is involved in this process (Chiang et al., 1989), Chaperone-mediated autophagy has not been widely explored in skeletal muscle (Smith et al., 2014). Chaperone-assisted selective autophagy involves the ubiquitin dependent degradation of a chaperone substrate by the lysosome (Arndt et al., 2010). Unlike Chaperone-mediated autophagy, there is strong evidence for Chaperone-assisted selective autophagy in skeletal muscle (Smith et al., 2014). Chaperone-assisted selective autophagy was first described in the *Drosophila* Z-disc as a mechanism by which Starvin (Drosophila Bag-3) mediates the autophagic turnover of filamin in a CHIP ubiquitination dependent manner (Arndt et al., 2010). It is likely that this role of Bag-3 is conserved in mammals as well, as Bag-3 homozygous null mice display normal Z-disc assembly, which deteriorates over time and results in eventual apoptosis (Homma et al., 2006). Bag-3 also appears to be important in humans, with a severe muscular dystrophy linked to loss of Bag-3 (Selcen et al., 2009). Because Bag-3 is considered to be an Hsp70 (or ubiquitous Hsc70) co-chaperone (Behl, 2016; Takayama et al., 1997) along with its many other proposed roles (Behl, 2016), the role of Hsp70 in muscle maintenance becomes an important and currently under-investigated question.

Evidence for chaperone and UPS collaboration comes from Chaperone-assisted proteasomal degradation, which describes the process by which a chaperone client is ubiquitinated and subsequently degraded by the proteasome (Arndt et al., 2007; Bercovich et al., 1997; Kettern et al., 2010). Evidence for Chaperone-assisted proteasomal degradation comes from the Hsc/Hsp70 co-chaperone Bag-1, which associates with the 26S proteasome and has been proposed to physically link chaperone and proteasome systems (Luders et al., 2000). Bag-1

has been shown to interact with CHIP (Demand et al., 2001), which provides a mechanism by which chaperone substrates could be ubiquitinated and targeted directly to the proteasome. Although CHIP is the only E3 ligase identified so far that binds to this complex, there are likely other E3 ligases involved in this role, as CHIP knockout mice do not have severe muscle defects (Dai et al., 2003). While it is likely that this process is abundant in skeletal muscle, it has not been widely studied to date.

Together, the collaboration of chaperones with both autophagic and proteasome degradation systems suggests a hypothesis by which chaperones respond to their client protein when damaged regardless of when the damage occurs. As many chaperones remain associated with their client proteins or are localized on nearby sarcomere structures after sarcomere assembly, this hypothesis makes sense. However, recent evidence that myosin damage may occur without a subsequent upregulated response of myosin chaperones contradicts this model (Etard et al., 2015). Differing from zebrafish with chaperone loss of function mutations, *steif* (Unc45b, Etard et al., 2015) and *still heart* (*smyd1b*; Prill et al., 2015), zebrafish with mutations outside the chaperone pathway, but with similar muscle disorganization, do not display an upregulation in myosin chaperones (Etard et al., 2015). The zebrafish mutation *sofa potato* (*sop*^{fixe}), affects an acetylcholine receptor, which results in grossly normal muscle ultrastructure but smaller myofibrils and disorganized slow myosin (Etard et al., 2005a). *Ache* has a mutation in acetyl cholinesterase, which results in gradual disorganization of myofibrils and a loss of slow myosin over time (Behra et al., 2002). Finally, *herzschlag* (*hel*) mutants carry an unknown titin paralog, *titin2*, mutation, that affects Titin2 protein somewhere between the I-band and A-band (Myhre et al., 2014b). This mutation results in initially normal sarcomere assembly, which degenerates over time (Myhre et al., 2014b).

The absence of myosin chaperone upregulation in these mutants, despite the myosin disorganization they display, suggests that myosin chaperones are not directly responding to the disorganized protein itself (Etard et al., 2015). Instead, it appears that Hsf-1 is responsible for inducing the myosin chaperone response (Etard et al., 2015). However, it is still unclear why these chaperones do not react in *sofa potato*, *ache*, or *herzschlag* embryos. One difference between these zebrafish and those with mutations in myosin chaperones is that the initial folding and assembly of myosin into the sarcomere is unimpeded. The difference in the myosin chaperone response is potentially due to the stage in which damage occurs, with myosin chaperones responding to initial folding and assembly defects through an Hsf-1 mediated response. Should damage occur post assembly due to normal wear and tear, an unc45b/hsp90/smyd1b/hsf-1 independent response to myosin occurs. Whether this response is entirely chaperone independent, or involves a subset of muscle maintenance chaperones collaborating with the UPS and autophagic systems, will be important to uncover.

1.4 Communication Between Protein Quality Control Systems

For many years it was believed that chaperone systems, autophagy, and the UPS existed as separate, competing, entities. However, recent evidence suggests that these systems communicate and even coordinate to maintain proteostasis (Esser et al., 2004; Kaushik and Cuervo, 2012b; Korolchuk et al., 2010). As discussed above, chaperones are connected with both the UPS and autophagy, but there is also evidence that the UPS and autophagy are connected themselves. Knockout of the E3 ligase Traf6 in mice was shown to lower the expression of autophagy markers after denervation and during cancer cachexia (Paul et al., 2010), and global inhibition of the proteasome system has been shown to increase autophagy (Ding et al., 2007), suggesting communication and coordination between these systems. The mechanisms behind this

phenomenon are still being uncovered, however (reviewed in Korolchuk et al., 2010), and will be discussed in section 1.5.

1.4.1 Refold or Degrade?

It is currently unclear what determines whether a damaged protein is salvaged and refolded by chaperone systems or simply targeted for degradation by autophagy or the UPS. While it is logical that a folded protein could be differentiated from an unfolded or misfolded protein due to the external exposure of hydrophobic domains, it is unclear how a misfolded/unfolded protein could be differentiated from a damaged protein. However, the lack of a misfolded myosin response in *sofa potato*, *ache*, or *herzschlag* embryos is evidence that such a differentiation does exist.

Many models of how damaged or misfolded proteins are recognized have been proposed (reviewed in Esser et al., 2004). In the simplest model, also known as the "kinetic model of protein triage", chaperones and the UPS exist as competing entities (Gottesman et al., 1997; Wickner et al., 1999; Figure 8A). In this model, chaperones respond to their misfolded client protein, likely recognizing exposed hydrophobic domains, and attempt to refold it to its proper conformation. A misfolded protein that is not successfully refolded may be bound again by its chaperone, or by an E3 enzyme that also recognizes exposed hydrophobic domains (Esser et al., 2004). In this model, whether a chaperone or an E3 enzyme binds the misfolded protein, is random (Gottesman et al., 1997; Wickner et al., 1999). However, concentrations of chaperones or E3 enzymes and damage to the client protein would play an important role in which outcome is favored. If the misfolded protein is bound by its chaperone, the attempt-to-refolded cycle continues. If an E3 enzyme binds the misfolded protein, it is targeted for degradation.

An alternate model of protein turnover suggests that when a chaperone binds a misfolded client protein, it is the recruitment of specific co-chaperones that determines whether the client protein will be refolded or degraded (Esser et al., 2004; Kettern et al., 2010; Figure 8B). Evidence for this model is abundant and mainly centers on the chaperones Hsp70 and Hsp90 and their substrates (Esser et al., 2004; Kettern et al., 2010). Co-factors Hip and Hop binding Hsp90 or Hsp70 has been shown to promote substrate folding (Connell et al., 2001; Nollen et al., 2001; Odunuga et al., 2004), while binding of CHIP or Bag-1 promotes substrate degradation (Connell et al., 2001; Luders et al., 2000; Murata et al., 2001; Wiederkehr et al., 2002). A lingering question remains as to how the appropriate co-chaperones are recruited. Like the previous model, refolding or degradation of the client protein likely depends on the initial damage to the protein as well as the presence and concentrations of its chaperone and co-chaperones. With all components being equal, this process will be stochastic (Gottesman et al., 1997). In support of this, the addition of CHIP to lysates containing HOP and Hsp90 significantly decreases the number of HOP/Hsp90 complexes (Connell et al., 2001), suggesting that HOP can be outcompeted by CHIP. Furthermore, CHIP and HOP appear to bind the same location of Hsp70/Hsp90 (Connell et al., 2001) as do Bag-1 and HIP, which sterically hinder the binding of its competitor (Kanelakis et al., 2000; Kettern et al., 2010).

A third model of protein turnover suggests that the binding of a co-factor such as CHIP results in the transformation of a chaperone/client complex into a degradation complex, which is then transported to the proteasome (Arndt et al., 2007; Esser et al., 2004; Wiederkehr et al., 2002). Rather than CHIP and Bag-1 being thought of as co-factors in this model, these proteins and the chaperones they bind form a complex that is thought of as one big E3 ligase (Arndt et al., 2007). Substrate specificity will come from the chaperone's affinity for their client (Kriegenburg

et al., 2012), CHIP ubiquitinates proteins in the complex and then the complex is transported to and docked on the 26S proteasome by Bag-1 (Luders et al., 2000; Figure 8C). This model differs from the "cofactor" model by the conceptualization of the entire complex as an active E3 ligase. Although these models are presented separately, they do not have to be mutually exclusive and it is feasible that certain co-factors promote folding, while others promote the transformation of the chaperone/substrate complex into a degradation complex. The binding and releasing of the folding co-factors or the degradation complex would be subject to competition, as outlined in the "kinetic model" making the best model of protein triage likely a combination of all three.

1.5 Striated Muscle Diseases

Striated muscle disease, or myopathies, are diseases of cardiac or skeletal muscle. Myopathies may affect solely cardiac or skeletal muscle, or a combination of both. Although myopathies can be grouped by the affected muscles, the genetic component, or the affected area of the sarcomere, historically myopathies have been classified by age of onset and diagnostic presentation. As such, myopathies fall into one of seven broad categories: congenital myopathies, muscular dystrophies, congenital muscular dystrophies, distal myopathies, metabolic myopathies, muscle channelopathies, and autophagic vacuolar myopathies (reviewed in Shieh, 2013). Many neuromuscular diseases are also associated with or included under the branch of myopathy (reviewed in Morrison, 2016), although they are outside the scope of this thesis. The advances in next generation sequencing has made identification of the genetic components of myopathies a reality, and delineating the borders between these categories is becoming increasingly difficult (Ravenscroft et al., 2018). As such, myopathies are becoming increasingly categorized by the genes involved (eg: titinopathies). Because Titin 2 and myosin

are the focus of this thesis, in addition to giving an overview of the above categories, this section will also include a list of myopathies associated with mutations in these genes.

1.5.1 Congenital Myopathies

Congenital myopathies are a group of myopathies characterized by non-progressive weakness and low muscle tone (hypotonia) which appear restricted to skeletal muscle and presents, in humans, within the first year of life (reviewed in Ravenscroft et al., 2018; Romero and Clarke, 2013; Shieh, 2013). Myopathies characterized as congenital myopathies have distinctive morphological defects in the muscle fibers. These morphological defects range from cores or holes in the muscle fiber (central core disease; multi-minicore disease; core-rod myopathy), protein aggregates in the muscle fiber (nemaline myopathy; actin filament aggregation myopathy; cap disease; myosin storage myopathy) abnormally located nuclei (myotubular myopathies; centronuclear myopathies), or alterations to slow twitch and fast twitch fiber distribution and/or size (congenital fiber type disproportion; congenital neuromuscular disease with uniform type 1 fibers). For a review of these myopathies, clinical presentations, and genetic components see (Romero and Clarke, 2013).

1.5.2 Muscular Dystrophies

Muscular dystrophies differ from congenital myopathies based on their progressive nature and cardiac involvement (reviewed in Chelly and Desguerre, 2013), although arguments have been presented for congenital myopathies to be reclassified as a subset of muscular dystrophies (Shieh, 2013). Dystrophic muscle fibers show variability in size, internally localized nuclei, and excessive connective tissue (fibrosis), associated with the continual damage and regeneration these fibers undergo (Chelly and Desguerre, 2013).

The most prevalent forms of muscular dystrophies, Duchennes muscular dystrophy and Beckers muscular dystrophy, result from mutations in dystrophin, a large cytoskeletal protein (Shieh, 2013). Dystrophin attaches the sarcolemma to the intermediate filaments of the cytoskeleton and maintains the integrity of the plasma membrane during muscle contractions (Gao and McNally, 2015). Mutations that interrupt this function result in contraction-induced damage (Goldstein and McNally, 2010) as well as increases in reactive oxygen-nitrogen species, intracellular calcium, and protease activation (Khairallah et al., 2012). Other common muscular dystrophies include facioscapulohumeral muscular dystrophy, myotonic dystrophy, and limb girdle muscular dystrophy, but this is not an exhaustive list. Facioscapulohumeral muscular dystrophy is caused by the deletion of a highly methylated region of chromosome 4, responsible for downregulating the expression of *dux4*, while myotonic dystrophy results from mutations in *dmpk* or *cnbp* that alter RNA structure and affect the splicing of downstream genes (Shieh, 2013). Currently 11 forms of limb-girdle muscular dystrophy exist, with multiple genetic loci involved (for a list of cognate genes, see Shieh, 2013. For clinical presentations, see Chelly and Desguerre, 2013).

1.5.3 Congenital Muscular Dystrophies

Congenital muscular dystrophies (reviewed in Falsaperla et al., 2016; Kirschner, 2013) differ from Congenital myopathies as they get progressively worse with age and lack the distinctive muscle fiber morphological changes characteristic of Congenital myopathies (Ravenscroft et al., 2018; Shieh, 2013). While congenital muscular dystrophies and muscular dystrophies both result in a gradual deterioration of muscle (dystrophy), muscle weakness associated with congenital muscular dystrophies presents at or before the first year of life (Falsaperla et al., 2016; Kirschner, 2013). Congenital muscular dystrophies often affect the brain

and other organ systems (Shieh, 2013), which also distinguish them from congenital myopathies and muscular dystrophies.

Classification of different congenital muscular dystrophies is complex and continually changing. Clinically, congenital muscular dystrophies are differentiated based on normal or abnormal mental development, but classification based on the genetic legion involved, inheritance pattern, or a combination of all three is becoming commonplace (Falsaperla et al., 2016). Mutations in collagen genes, laminin, or sarcoplasmic reticulum genes cause congenital muscular dystrophies with normal mental development (for a list of cognate genes see Kirschner, 2013). Congenital muscular dystrophies that present with brain defects and cognitive impairment (Fukuyama congenital muscular dystrophy; muscle-eye-brain disease; Walker-Warburg syndrome) result from improper glycosylation of α-dystroglycan (for a list of cognate genes see Kirschner, 2013), a protein in the dystrophin-associated protein complex, that links laminin to dystrophin (Johnson et al., 2013). However, there are some congenital muscular dystrophies caused by defects in α-dystroglycan that do not result in cognitive impairment (congenital muscular dystrophy type 1C; congenital muscular dystrophy with partial merosin deficiency; LARGE related congenital muscular dystrophy). For reviews of clinical presentations, see (Falsaperla et al., 2016; Kirschner, 2013).

1.5.4 Distal Myopathies

Distal myopathies (reviewed in Dimachkie and Barohn, 2014; Mankodi et al., 2015) are characterized by weakness of the distal skeletal muscles of the body, including muscles of the hands, feet, shoulders, legs, and face. While symptoms usually present in early or late adulthood, some distal myopathies are symptomatic as early as 4 years of age (Laing et al., 1995). Although distal myopathies are classified based on skeletal muscle weakness and atrophy, there is cardiac

involvement in some cases (ie: desminopathies; Strach et al., 2008). Like other myopathies, the classification of distal myopathies is changing as genetic loci are being identified. However, many distal myopathies are still classified by age of onset, inheritance pattern, and affected muscle groups. Currently, more than 20 genes have been implicated in distal myopathies ranging from mRNA binding proteins (TIA1; Welander distal myopathy, matrin3; matrin3 distal myopathy), sarcomere structural proteins (titin; tibial muscular dystrophy, nebulin; distal nebulin myopathy, myotilin; distal myotilinopathy), signalling proteins (ZASP; ZASPopathy), and ubiquitin ligases (KLHL9; KLHL9 mutated distal myopathy), among others. For a full list of distal myopathies, cognate genes, and clinical presentations, see Palmio and Udd, 2016; Udd, 2014.

1.5.5 Metabolic Myopathies, Muscle Channelopathies, and Autophagic Vacuolar Myopathies

In addition to mutations in structural proteins and chaperones, alterations in the excitation contraction cycle can lead to myopathies, whether through energy misregulation or ion conductance abnormalities. These myopathies include metabolic myopathies, muscle channelopathies, and autophagic vacuolar myopathies (Shieh, 2013).

Metabolic myopathies refer to a group of diseases that affect the production of ATP by mitochondria through defects in oxidative phosphorylation, glycogen, or fatty acid metabolism (reviewed in Berardo et al., 2010). Metabolic myopathies can present at birth or during adulthood and symptoms can range from continual to exercised-induced. Common metabolic myopathies and their clinical presentations can be found in (Shieh, 2013).

Muscle channelopathies include nondystrophic myotonias, and periodic paralysis (Raja Rayan and Hanna, 2010). Nondystrophic myotonias present as muscle stiffness caused by a failure or delay of the muscle to relax after contraction, usually due to mutations in voltage-gated sodium (paramyotonia congenita) or chloride channels (myotonia congenita). Nondystrophic myotonias differ from muscle dystrophies in their absence of non-muscle system symptoms (Matthews et al., 2010). Periodic paralysis results from mutations in potassium, sodium, or calcium channels. Clinical features of these myopathies and their genetic loci can be found in (Raja Rayan and Hanna, 2010; Shieh, 2013).

Autophagic vacuolar myopathies describe a category of myopathies resulting from abnormal lysosomal proteins (reviewed in Nishino, 2006). Of the autophagic vacuolar myopathies, the most well characterized are acid maltase deficiency and Danon disease. Acid maltase deficiency results from a loss of function of the lysosomal enzyme, acid maltase, and subsequent aggregation of glycogen. The glycogen aggregation results in hypotona and in severe cases, cardiac and respiratory consequences (Nishino, 2006). Danon disease (Danon et al., 1981) is an X-linked dominant myopathy that has similar clinical features to acid maltase deficiency, but with increased instances of cardiac and intellectual defects and the absence of glycogen aggregates (Nishino, 2006). Danon disease results from mutations in LAMP-2, a structural protein of the lysosomal membrane (Nishino, 2006). Clinical features of these myopathies can be found in (Nishino, 2006).

1.5.6 Titinopathies:

Titin, originally called connectin, is a striated muscle protein, with both cardiac and skeletal isoforms. Titin is the largest mammalian protein discovered, which has made a thorough analysis of its role in developing muscle difficult due to its sheer size and complexity. Titin

stretches one half of a sarcomere (1.2um), with protein domains that correspond to specific regions of the sarcomere (reviewed in Chauveau et al., 2014). These domains are responsible for various functions in sarcomere assembly and maintenance, and are still being actively studied (see Granzier and Labeit, 2004, 2006; Gregorio et al., 1999; Krüger and Kötter, 2016; Krüger and Linke, 2011; Labeit and Kolmerer, 1995; Linke, 2008; Myhre and Pilgrim, 2014; Tskhovrebova and Trinick, 2002; Tskhovrebova and Trinick, 2010 for reviews on the functions of titin).

The human titin gene is located on chromosome 2q31, and contains 363 (now considered to be 364 as the first exon is non-coding) exons (reviewed in Chauveau et al., 2014). Human titin mRNA consists of over 1kb, and theoretically can produce a protein containing over 38 000 amino acids and weighing over 4 kDa (reviewed in Chauveau et al., 2014). Due to its sheer size and numerous binding partners, it is unsurprising that titin mutations result in myopathies. With the increasing availability of next generation sequencing, titin mutations are being more readily identified as historical sequencing methods are not amenable to diagnosing titin mutations. As of 2014, 127 titin mutations resulting in 10 titinopathies have been identified (Table 1; reviewed in Chauveau et al., 2014). Mutations in the M-line and A-band of titin are over represented compared to Z-disc and I-band mutations (Chauveau et al., 2014), suggesting mutations in these regions are underdiagnosed due to them being asymptomatic, overlooked, or embryonic lethal.

Tibial muscular dystrophy (Udd et al., 1991) was the first myopathy linked to a titin mutation (Hackman et al., 2002). Sequencing of titin identified the tibial muscular dystrophy mutation to be in exon 363 of titin's 363 exons, which results in a change of four amino acids and commonly called the FINmaj mutation (EITW to VKEK; Hackman et al., 2002). Since then, other mutations in exon 363 of titin have shown to result in tibial muscular dystrophy (reviewed

in Chauveau et al., 2014; Udd, 2013; Table 1; Figure 9). When heterozygous, these titin mutations cause tibial muscular dystrophy, a late onset disease characterized by weakness in the ankles and feet as well as atrophy of the lower leg muscles (reviewed in Udd, 2013). When homozygous, this mutation causes the more severe limb-girdle muscular dystrophy type 2J (LGMD2J; Hackman et al., 2008; Hackman et al., 2002).

A subset of patients with FINmaj mutations but presenting with an unusually severe form of tibial muscular dystrophy (now designated as young or early adult onset recessive distal titinopathy; Evilä et al., 2017; Savarese et al., 2016) were shown to have secondary (compound or homozygous) mutations in the titin A-band (Evilä et al., 2017; Evila et al., 2014), which further highlights the importance of next generation sequencing as a diagnostic tool in identifying titinopathies. Currently, no treatments for tibial muscular dystrophy or LGMD2J exist, although experiments in mouse models of tibial muscular dystrophy suggest the pathology behind the titin mutation is due to overactivity of calpain-3, which binds the titin I-band and M-line (Charton et al., 2010; Figure 9&10). However, calpain-3 activity cannot solely explain the muscle consequences associated with the more severe LGMD, as these patients have cardiac defects and calpain-3 protein is not expressed in the adult heart (Fougerousse et al., 2000).

Early-onset myopathy with fatal cardiomyopathy, or Salih myopathy, was the second myopathy found to result from titin mutations (Carmignac et al., 2007). Early-onset myopathy with fatal cardiomyopathy is caused by a frameshift mutation in the titin C-terminus, resulting in 21 amino acid changes before a premature stop codon and a truncation of 447 amino acids in one family, while another family had an insertion of 8 amino acids, followed by a stop codon and a truncation of 808 amino acids (Carmignac et al., 2007; Figure 9). As a result, patients between 5-12 years old displayed weakness of the distal muscles and lower limb muscle atrophy as well as

dilated cardiomyopathy that progressed into heart failure (Carmignac et al., 2007). No therapies currently exist for Early-onset myopathy with fatal cardiomyopathy, but cardiac transplants have shown to extend the lifespan of the patient (Carmignac et al., 2007).

Hereditary myopathy with early-onset respiratory failure was first described by Edstrom and colleagues as a disease characterized by distal muscle weakness, thin filament aggregation, early (onset at between the second and fifth decade of life) respiratory failure, and absence of cardiac involvement (1990). Hereditary myopathy with early-onset respiratory failure was later linked to a missense mutation in the titin kinase domain of the titin M-line (Lange et al., 2005). However, since then many other missense mutations in exon 343, corresponding to the titin A-band, have been identified, which result in hereditary myopathy with early-onset respiratory failure (reviewed in Tasca and Udd, 2018; see Table 1, Figure 9&11). The mechanism behind hereditary myopathy with early-onset respiratory failure pathology remains unknown, however dysregulation of titin binding partners and subsequent interruption of autophagy is an attractive hypothesis (Tasca and Udd, 2018) as improper lysosomal activity has been observed in the muscles of these patients (Edström et al., 1990).

Centronuclear myopathy is a congenital myopathy whose cognate genes are usually related to excitation contraction coupling, including ryanodine receptors, myotubularin, and dynamin (reviewed in Romero, 2010). However, 5 patients diagnosed with centronuclear myopathy were found to have mutations predicting C-terminal truncations in both alleles of titin (Ceyhan-Birsoy et al., 2013; Table 1; Figure 9-11). Another subset of patients presenting with skeletal muscle symptoms reminiscent of Emery-Dreifuss muscular dystrophy, a myopathy also not historically linked to titin, were shown to have homozygous C-terminal titin truncations (De Cid et al., 2015; Table 1; Figure 9).

The most prevalent myopathy linked to titin mutations is dilated cardiomyopathy (DCM), with 25% of DCM patients carrying titin mutations (Herman et al., 2012). Dilated cardiomyopathy is characterized as dilation of the left ventricle and subsequent cardiac dysfunction, in the absence of arterial blockages and ventricle filling/arterial loading defects (reviewed in Weintraub et al., 2017). There are over 60 titin mutations linked to DCM (for a full list of mutations see Chauveau et al., 2014; Herman et al., 2012; Table 1, Figure 9-11). Titin mutations have also been linked to hypertrophic cardiomyopathy (HCM), which results in excessively large ventricular muscles impeding cardiac function (reviewed in Frey et al., 2011; Maron and Maron, 2013). However, in contrast to DCM, only 4 HCM causing titin mutations have been identified (Chauveau et al., 2014; Matsumoto et al., 2005; Satoh et al., 1999; Table 1, Figure 11). A third cardiomyopathy linked to titin is arrhythmogenic right ventricular cardiomyopathy, which results from dilation of the right ventricle and fibrosis of cardiac muscle (Taylor et al., 2011). Eight titin mutations have currently been identified in patients with arrhythmogenic right ventricular cardiomyopathy (Taylor et al., 2011). DCM, HCM, and arrhythmogenic right ventricular cardiomyopathy each have multiple genetic causes, and therefore it is not surprising that the titin mutations that affect cardiac function are commonly associated with dysregulation of titin binding partners (Table 1).

1.5.7 Myosinopathies

Myopathies resulting from mutations in the thick filament protein, myosin, are widespread with over 200 myosin mutations resulting in familial mypertrophic cardiomyopathy and DCM alone (reviewed in Tajsharghi and Oldfors, 2013). Mutations in an embryonic myosin (MYH3) as well as the fast twitch myosin (MYH2) and slow twitch myosin (MYH7) have been linked to myosinopathies (reviewed in Goebel and Laing, 2009; Tajsharghi and Oldfors, 2013;

Table 2). Myosinopathy causing mutations exist in non-muscle myosins, as well as the atrial specific, MYH6 (Carniel et al., 2005; Ching et al., 2005), but they are outside the scope of this thesis.

Distal arthrogryposis describes a group of diseases characterized by contractures (permanent shortening) of the joints and muscles in the absence of an underlying neurological disorder (reviewed in Scala et al., 2018). Mutations in embryonic myosin, MYH3, has been linked to four types of distal arthogryposis, Freeman-Sheldon syndrome, Sheldon-Hall syndrome, autosomal-dominant multiple pterygium syndrome (Chong et al., 2015), and digitotalar dysmorphism (Alvarado et al., 2011; Toydemir and Bamshad, 2009; Toydemir et al., 2006). Freeman-Sheldon syndrome is the most severe of the distal arthogryposes, with facial muscle involvement as well as distal limbs (Stevenson et al., 2006). Nearly all the myosin mutations causing Freeman-Sheldon syndrome lie in the globular head domain of myosin and are predicted to interrupt ATP hydrolysis and interfere with myosin activity (Toydemir et al., 2006; Walklate et al., 2016). Although myosin mutations causing Sheldon-Hall syndrome also localize primarily to the globular head domain of myosin, it is proposed that these residues are important for actin and troponin binding or forming myosin thick filaments, rather than ATP hydrolysis (Toydemir et al., 2006). Mutations in the head domain of myosin also can result in the abnormal bone development found in autosomal-dominant multiple pterygium syndrome and digitotalar dysmorphism, although the mechanism underlying MYH3 and skeletal development has yet to be elucidated (Carapito et al., 2016; Chong et al., 2015).

Laing distal myopathy results from mutations in the slow muscle/ventricular myosin, MYH7 (Table 2), and presents with early onset (before 5 years of age) weakness in the distal muscles, especially foot and finger (reviewed in Tajsharghi and Oldfors, 2013). Cardiac

involvement in Laing distal myopathy is rare, and usually linked to mutations in the globular head domain of myosin rather than mutations in the coiled tail domain. However, MYH7 mutations can have cardiac consequences and missense mutations in MYH7 are linked to familial hypertrophic cardiomyopathy and DCM (Table 2; Walsh et al., 2017).

Myosin storage myopathies are characterized by inclusion bodies of myosin proteins in the myofibrils (reviewed in Goebel and Laing, 2009), and also caused by mutations in the rod domain of MYH7 (Table 2). These mutations are proposed to interfere with the dimerization of myosin (Laing et al., 2005). The severity of myosin storage myopathies varies with the mutated residues, with the most common R1845W mutation presenting with distal muscle weakness (Tajsharghi et al., 2003), while the other mutations exhibit severe cardiac and respiratory symptoms (Goebel and Laing, 2009).

1.6 Mechanisms of Muscle Atrophy

Common to many of the myopathies listed above is the wasting, or atrophy, of muscle. Although this is a prevalent phenotype, molecular mechanisms behind muscle atrophy and cross talk between protein quality control systems are still being uncovered.

The pathway most heavily implicated in muscle atrophy is the PI3K/Akt axis (reviewed in Bilodeau et al., 2016; Bonaldo and Sandri, 2013). Control of Akt expression is critical for muscle homeostasis as Akt regulates both protein synthesis and protein turnover (Figure 12). High expression of Akt inhibits the transcription factor FOXO, which can induce Atrogin-1 and MuRF1 expression (Sandri et al., 2004; Stitt et al., 2004), and Akt simultaneously promotes protein synthesis through mTOR signalling (Stitt et al., 2004). The PI3K/Akt axis is initiated by insulin-like growth factors that are produced in skeletal muscle, especially after exercise

(Bonaldo and Sandri, 2013). However, many other factors can influence Akt expression, including direct inhibition by E3 ligases (Trim32; Cohen et al., 2009), glucocorticoids (Kukreti et al., 2013), and cross talk from other signalling pathways, such as NFkB signalling (Figure 12). NFkB signalling (reviewed in Peterson et al., 2011) can be initiated through an inflammatory or immune response which activates TNF-α, although NFkB activation independent of TNF-α appears to be the primary pathway responsible for denervation induced muscle atrophy (Cai et al., 2004; Mittal et al., 2010; Paul et al., 2010). Once activated, NFkB can initiate transcription of MuRF1 (Cai et al., 2004) and halt protein synthesis (Li et al., 2008) which leads to muscle atrophy.

ER stress and the Unfolded Protein Response (reviewed in Bohnert et al., 2018 are also critically involved in muscle atrophy, especially under starvation conditions (Paul et al., 2012), during sarcopenia (Deldicque, 2013), or during cachexia (Bohnert et al., 2016; Figure 12). The E3 ligase TRAF6 appears to be involved in activation of this system (Paul et al., 2012), and is also involved in NFkB and MAPK mediated muscle atrophy, providing additional evidence that cross-talk between various mechanisms controls muscle atrophy.

However, due to the tightly organized structure of the sarcomere, it is likely that additional sarcomere components sense and report sarcomere damage. The protein titin, which stretches one-half sarcomere from Z-disc to M-line has been associated with sarcomere monitoring functions (Gautel, 2011; Krüger and Linke, 2011) and is a good candidate for regulating proteostasis. Links between titin and protein turnover have been established with the C-terminal titin- kinase domain shown to be a binding site of the muscle specific ubiquitin ligases, MuRF1 (Mrosek et al., 2007), MuRF2 (Lange et al., 2005), as well as the protease calpain 3 (Beckmann and Spencer, 2008; Keira et al., 2003; Sorimachi et al., 1989). One role of

this titin-kinase domain is to regulate gene expression in a contraction dependent manner, with MuRF2 and Serum Response Factor (SRF) translocating to the nucleus during an absence of contractions and regulating expression of genes such as myomesin (Lange et al., 2005). However, as this domain also behaves as a reservoir for proteins involved in muscle maintenance, there is an obvious connection between titin and protein turnover that has yet to be fully elucidated.

1.6.1 Titin Proteostasis:

Although this thesis focuses primarily on myosin turnover, titin and its binding partners are implicated in protein quality control. Therefore, regulation of titin proteostasis is an important question in understanding sarcomere health and maintenance.

Due to its enormous size, protein quality control of titin must be an extensive process. However, titin turnover must occur as, with any other protein, wear and tear damage is inevitable. Fluorescence recovery after photobleaching experiments suggests that cardiomyocyte titin can be replaced 14 hours after injury, independent of protein synthesis, suggesting the large protein is quite mobile (da Silva Lopes et al., 2011). Although titin degradation products are prevalent in cardiac pathologies to the extent that they have been proposed as a biomarker of cardiac injury (Vassiliadis et al., 2012), how titin is removed and replaced into the mature sarcomere is still an unanswered question.

Matrix metalloproteinases (MMP) are best known for extracellular matrix remodelling (reviewed in Clark et al., 2008), but have also been implicated in turnover of troponin I (Wang et al., 2002) and myosin light chain 1 (Sawicki et al., 2005). More recently, MMP2 has been shown to localize to the N-terminus of titin, and increasing concentrations of MMP2 correlates with an increase in titin degradation products in a concentration dependent manner (Ali et al., 2010).

Furthermore, inhibition of MMP2s have shown to reduce titin degradation products in hearts subjected to ischemia reperfusion injury (Ali et al., 2010). As titin degradation products are associated with cardiac pathologies including ischemic reperfusion injury (Ali et al., 2010),ventricular hypertrophy (Warren et al., 2003), and acute myocardial infarction (Vassiliadis et al., 2012), MMP2 inhibitors could prove therapeutic in a number of cardiac diseases.

1.7 Zebrafish Muscle Mutants

While muscle diseases have previously been studied in cell culture, avian, and murine models, zebrafish has emerged as a model system for studying muscle development because of some unique advantages (reviewed in Lieschke and Currie, 2007). Zebrafish develop externally to the mother and develop transparently, which allows muscle phenotype screening to be done without surgery or sacrificing the animal. Cardiac and skeletal muscle develop rapidly in zebrafish, and these processes can continue in the absence of a functioning circulatory system. This has led to the identification of novel genes controlling the early development of striated muscle, which were not recoverable in other systems due to the mutations being fatal very early in development. The ability of zebrafish to complete skeletal muscle development in the absence of a functioning heart also provides a unique ability to study the skeletal muscle consequences of fatal myopathies, as other vertebrate model systems would die *in utero* from the consequences to cardiac muscle before the skeletal muscle had developed. Unlike mice, zebrafish have spatial segregation of slow and fast muscle tissue, which benefits studying diseases that are unique to fiber type. The development of genetic tools for zebrafish, their large brood sizes, and their relatively short generation time gives them the advantages of invertebrate systems, in a vertebrate model. Many zebrafish mutant lines exist thanks to forward genetic screens performed in the 1990s (Felsenfeld et al., 1990; Granato et al., 1996), and the genetic tractability of the

system allows creation of new mutations at will. Because many zebrafish muscle mutations recapitulate the phenotypes in human diseases (reviewed in Bassett and Currie, 2003), the ability to create zebrafish lines carrying mutations identical to human patients is becoming a powerful tool in personalized medicine. Zebrafish are excellent organisms in which to perform high throughput small molecule drug screens, which can identify novel pharmaceutical therapies as well as personalize treatment to the patient.

1.8 Hypothesis

From the above sections, it is obvious that protein quality control is imperative during both sarcomere assembly and maintenance to maintain muscle health. I chose to study skeletal muscle and hypothesize that these protein quality control and turnover mechanisms differ when damage occurs during sarcomere assembly or when it occurs during sarcomere maintenance, with emphasis on the protein myosin. In order to test this hypothesis, I needed to separate sarcomere assembly from sarcomere maintenance, which I did with the selection of specific zebrafish mutants for either process.

The zebrafish mutant *steif* encodes a loss of function mutation in the myosin chaperone, *unc45b* Etard et al., 2007 and is expected to be unable to fold and incorporate myosin into thick filaments. I propose that *steif* is a sarcomere assembly mutant, with respect to myosin thick filaments. The zebrafish *titin2* mutant, *herzschlag*, has been shown to assemble thick filaments *in vitro* (Myhre et al., 2014b), and therefore I propose that *herzschlag* is a sarcomere maintenance mutant, with respect to myosin thick filaments. Furthermore, I hypothesize that titin plays a role in protein quality control and protein turnover and expect the *herzschlag* mutation to affect protein turnover in the *herzschlag* mutant.

Table 1. Titin Mutations Causing Titinopathies

Titinopathy	OMIM	Inheritance Pattern	Region of Titin	Affected Exons	Affected Binding Partners	Affected Muscle Type	Mutation List
Arhythmogenic Right Ventricular Cardiomyopathy (ARVC)	#602087	Autosomal dominant	I-band; A-band; M-line	37 (missense); 97 (missense); 108 (missense); 298 (missense); 305 (missense); 313 (missense); 357 (missense); 362 (missense)		Cardiac	Taylor et al., 2011
Centronuclear Myopathy (CNM)	#255200	Autosomal Dominant	I-band; A band; M-line	41 (nonsense); 86 (deletion); 203 (insertion); 219 (missense); 298 (frameshift); 326 (frameshift, nonesense); 358 (frameshift, nonsense); 363 (frameshift)	Calpain-3; Nebulin	Skeletal	Ceyhan-Birsoy et al., 2013; Fattori et al., 2015
Dilated Cardiomyopathy (DCM)	#604145	Autosomal Dominant	Z-disc; I-band; A-band; M-line	3 (missense); 14 (missense); 18 (missense); 28 (frameshift); 49 (nonsense); 50 (missense); 119 (slpice variant)	T-Cap; telethonin; α-actinin	Cardiac	Chauveau et al., 2014; Herman et al., 2012

Titinopathy	OMIM	Inheritance Pattern	Region of Titin	Affected Exons	Affected Binding Partners	Affected Muscle Type	Mutation List
Dilated Cardiomyopathy (DCM)	#604145	Autosomal Dominant	Z-disc; I-band; A-band; M-line	220 (splice varient); 234 (splice varient); 236 (frameshift); 246 (nonsense); 265 (splice varient); 267 (frameshift); 268 (splice varient); 279 (nonsense); 281 (nonsense); 284 (splice varient); 292 (nonsense); 295 (nonsense); 296 (nonsense); 297 (frameshift); 300 (nonsense); 302 (splice varient); 303 (splice varient); 305 (nonsense); 307 (nonsense); 319 (splice varient); 320 (nonsense); 322 (splice varient); 327 (nonsense, frameshift, splice varient); 328 (nonsense); 329 (nonsense); 336 (frameshift);	T-Cap; telethonin; α-actinin	Cardiac	Chauveau et al., 2014; Herman et al., 2012

Titinopathy	OMIM	Inheritance Pattern	Region of Titin	Affected Exons	Affected Binding	Affected Muscle	Mutation List
Dilated Cardiomyopathy (DCM)	#604145	Autosomal Dominant	Z-disc; I-band; A-band; M-line	340 (nonsense, frameshift); 344 (nonsense, splice varient); 346 (frameshift); 348 (frameshift); 350 (splice varient); 353 (nonsense); 355 (nonsense); 356 (splice varient); 358 (nonsense); 359 (missense)	T-Cap; telethonin; α-actinin	Cardiac	Chauveau et al., 2014; Herman et al., 2012
Early-Onset Myopathy with Fatal Cardiomyopathy (EOMFC)	#611705	Autosomal recessive	M-line	358 (8bp deletion); 360 (1bp deletion)		Skeletal, Cardiac	Carmignac et al., 2007
Emery-Dreifuss-Like Muscular Dystrophy	Not available	Autosomal recessive	M-line	358 (frameshift); 360 (nonsense)	Calpain-3	Skeletal	De Cid et al., 2015
Hereditary Myopathy with Early-Onset Respiratory Failure (HMERF)	#603689	Autosomal dominant	A-band; M-line	343 (missense; frameshift); 359 (missense)		Skeletal	Tasca and Udd, 2018

Titinopathy	OMIM	Inheritance Pattern	Region of Titin	Affected Exons	Affected Binding	Affected Muscle	Mutation List
Hypertrophic Cardiomyopathy (HCM)	#613765	Autosomal Dominant	Z-disc; I-band;	14 (missense); 49 (missense); 103 (missense); \104 (missense)	α-actin; DRAL/FHL2; T–CARP	Cardiac	Chauveau et al., 2014
Limb-Girdle Muscular Dystrophy Type 2J (LGMD2J)	#608807	Autosomal dominant (homozygous)	See TMD	See TMD	See TMD	Skeletal, Cardiac	See TMD
Tibial Muscular Dystrophy (TMD)	#600334	Autosomal dominant (heterozygous)	A-band; M-line	304* (missense); 339* (missense); 362-363 (11bp change - FINmaj); 363 (missense, frameshift, nonsense, deletion)	Calpain-3	Skeletal	Chauveau et al., 2014; Savarese et al., 2016
Young or Early Adult Onset Recessive Distal Titinopathy	Not available	Autosomal recessive	A-band; M-line	318* (frameshift); 339* (missense); 352* (frameshift); 357* (frameshift); 361* (nonsense); 362* (missense, frameshift); 363 (frameshift)		Skeletal	Evilä et al., 2017; Savarese et al., 2016
*denotes mutations only identified as symptomatic when compound heterozygous with a second titin mutation							

Table 2. Myosin Mutations Causing Myosinopathies

Myosinopathy	OMIM	Inheritance Pattern	Myosin Isoform	Region of Myosin Affected	Mutation	Affected Muscle Type	Citations
Autosomal Dominant Myopathy with Congenital Joint Contractures, Ophthalmoplegia and Rimmed Vacuoles	#605637	Autosomal Dominant	MYH2	Head	Exon 19: E706L	Skeletal Fast Twitch Fibers	Martinsson et al., 2000
Autosomal-Dominant Multiple Pterygium Syndrome (DA8)	#178110	Autosomal Dominant	MYH3	Head, Rod	Exon 8: S243del; Exon 25: N1072dup, Q1075P	N/A	Chong et al., 2015
Digitotalar Dysmorphism (DA1)	#108120	Autosomal Dominant	MYH3	Head	Exon 6: G184A; Exon 7: A234T; Exon 14: F437I; Exon 15: K504N	Skeletal Fast Twitch Fibers	Alvarado et al., 2011; Beck et al., 2013
Dilated Cardiomyopathy (DCM)	#613426	Autosomal Dominant	MYH7	Head; Neck; Rod	Exon 5: G144V; Exon 6: G178R; Exon 7: G181R, V197I; Exon 8: R243H, Exon 12: M349V;	Cardiac	Walsh et al., 2017

Myosinopathy	OMIM	Inheritance Pattern	Myosin Isoform	Region of Myosin Affected	Mutation	Affected Muscle Type	Citations
Dilated Cardiomyopathy (DCM)	#613426	Autosomal Dominant	MYH7	Head; Neck; Rod	Exon 18: C672F; Exon 22: I814S, R819W, R819Q; Exon 23: E894D; Exon 26: E1095G; Exon 27: G1155E; Exon 30: S1335L, E1350K; Exon 31: R1434C; Exon 33: E1546D; Exon 34: E1548V; Exon 35: V1674L; Exon 37:A1777T; Exon 38: E1844K	Cardiac	Walsh et al., 2017
Familial Hypertrophic Cardiomyopathy (FHC)	#192600	Autosomal Dominant	MYH7	Head; Neck; Rod	Exon 3: Q27R, V39M; Exon 4: A100T; Exon 5: Y115H, Y115X, R143W, R143Q, T167Q; Exon 7: T188N, Q193R, A199T, R204H, K207Q, P211L; Exon 8: G214D, A226V, N232H, N232S, R237Q, D239N, R243H, F244C, K246I;	Cardiac	Richard et al., 2003; Walsh et al., 2017

Myosinopathy	OMIM	Inheritance Pattern	Myosin Isoform	Region of Myosin Affected	Mutation	Affected Muscle Type	Citations
Familial Hypertrophic Cardiomyopathy (FHC)	#192600	Autosomal Dominant	MYH7	Head; Neck; Rod	Exon 9: R249Q, G256E, I263T, I236M, T265S, L267V, K270R; Exon 10: L302M, P307H, D309N; Exon 11: V320M, S322T, A326P, E328G; Exon 12: M349V, K351E, A355T, A355S; Exon 13: E374V, A381D, D394E, R403G, R403L, R403Q, R403W, V406M, Y410D, V411I, A423V, L427M; Exon 14: A428V, V440M, R422C, T449S, T449I, R453C, R453H, I457T, D469N; Exon 15: I478N, N479S, E483K, M493V, M493L, M493I, M515T, P527T;	Cardiac	Richard et al., 2003; Walsh et al., 2017

Myosinopathy	OMIM	Inheritance Pattern	Myosin Isoform	Region of Myosin Affected	Mutation	Affected Muscle Type	Citations
Familial Hypertrophic Cardiomyopathy (FHC)	#192600	Autosomal Dominant	MYH7	Head; Neck; Rod	Exon 16: K542R, I585F, V586A, D587N, N602Y, V606M, T619I; Exon 18: R652G, M659I, R663S, R663H, R671C; Exon 19: M690T, R694H, I702V, P710H, G716R, R719W, R719Q, R723C, R723G, A728V; Exon 20: R723C, G733E, I726T, K740N, G741W, G741R, F758C, K766Q, G786R; Exon 21: G768R, D778E, R783H, I785V, R787C, R787H, A797P, A797T; Exon 22: V824A, F834Y, E846Q, K847E, M849T, A850D, M852T, R858C, R858H, A868P, R869H, R869L, R869G,	Cardiac	Richard et al., 2003; Walsh et al., 2017

Myosinopathy	OMIM	Inheritance Pattern	Myosin Isoform	Region of Myosin Affected	Mutation	Affected Muscle Type	Citations
Familial Hypertrophic Cardiomyopathy (FHC)	#192600	Autosomal Dominant	MYH7	Head; Neck; Rod	Exon 22: R870H, E875del, M877I, E883del; Exon 23: E894K, E894G, Q895K, D900E, A901P, E903Q, R904H, D906G, L908V, I913T, E924K, E924Q, L926V, E927K, E929K, E930K, E930del, L961V, E965G, H969P; Exon 24: K1016E, K1022E, Exon 25: R1045C, R1045L, M1046I, R1053Q, G1057D, E1070K, Exon 26: D1077E, E1097K, K1109E; Exon 27: R1114H, E1116K, E1125Q,L1135R, L1143R, V1159M, E1162K, K1165E, L1183Q, R1193H, D1198G, D1208N, V1213M, E1218Q; Exon 28: R1268P	Cardiac	Richard et al., 2003; Walsh et al., 2017

Myosinopathy	OMIM	Inheritance Pattern	Myosin Isoform	Region of Myosin Affected	Mutation	Affected Muscle Type	Citations
Familial Hypertrophic Cardiomyopathy (FHC)	#192600	Autosomal Dominant	MYH7	Head; Neck; Rod	Exon 29: Q1300L, A1325V; Exon 30: Q1334X, S1335L, R1344W, E1350K, E1356K, Q1370K, Y1375C, T1377M, E1377M, D1378H, A1379T, R1382W; Exon 21: R1420W, R1420Q, R1420L, E1426K, N1448S; Exon 32: E1473G; Exon 33: D1511A, E1546Q; Exon 34: E1554K, E1555G, S1596L, R1606H, Q1640R; Exon 35: D1652Y, R1662H, K1668E, R1677C, V1691M, E1696D, Q1704X, R1712Q; Exon 36: I1724M; Exon 37: M1764K, S1776G, A1777T, Q1794K, N1824S; Exon 39: T1854M, R1863W, E1883K;	Cardiac	Richard et al., 2003; Walsh et al., 2017

Myosinopathy	OMIM	Inheritance Pattern	Myosin Isoform	Region of Myosin Affected	Mutation	Affected Muscle Type	Citations
Familial Hypertrophic Cardiomyopathy (FHC)	#192600	Autosomal Dominant	MYH7	Head; Neck; Rod	Exon 40: R1897H, E1902Q, R1909W, E1914K, R1925C	Cardiac	Richard et al., 2003; Walsh et al., 2017
Freeman-Sheldon Syndrome (FSS; DA2A)	# 193700	Autosomal Dominant	MYH3	Head; Neck	Exon 5: T178I, T178M; Exon 14: E498G; Exon 15: Y583S; Exon 17: R672C, R672H; Exon 21: V825D	Skeletal Fast Twitch Fibers	Scala et al., 2018; Tajsharghi et al., 2008; Toydemir et al., 2006
Laing Distal Myopathy	#160500	Autosomal Dominant	MYH7	Head; Neck; Rod	Exon 14: T441M; Exon 16: V606M; Exon 21: R783P; Exon 32: R1500P; Exon 34: K1617del, L1591P, A1603P; Exon 35: A1663P, L1706P; Exon 36: K1729del; Exon 37: E1508del; K1784del; E1856K; E1801K;	Skeletal Slow Twitch Muscle; Some Cardiac Defects	Tajsharghi and Oldfors, 2013
Myosin Storage Myopathies (MSM)	#608358	Autosomal Dominant	MYH7	Rod	Exon 37: R1845W, K1738del; L1793P; Exon 38: E1883K; Exon 39: H1901L;	Skeletal Slow Twitch Muscle	Tajsharghi and Oldfors, 2013

Myosinopathy	OMIM	Inheritance Pattern	Myosin Isoform	Region of Myosin Affected	Mutation	Affected Muscle Type	Citations
Myosin Storage Myopathies (MSM)	#608358	Autosomal Dominant	MYH7	Rod	Exon 40: X1936W	Skeletal Slow Twitch Muscle	Tajsharghi and Oldfors, 2013
Sheldon-Hall Syndrome (DA2B)	#601680	Autosomal Dominant	MYH3	Head; Neck; Rod	Exon 5: T178I; Exon 7: A234T; Exon 8: G264A, S261F; Exon 9: S292C; Exon 10: F287V; Exon 11: E375K; Exon 12: L340Q; Exon 13: D462G; Exon 14: D517Y, F466C; Exon 20: G769V; Exon 21: K838E, L841del; Exon 22: F835del; Exon 33: D1622A, A1637V	Skeletal Fast Twitch Fibers	Beck et al., 2013; Tajsharghi et al., 2008; Toydemir et al., 2006
Spondylocarpotarsal Synostosis	#272460	Autosomal Recessive	MYH3	Head; Rod	Exon 11: T333R; Exon 30: L1344P	N/A	Carapito et al., 2016

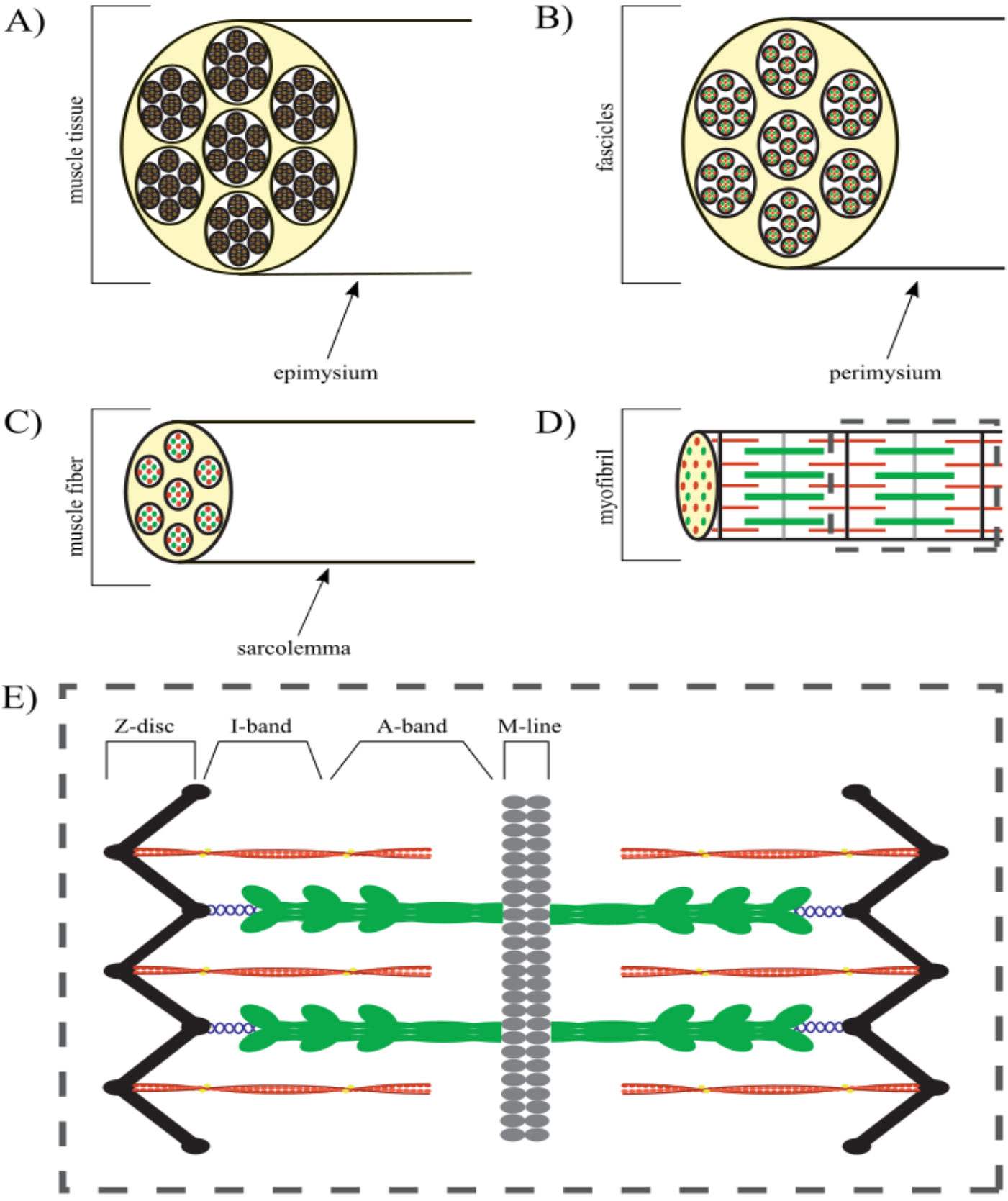
A)
muscle tissue
epimysium
B)
fascicles
perimysium
C)
muscle fiber
sarcolemma
D)
myofibril
E)
Z-disc
I-band
A-band
M-line

Figure 1: Simplified Diagram of Striated Muscle Organization.

(A) Striated muscle is composed of bundles of fascicles bound together by epimysium. Fascicles (B) are held together by an outer tissue layer called perimysium, and are composed of bundles of muscle fibres and endomysium. Muscle fibres (C) contain bundled myofibrils encased in a membrane called the sarcolemma. Myofibrils (D) can be broken down into repeating units known as the sarcomere (E), the basic unit of striated muscle. The sarcomere is composed of four regions: the Z-disc, I-band, A-band, and M-line.

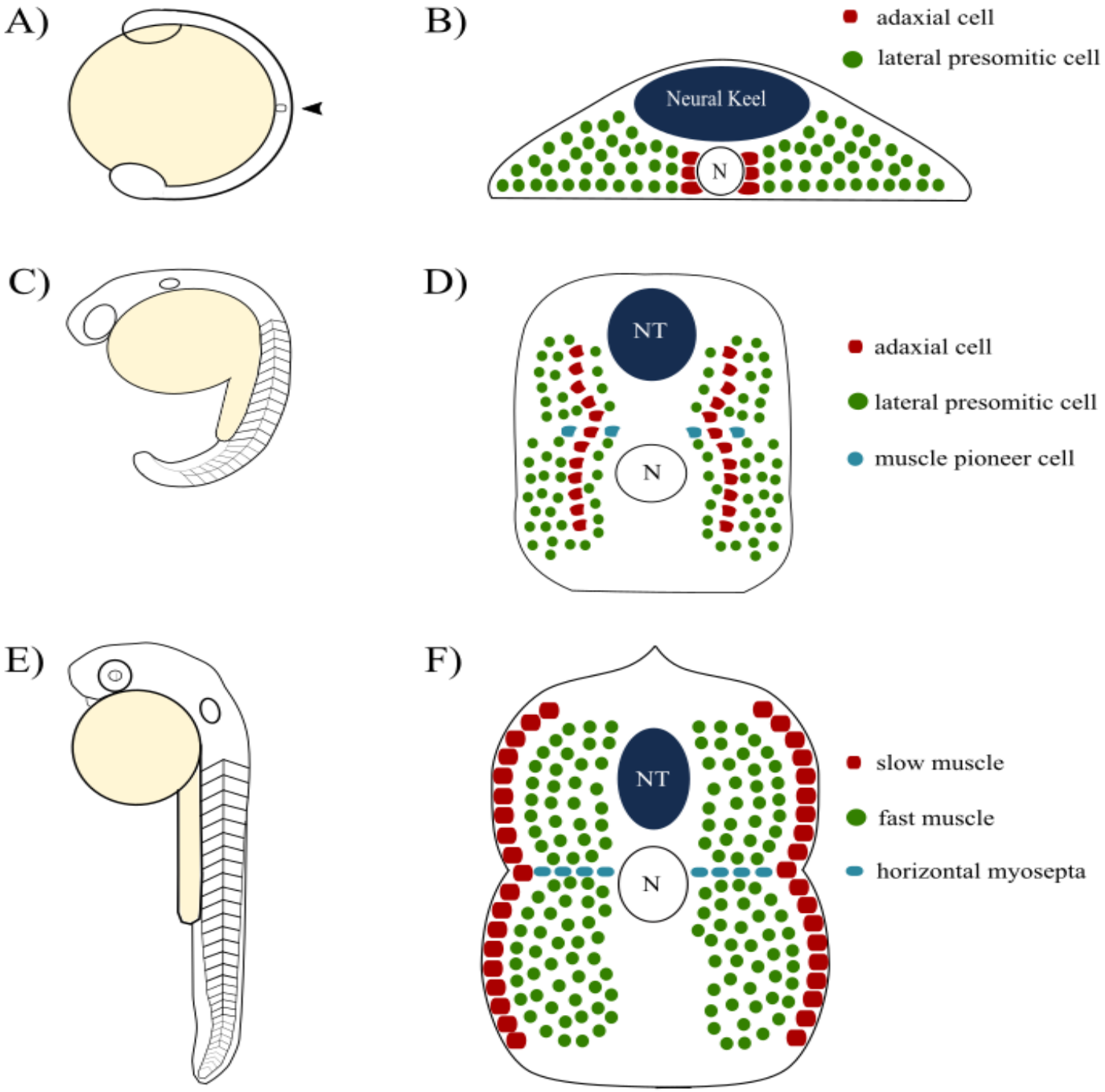
A)
B)
adaxial cell
lateral presomitic cell
Neural Keel
N
C)
D)
NT
N
adaxial cell
lateral presomitic cell
muscle pioneer cell
E)
F)
NT
N
slow muscle
fast muscle
horizontal myosepta

Figure 2: Zebrafish Skeletal Muscle Development.

(A) The first somite (arrowhead) develops at 10.3 hpf. B) Cross section of the somite shows adaxial cells adjacent to the notochord while lateral presomitic cells are more peripheral. C) At 19 hpf (20 somites), slow muscle sarcomeres have begun to develop (D) as the adaxial cells differentiate and migrate radially outwards, past the lateral presomitic cells. A subset of adaxial cells migrate to the midline of the zebrafish and are known as muscle pioneer cells. E) At 24 hpf (30 somites), muscle development is largely complete (F) with clear differentiation between fast and slow muscle and formation of the horizontal myosepta. N: notochord. NT: neural tube.

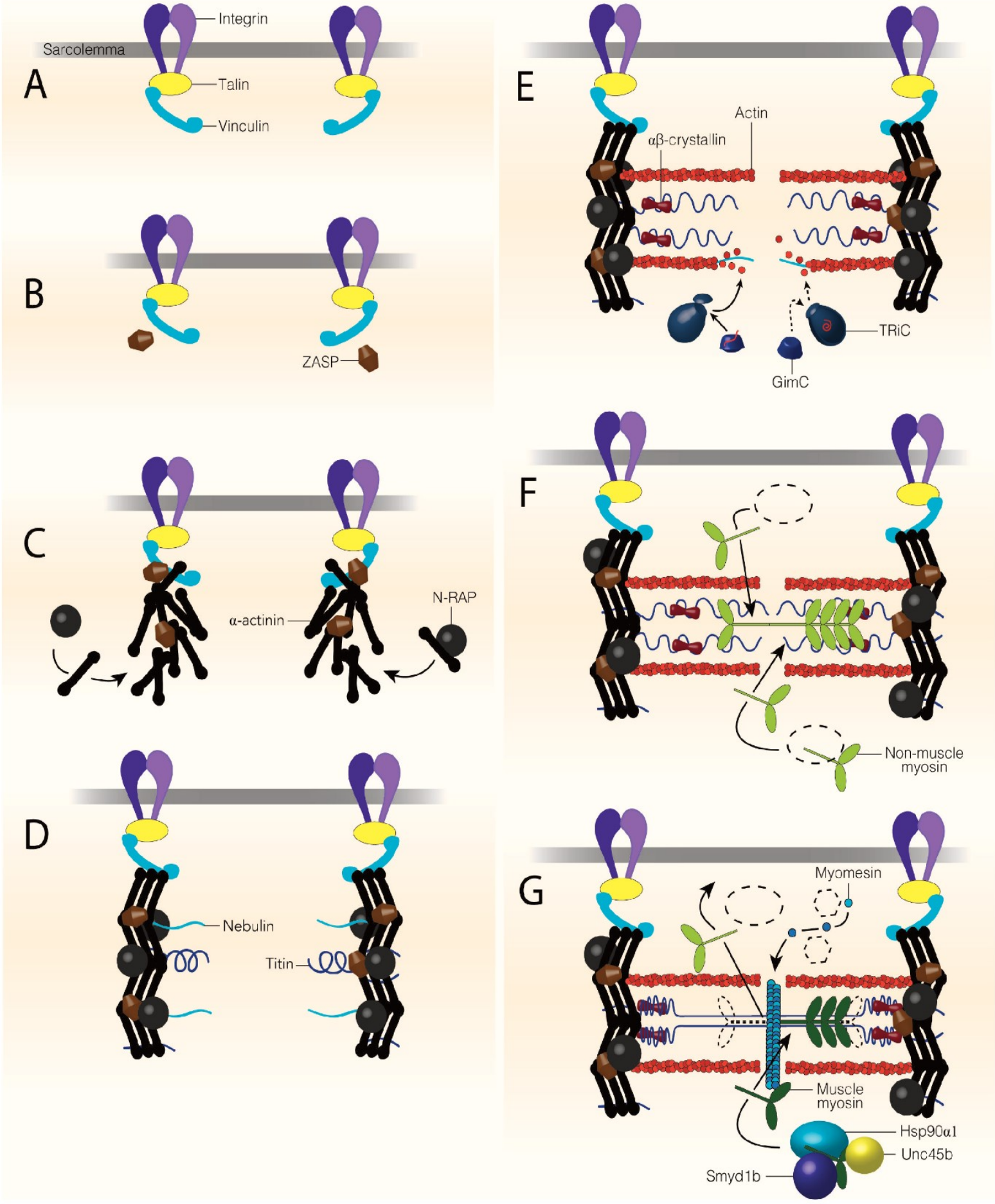
A
Integrin
Sarcolemma
Talin
Vinculin
B
ZASP
C
α-actinin
N-RAP
D
Nebulin
Titin
E
Actin
αβ-crystallin
TRiC
GimC
F
Non-muscle
myosin
G
Myomesin
Muscle
myosin
Hsp90α1
Unc45b
Smyd1b

Figure 3: The Premyofibril Model of Sarcomere Assembly.

Sarcomere assembly begins with the dimerization of integrins in the sarcolemma. Integrins recruit talin and viniculin to the sarcolemma to form protocostameres (A). ZASP localizes to the protocostameres to recruit α-actinin, which is folded and incorporated by its chaperone, N-RAP (B,C). The organization of α-actinin into Z-bodies likely recruits the protein giants nebulin and titin to the developing Z-discs (D). Nebulin and titin extend out from the Z-discs to the sarcomere center as Z-discs migrate away from one another to reach mature sarcomere length (D). GimC and TRiC fold actin before incorporating into thin filaments along the nebulin scaffold (E). Titin folding and integrity is maintained, in part, by αβ-crystallin during sarcomere assembly and muscle development (E). Non-muscle myosin II is proposed to aid in the alignment and formation of the thin filaments but the factors required for non-muscle myosin folding and incorporation are unknown ((F); dotted shape). In the final stages of sarcomere assembly, non-muscle myosin is replaced by muscle myosin II to form the thick filaments, which are assembled by Hsp90α1, Unc45b and Smyd1b (G). The M-line assembles either immediately after or simultaneously to thick filament formation and incorporates the tails of myosin heavy chains and the C-terminus of titin (G).

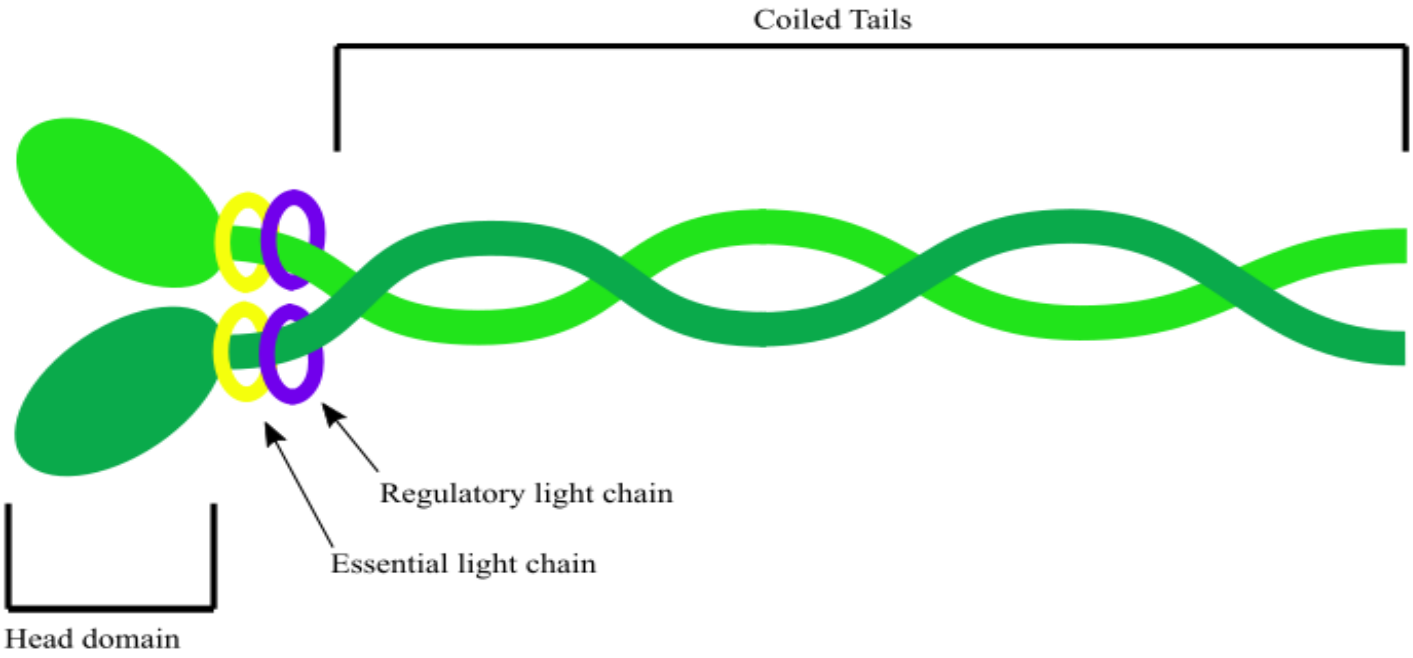
Coiled Tails
Regulatory light chain
Essential light chain
Head domain

Figure 4: Diagram of Type II Myosin.

Muscle myosin (Type II) is the primary component of the sarcomere A band. Each myosin is composed of two heavy chains (~200KDa) and two light chains (~20KDa). Myosin heavy chains have a globular head domain and an α helical tail domain, and two light chains associated with the neck region. Myosin heavy chains dimerize and the globular head domains bind and release from actin thin filaments to promote muscle contraction.

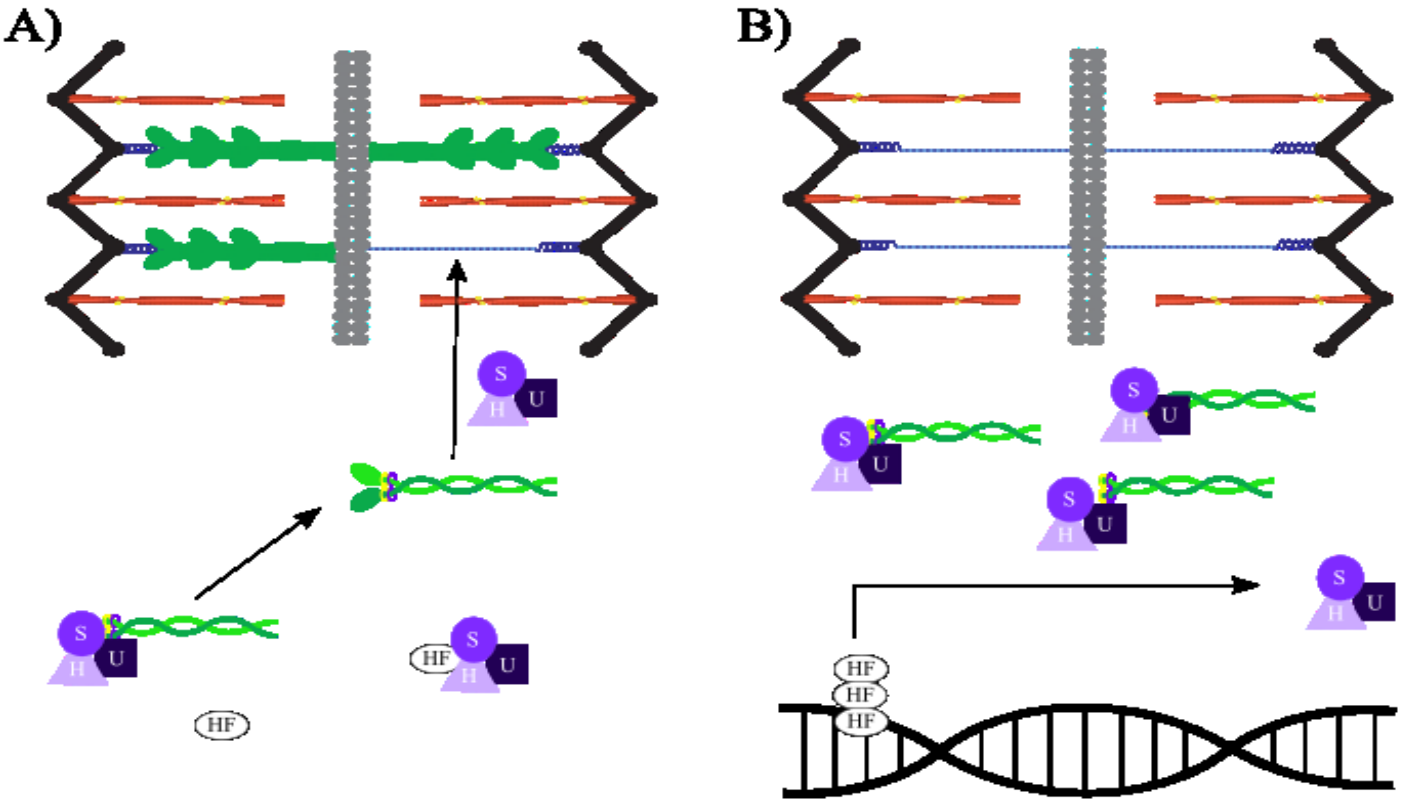
A)
B)
S
H
U
HF

Figure 5: The Misfolded Myosin Response.

A) During normal thick filament assembly, myosin is synthesized and the head domains folded by myosin chaperones Smyd1b (S), Hsp90α1 (H), and Unc45b (U). Properly folded myosin is then inserted into the sarcomere by some or all of these chaperones. B) Under conditions where the myosin head cannot be folded properly, myosin chaperones dissociate from the transcription factor HSF-1 (HF) and bind the head domain. As myosin is continuously synthesized, but not folded, more chaperones dissociate from HSF-1. HSF-1 trimerizes and translocates to the nucleus where it promotes the transcription of myosin chaperones in a phenomenon known as the misfolded myosin response (Etard *et al*., 2015).

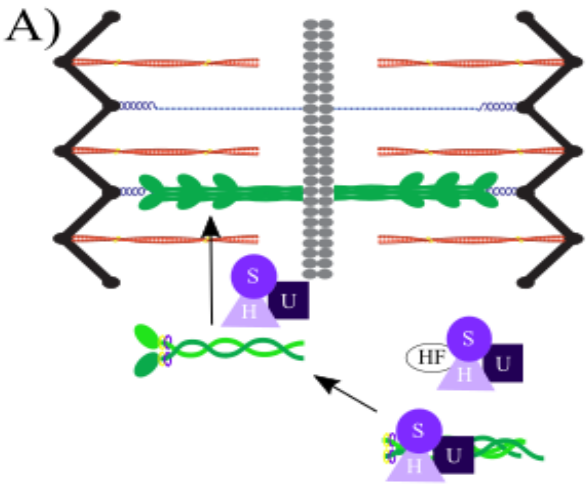
A)
S
H
U
HF
S
H
U
S
H
U

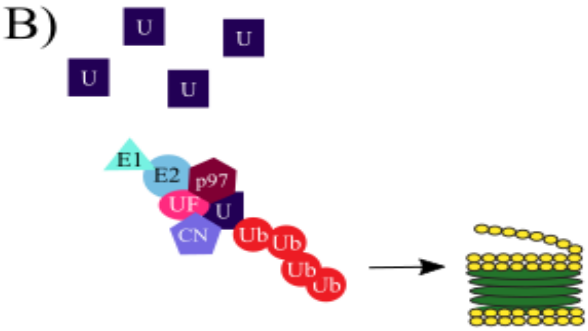
B)
U
U
U
E1
E2
p97
UF
U
CN
Ub
Ub
Ub
Ub

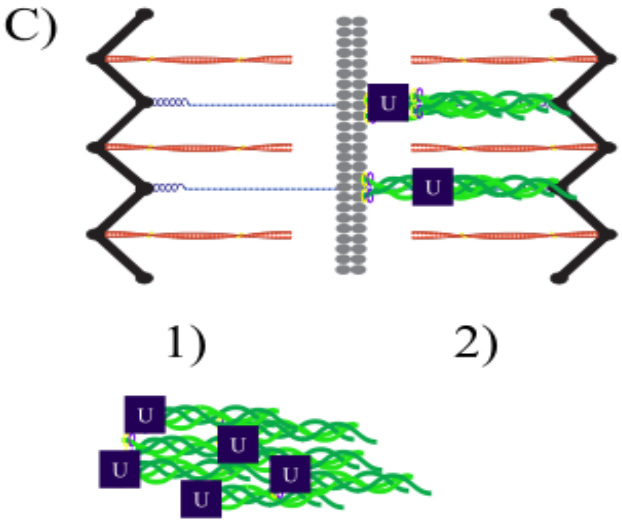
C)
U
U
1)
2)
U
U
U
U
U

Figure 6: Regulation of Unc45 Protein Levels.

A) During normal thick filament assembly, myosin is synthesized and the head domains folded by myosin chaperones Smyd1b (S), Hsp90α1 (H), and Unc45 (U). Properly folded myosin is then inserted into the sarcomere by some or all of these chaperones. (B) Regulation of Unc45 protein levels is controlled by binding of p97, UDF-2 (UF), and CHN-1 (CN) in a complex and recruitment of E1 and E2 enzymes. Excess Unc45 is polyubiquitinated and degraded by the 26S proteasome. (C) Overexpression of Unc45 is hypothesized to cause either (1) aggregation of unfolded myosin bound to Unc45, (2) Improperly assembled thick filaments, or a combination of both.

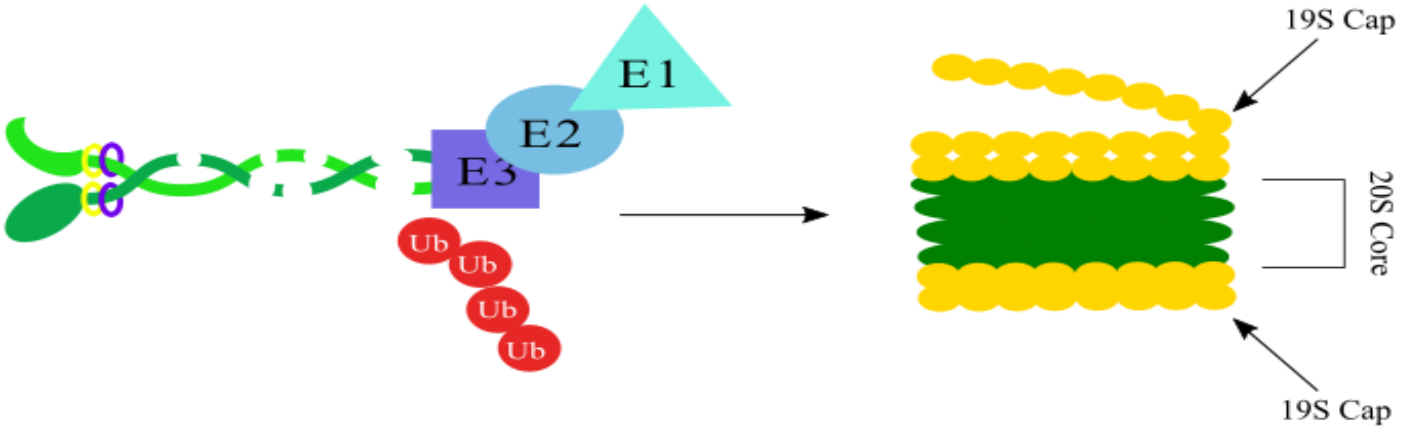
E1
E2
E3
Ub
Ub
Ub
Ub
19S Cap
20S Core
19S Cap

Figure 7: The Ubiquitin Proteasome System.

The ubiquitin proteasome system is composed of three main proteins, E1, E2, and E3, which respectfully, activates, transfers, and attaches the ubiquitin molecule (Ub) to the target protein. Once polyubiquitinated, the target protein is transferred to the 26S proteasome and degraded in an ATP dependent mechanism (Hershko and Ciechanover, 1998).

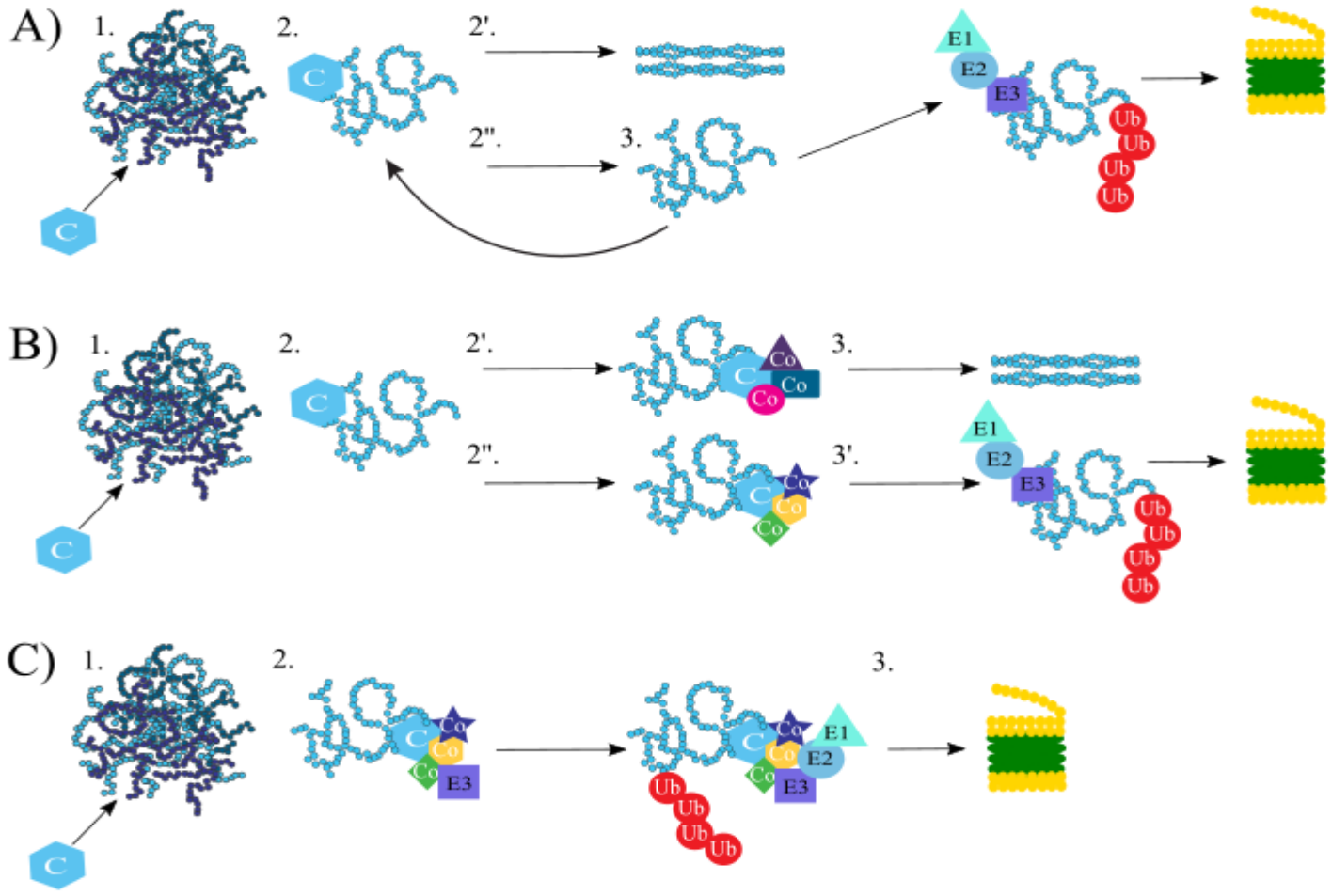
A)
1.
2.
2'.
2".
3.
C
E1
E2
E3
Ub
B)
1.
2.
2'.
2".
3.
3'.
C
Co
E1
E2
E3
Ub
C)
1.
2.
3.
C
Co
E1
E2
E3
Ub

Figure 8: Models of Chaperone and UPS Cooperation in Protein Quality Control.

A) Kinetic model of protein triage. 1. Protein aggregate forms and chaperones (C) are recruited. 2. Chaperones bind client protein and either succeed in refolding (2') or fail (2"). 3. Misfolded proteins either rebinds chaperone or is targeted for degradation by the UPS. B). Cofactor mediated model of protein turnover. 1. Protein aggregate forms and chaperones are recruited. 2. Chaperone binds client protein and co-chaperones (co) are recruited and either promotes refolding of client protein (2'-3) or degradation (2"-3'). C) Degradation complex model of protein triage. 1. Protein aggregate forms and chaperones are recruited. 2. Chaperone binds client protein and co-chaperones are recruited, transforming the chaperone complex into the E3 ligase complex. 3. E3 complex is targeted to the proteasome for degradation. Figure modified from (Carlisle et al., 2018).

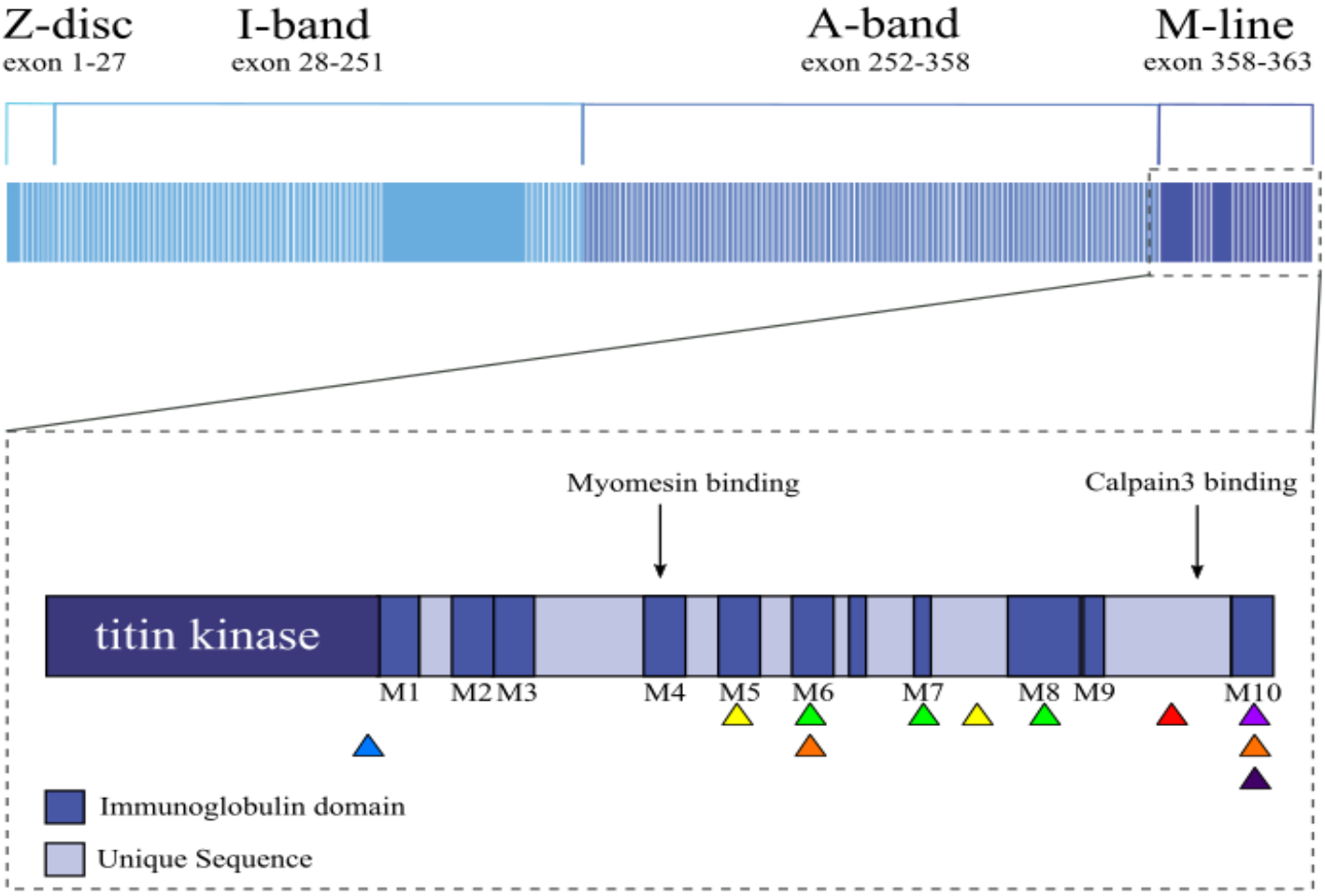

ARVC
EMOFC
HMERF
YEAORDT
CNM
EDLMD
TMD

Figure 9: M-line Titin Mutations Causing Titinopathies.

Schematic of the proposed human full length titin protein (Uniprot: Q8WZ42-1). Inset: M-line region of titin. Titinopathy-causing mutations are indicated by arrrowheads and colour coded to their respective titinopathy. ARVC (Arhythmogenic Right Ventricular Cardiomyopathy); CNM (Centronuclear Myopathy); EMOFC (Early-Onset Myopathy with Fatal Cardiomyopathy); EDLMD (Emery-Dreifuss Like Muscular Dystrophy); HMERF (Hereditary Myopathy with Early-Onset Respiratory Failure); TMD (Tibial Muscular Dystrophy); YEAORDT (Young or Early Adult Onset Recessive Distal Titinopathy).

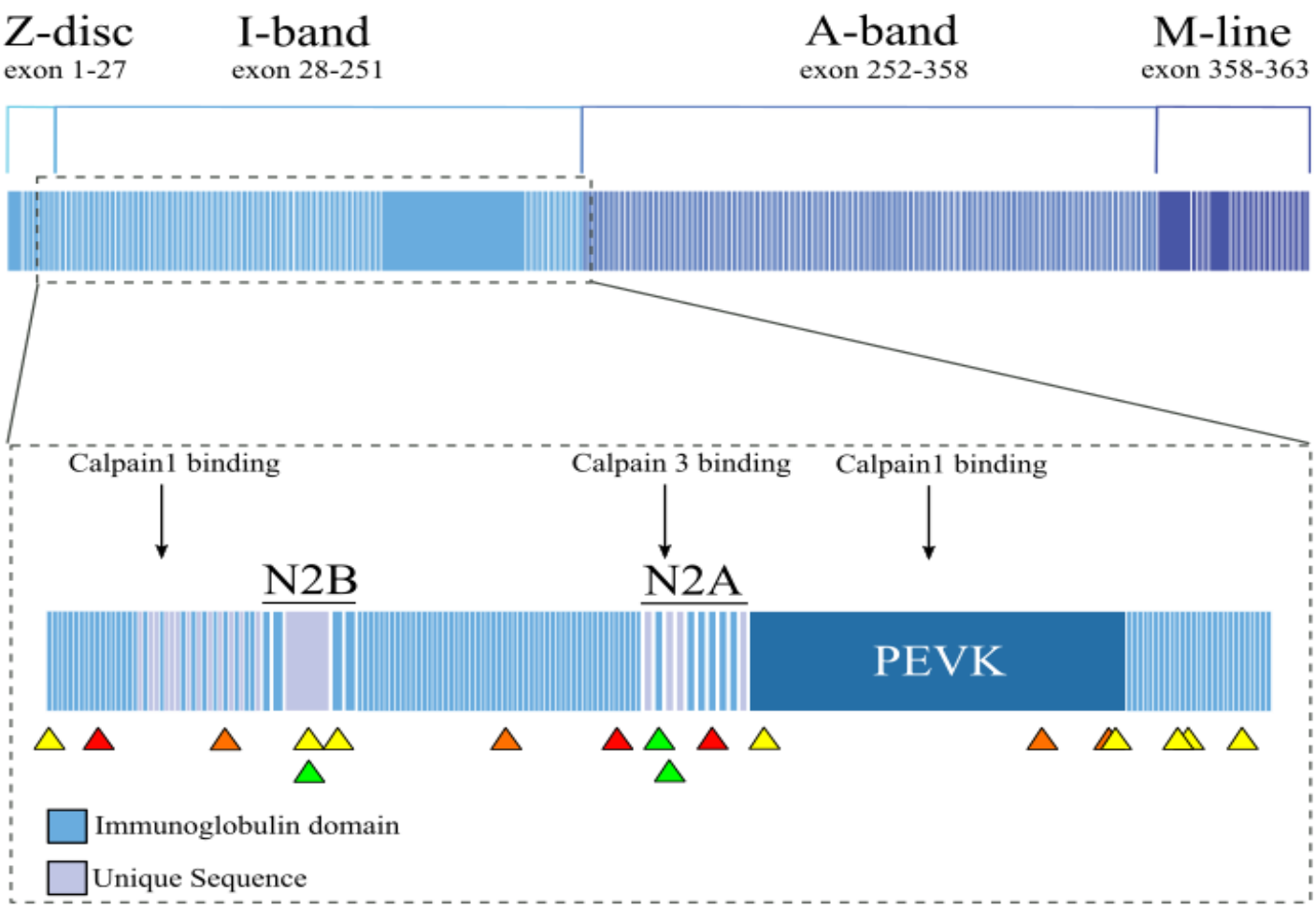
Z-disc
exon 1-27
I-band
exon 28-251
A-band
exon 252-358
M-line
exon 358-363
Calpain1 binding
Calpain 3 binding
Calpain1 binding
N2B
N2A
PEVK
Immunoglobulin domain
Unique Sequence


ARVC
DCM
CNM
HCM

Figure 10: I-band Titin Mutations Causing Titinopathies.

Schematic of the proposed human full length titin protein (Uniprot: Q8WZ42-1). Inset: I-band region of titin. Titinopathy causing mutations are indicated by arrrowheads and colour coded to their respective titinopathy. ARVC (Arhythmogenic Right Ventricular Cardiomyopathy); CNM (Centronuclear Myopathy); DCM (Dilated Cardiomyopathy); HCM (Hypertrophic Cardiomyopathy).

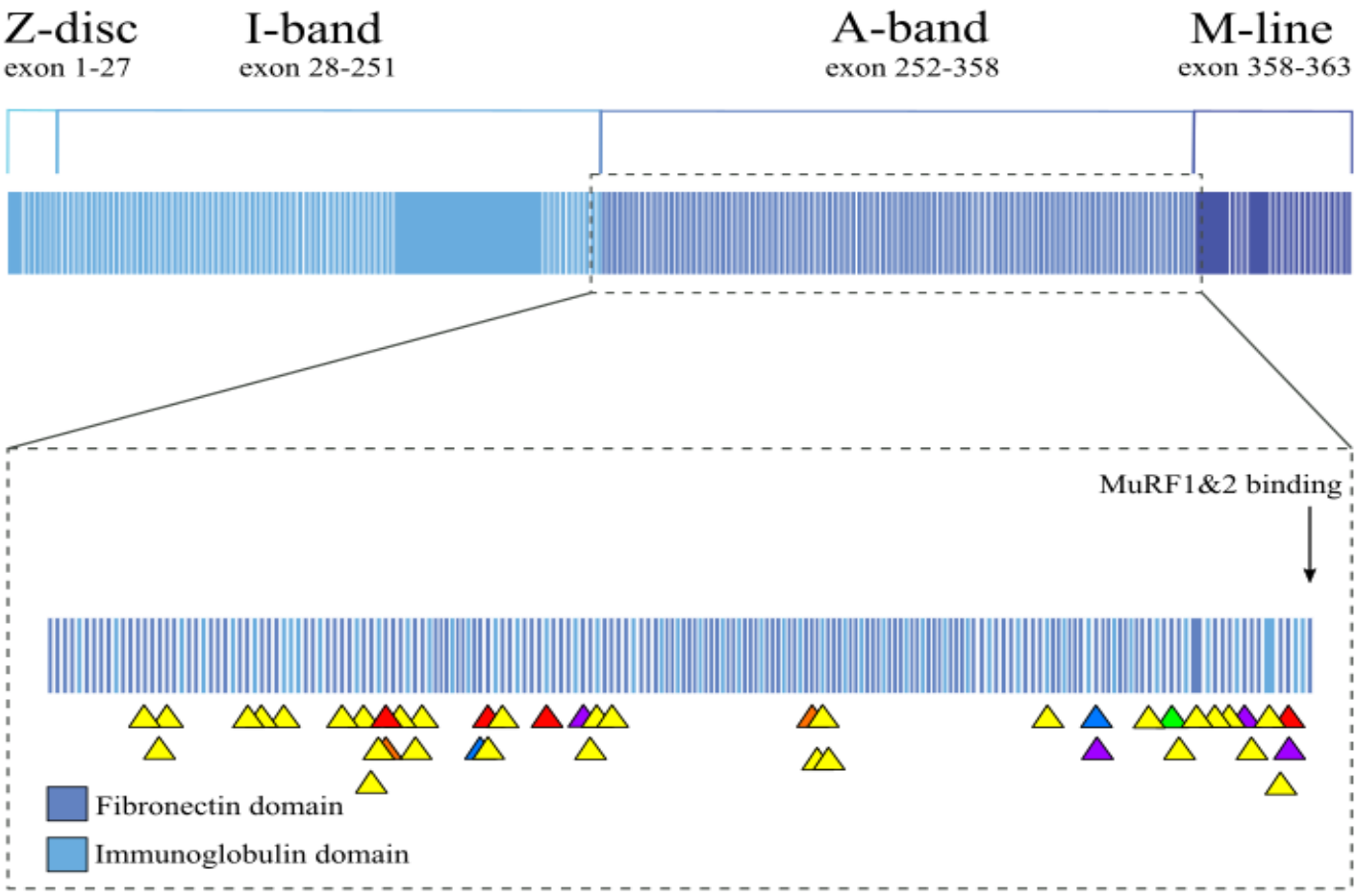
Z-disc
exon 1-27
I-band
exon 28-251
A-band
exon 252-358
M-line
exon 358-363
MuRF1&2 binding
Fibronectin domain
Immunoglobulin domain


ARVC
DCM
TMD
CNM
HMERF
YEAORDT

Figure 11: A-band Titin Mutations Causing Titinopathies.

Schematic of the proposed human full length titin protein (Uniprot: Q8WZ42-1). Inset: A-band region of titin. Titinopathy causing mutations are indicated by arrrowheads and colour coded to their respective titinopathy. ARVC (Arhythmogenic Right Ventricular Cardiomyopathy); CNM (Centronuclear Myopathy); DCM (Dilated Cardiomyopathy); HMERF (Hereditary Myopathy with Early-Onset Respiratory Failure); TMD (Tibial Muscular Dystrophy); YEAORDT (Young or Early Adult Onset Recessive Distal Titinopathy).

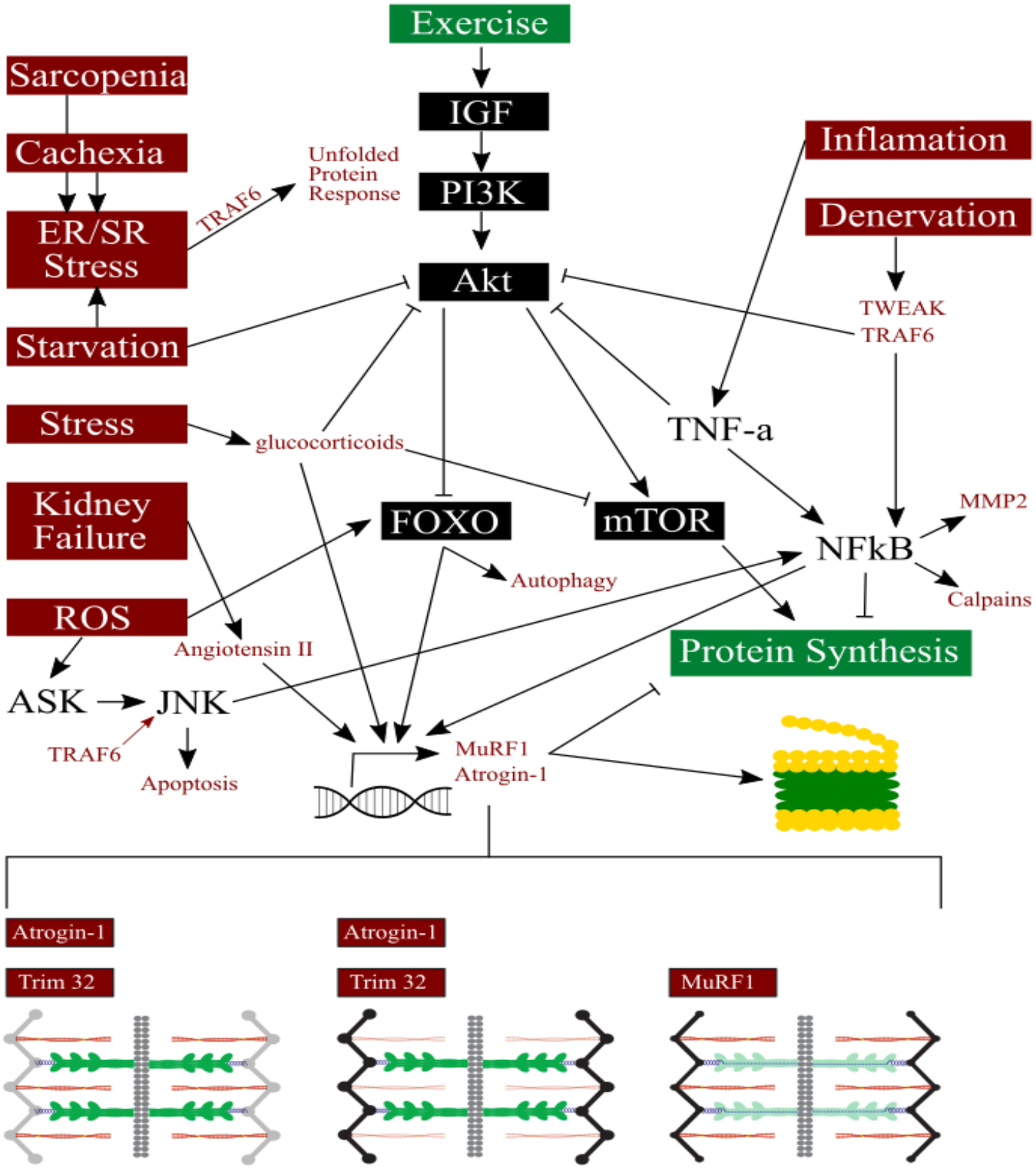
Exercise
IGF
PI3K
Akt
Sarcopenia
Cachexia
ER/SR Stress
TRAF6
Unfolded Protein Response
Starvation
Stress
glucocorticoids
Kidney Failure
ROS
Angiotensin II
ASK
JNK
TRAF6
Apoptosis
FOXO
mTOR
Autophagy
Inflamation
Denervation
TWEAK
TRAF6
TNF-a
NFkB
MMP2
Calpains
Protein Synthesis
MuRF1
Atrogin-1
Atrogin-1
Trim 32
Atrogin-1
Trim 32
MuRF1

Figure 12: Mechanisms of Muscle Atrophy.

The PI3K/Akt axis (black boxes) is heavily involved in muscle homeostasis and can regulate protein synthesis as well as protein degradation. External factors can push this network towards protein degradation (red boxes), or protein synthesis (green boxes). NFkB signalling and MAPK signalling are also implicated in muscle atrophy (black text, no boxes). Factors that promote muscle atrophy result in the upregulation of E3 ligases, either indirectly through FOXO, or directly by binding response elements on E3 ligase promoters. E3 ligases target different areas of the sarcomere (bracket) with Trim32 and Atrogin-1 being primarily responsible for degradation of the Z-disc and I-band, while MuRF-1 is implicated in thick filament degradation. No M-line targeted E3 ligase has yet been identified.

CHAPTER 2. MATERIALS AND METHODS:

2.1 Zebrafish Lines and Husbandry

2.1.1 Line Maintenance

All zebrafish were kept at 28°C on a 14/10 hr light/dark cycle in the aquatics facility. in a recycled water circuit. Larval zebrafish (1-6 weeks old) were fed Gemma Micro 75 powder (Skretting Canada) twice a day, while juvenile zebrafish (6-12 weeks old) were fed Premium Brine Shrimp (95% hatch out rate, Great Salt Lake Artemia). Adult zebrafish (greater than 12 weeks old) were fed a mixture of trout chow and Zeigler diet, followed by Brine Shrimp (85% hatch out rate, Great Salt Lake Artemia).

Zebrafish were bred once every week and the resulting embryos were collected and switched to embryo media (15 mM NaCl, 50 μM KCl, 1.3 mM $CaCl_2$, 150 μM KH_2PO_4, 50 μM Na_2HPO_4, 1 mM $MgSO_4$ and 0.71 mM $NaHCO_3$; Westerfield, 2007). Embryos were raised at 28°C until a maximum of 7 days post fertilization (dpf). All staging was done according to the zebrafish book (Westerfield, 2007). All protocols were carried out following the guidelines stated by the Canadian Council for Animal Care and the University of Alberta.

2.1.2 Zebrafish Strains

Four mutant strains were used in experiments: *still heart*, *herzschlag*, *steif*, and *jam*. The Nusslein-Volhard lab generated and identified the *herzschlag* (*hel*^{tg278}), *still heart* (*sth*^{tm123a}), and *jam* (*jam*^{tr254a}) mutations in the TB (Tubingen) background through an N-ethyl-N-nitrosourea mutagenesis screen (Chen et al., 1996; Granato et al., 1996). These strains were obtained from the Max-Planck-Institut für Entwicklungsbiologie (Tübingen, Germany), and maintained as heterozygotes by outcrossing them to our AB strain (obtained from the Zebrafish International

Resource Center (Eugene, OR). *Steif* (*stf*) was a generous gift from Dr. Uwe Strahle (Karlsruhe, Germany), and was also outcrossed to AB to be maintained as a heterozygous line.

Still heart was identified as a mutation in *smyd1b* by complementation crossing to another *smyd1b* mutant, *flatline* (Just et al., 2011a; Prill et al., 2015). *Steif* encodes a truncation in *unc45b*, where a C-A point mutation results in a premature stop codon (Etard et al., 2007). The *herzschlag* mutation was identified previously by our lab in the gene *titin2* (Myhre et al., 2014b). Currently the cognate gene of *jam* is unidentified. Fish designated as 'Wild-type' in figures were either of the AB background or phenotypically wild-type siblings of heterozygous line in-crosses, as stated in figure legends. Embyros designated as 'mix brood' were products of a heterozygous in-cross where the entire clutch was taken and analyzed at a timepoint before homozygous mutants could be phenotypically identified.

2.2 Whole Mount *in situ* Hybridization

2.2.1 RNA Probe Synthesis

3' untranslated region sequences of candidate gene mRNA were obtained and primers designed (see Table 3) to amplify fragments of 500 bp. Templates for amplification were cDNA of various stages (between 19 hpf and 48 hpf), selected based on when the gene was expected to be most strongly expressed. Once amplified, PCR products were size-separated via gel epectrophoresis on a 0.8% agarose gel with ethidium bromide. Gels were imaged under ultraviolet light and either a band was extracted, or a PCR cleanup (RBC Bioscience) was used and the product (2 µL) was cloned into a pGEM-T plasmid (Promega: A1360).

Frozen 150 µL aliquots of DH5α competent bacterial cells were thawed on ice for 20 minutes, then 50 µL of competent cells were mixed with plasmid ligations and left for another 20

minutes on ice. Competent cell/plasmid mixtures were heat shocked at 42°C for 45 seconds, rested on ice for 2 minutes, and allowed to recover in 100 µL of prewarmed LB at 37°C for a minimum of 1 hour. The entire transformation was plated on LB+Ampicillin (100 µg/mL) or LB+Carbenicillin (100 µg/mL) and incubated at 37°C overnight. Three colonies were randomly selected for inoculation in 5 mL LB+Ampicilin or LB+Carbenicillin and left in a 37°C agitator overnight. Plasmids were recovered by minipreps (Qiagen Miniprep Kit) and sent for sequencing at the Molecular Biology Service Unit at the University of Alberta.

Using BLAST, I identified plasmids containing sequences that matched the gene of interest. 5 µg of those plasmids were digested with restriction enzymes Nco1 or Nde1, depending on insert orientation, for 2 hours at 37°C. Subsets of the digests were electrophoresed on a 0.8% gel, alongside an undigested control, to ensure they were digested. If the plasmid had been incompletely digested, the digested band was extracted using a gel extraction kit (Qiagen). If the plasmid was completely digested the remainder that was not run on a gel was purified by phenol/chloroform precipitation. For phenol/chloroform precipitations, 160 µL Diethyl pyrocarbonate and 1 volume of phenol was added to the digest and the sample was vortexed for 20 seconds. Digests were centrifuged (12 000 RPM) for 5 minutes at room temperature and the aqueous layer was transferred to a new centrifuge tube. 1 volume of chloroform was added to the aqueous layer and vortex for 20 seconds before centrifuging (12 000 RPM) for 5 minutes at room temperature. The aqueous layer was transferred to a new tube and 2 volumes of 95% ethanol was added, tubes were inverted, and allowed to precipitate on ice for 30 minutes. A final 10 minute centrifuge (12 000 RPM) at room temperature pelleted DNA, ethanol was removed, and pellets were allowed to air dry for 5 minutes before being resuspended in 30 µL Diethyl pyrocarbonate.

Both sense and antisense RNA probes were synthesized from 10 µL of the purified digests using T7 RNA Polymerase (Ambion) and digoxigenin RNA Labelling Mix (Roche). Mixtures were incubated at 37°C for 2 hours. 30 µL of 7.5 M LiCl (Thermo Fisher Scientific) was added to the mixtures and left overnight at -20°C for at least overnight. Probes were centrifuged (12 000 RPM) at 4°C for 15 minutes and supernatant removed. 50 µL 70% ethanol/Diethyl pyrocarbonate was added to pellets before centrifuging for another 15 minutes at 4°C (12 000 RPM). Supernatant was removed and pellets left to air dry for 2 minutes (on ice) before resuspending in 20 µL Diethyl pyrocarbonate. Probes were measured for purity and concentration by spectrophotometry (NanoDrop) and diluted 2 ng/µL in hyb (25mL 50% formamide, 12.5 mL 20X SSC, 50 µL of 50 mg/mL heparin, 250 µL Tween-20, and MilliQ) and stored at -20°C until used.

2.3.2 Hybridization Protocol

Embryos were collected, staged, and fixed in 4% paraformaldehyde/MilliQ overnight at 4°C. Embryos underwent 5x 5 minute washes in PBST (Phosphate buffered saline + 2% Tween-20) and dechorionated manually after the second wash. 1 µl/mL of Proteinase K (New England Biolabs, 800 U/mL) was used to permeabilize tissue at room temperature for 45 minutes (5 dpf), 15 minutes (24 hpf or older), 5 minutes (18 hpf or younger), or 3 minutes (for any heart probes). After permeabilization, embryos were re-fixed in 4% PFA at room temperature for at least 40 minutes. Fixative was removed and embryos were washed 5x in PBST for 5 minutes before prewarmed prehyb (25 mL 50% formamide, 12.5 mL 20X SSC, 50 µL of 50 mg/mL heparin, 500 µL of 50 mg/mL tRNA, 250 µL Tween-20, and MilliQ) at 65°C for 1 hour. Prehyb was removed and prewarmed probe was placed on the embryos and left at 65°C overnight.

Probes were removed (and kept for reuse at -20°C) and embryos underwent a series of prewarmed stringency washes at 65°C in the order: 5 minutes in 66% hyb/33% 2X SSC, 5 minutes in 33% hyb/66% 2X SSC, 5 minutes in 2X SSC, 20 minutes in 0.2X SSC+0.1% Tween-20, and two 20 minute washes in 0.1X SSC+0.1% Tween-20. At room temperature, embryos were then washed with 66% 0.2X SSC/33% PBST for 5 minutes, 66% PBST/33% 0.2X SSC for 5 minutes, and finally 5 minutes in PBST. Embryos were then incubated in blocking solution (2% sheep serum, 2 mg/mL Bovine Serum Albumin, in PBST) for a minimum of 1 hour at room temperature. For heart *in situ* hybridizations, blocking was done on a rocker. After blocking, embryos were incubated in blocking solution + 1/5000 anti-digoxigenin-AP antibody (Roche: 11093274910) for 2 hours on a rocker at room temperature (heart *in situ* hybridizations) or overnight at 4°C

After incubation in antibody, embryos underwent 5-7x 15 minute PBST washes (depending on whether they were incubated for 2 hours or overnight) and then 4x 5 minute washes in colouration buffer (5mL 1M Tris-HCl pH 9, 2.5mL 1M $MgCl_2$, 1mL 5M NaCl, 250uL Tween-20, and MilliQ up to 50mL). 10mL of colouration buffer was kept aside and (with the lights off) 45uL of nitro-blue tetrazolium (NBT) and 35uL 5-bromo-4-chloro-3-indolyl phosphate (BCIP) were added to make colouration agent. Embryos were incubated in the dark in colouration agent at 28°C for 45 minutes and checked for staining. This was repeated twice. If no staining had occurred by 90 minutes, embryos were placed at 4°C overnight in colouration agent. Staining was stopped by 5 rapid PBST washes, followed by 3x 10 minute PBST washes and stored in PBST at 4°C until imaged. Embryos were imaged using the program Q-Capture on a Zeiss Axioskop mot *plus* microscope (QImaging, Retiga ex*i* camera) within 1-2 weeks of the staining protocol.

2.3 Quantitative Polymerase Chain Reaction

2.3.1 RNA Extraction

Embryos were collected, staged, and flash frozen in liquid nitrogen and stored at -80°C until they underwent RNA extraction. 500 µL of TRIzol (Invitrogen) was added to flash frozen embryos and they were homogenized with an RNAse-free pestle, on ice, for a strict maximum of 5 minutes. After homogenization, 300 µL chloroform was added and tubes were inverted 3-6 times, and centrifuged at 4°C for 10 minutes (12 000 RPM). The aqueous phase was transferred to a new RNAse-free microcentrifuge tube, on ice, and 1 volume of chloroform was added. Tubes were inverted 3-6 times and centrifuged at 4°C for 10 minutes (12 000 RPM). The aqueous phase was transferred to a new RNAse-free microcentrifuge tube, on ice, and 2 volumes of ice cold RNAse free 95% ethanol was added. Tubes were inverted twice, and left to precipitate on ice for 30 minutes. Tubes were then centrifuged at 4°C for 10 minutes (12 000 RPM), ethanol was removed, and pellets left to air dry, on ice, for 5 minutes. Pellets were rehydrated in 89 µL diethyl pyrocarbonate, 10 µL DNAse buffer (Ambion), and 1 µL DNAse (Ambion) and left at 37°C for 30 minutes before being placed back on ice. Spectrophotometry (NanoDrop) was used to measure samples for purity (only those with a 260/280 absorbance ratio between 1.9-2.0 were kept) and concentration and then diluted to 100 ng/µL. Extracted RNA was stored at -20°C.

2.3.2 Complimentary DNA Synthesis

RNA standardized to 100 ng/µL was used to make cDNA using qScript cDNA SuperMix (Quanta Biosciences). Each cDNA reaction was set up on ice, and contained 1 µg RNA, 6 µl Diethyl pyrocarbonate, and 4 µL qScript. Reactions were run through a thermocycler (5 minutes

at 25°C, 30 minutes at 42°C, and 5 minutes at 85°C; Veriti 96-Well Thermal Cycler Thermo Fisher Scientific) and stored at 4°C.

2.3.3 qPCR Protocol

qPCR primers (Table 4) were designed to be approximately 100bp in length and spanning an exon-exon boundary near the 3' end of the gene sequence. Primers were rehydrated in MilliQ to 100 µM and then diluted in MilliQ (8 µL forward primer, 8 µL reverse primer, 484 µL MilliQ) to generate working stocks. qPCR master mix was generated using 2:1 SYBR buffer mix (Molecular Biology Services Unit, University of Alberta) to primer working stock. Primers were tested by running a standard curve of known cDNA dilutions and were required to have slope values between -3.1 and -3.6 in order to ensure that exponential amplification of one target was occurring. Only primers that passed the standard curve were used for examination of relative expression.

To determine relative expression, 7.5 µL of master mix and 2.5 µL of cDNA (various dilutions, see Table 4) were used to compare expression of genes of interest in mutant fish to wild-type (AB) fish. The housekeeping gene, *ef1a*, was used to normalize expression using the $2^{-\Delta\Delta CT}$ method (Schmittgen and Livak, 2008). A sample calculation can be found in Appendix 7.1. qPCR plates were run in an EcoTM Real-Time PCR System (Illumina) using the EcoTM and Eco-Study Software (Illumina). Results were analyzed in Microsoft Excel and ΔΔCT values with error bars representing standard deviation were graphed using GraphPad.

2.4 Whole Embryo Immunofluorescence

Embryos were staged morphologically, manually dechorionated, collected, and fixed in 4% paraformaldehyde overnight at 4°C, then moved to PBST for 3 days at 4°C. Embryos were

washed 4x with PBST at room temperature before permeabilization in chilled acetone at -20°C for 1 hour (24 hpf, 48 hpf, and 5 dpf). Embryos younger than 24 hpf were not permeabilized in chilled acetone. After 3 more PBST washes (room temperature), embryos were left in blocking solution (PBST+5% goat serum) on a rotator at room temperature for 1 hour before incubation in a 3% goat serum/PBST+10% primary antibody solution (**F59**, DSHB, Iowa, USA; **T11**, T9030, Sigma, **T12** (this monoclonal antibody was a generous gift of Dr. Elizabeth Ehler, London, UK; **M8M9** (a generous gift from Dr. Siegfried Labeit), **F310**, DSHB, Iowa, USA; **mMaC myomesin B4**, DSHB, Iowa, USA) overnight at 4°C. After four PBST washes (room temperature), embryos were moved to a 4% goat serum/PBST solution containing 5% secondary antibody (AlexaFluora 488 goat anti mouse, Invitrogen) and 1% phalloidin (Alexa 568, Thermo Fischer Scientific). Embryos were left overnight at 4°C in this solution. Embryos were washed 3 more times in PBST (room temperature) to remove residual secondary before imaging and processing as previously described (Myhre et al., 2014b) by wet-mounting whole embryos and imaging on a confocal microscope (Nikon Eclipse 80i). Images were processed using NIS Elements and Adobe Photoshop. Experiments were conducted at least 3 times with a minimum of 15 embryos per replicate.

2.5 Transmission Electron Microscopy

Transmission electron microscopy was performed at the Advanced Microscopy Unit at the University of Alberta. Embryos were staged, manually dechorionated, and 3-5 were fixed in electron microscopy fixative (2.5% glutaraldehyde, 2% paraformaldehyde, in 0.1M phosphate buffer, pH 7.2-7.4) for at least 2 days at room temperature. Fixed embryos underwent three 10 minute washes in 0.1M phosphate buffer (ph 7.2-7.4) before ‘re-fixing’ in 1% osmium tetroxide for 1 hour. Embryos underwent another three 10 minute washes in phosphate buffer before they

undergoing a series of dehydration washes (15 minutes each at room temperature) in increasing concentrations of ethanol (15% Ethanol/water, 70% Ethanol/water, 90% Ethanol/water, and three 100% Ethanol washes). After dehydration, embryos were washed in 50% Ethanol/Spur's resin (Spurr's low viscosity resin) for 2 hours on a rocker before changing to pure resin overnight. Early the next morning, embryos were moved to fresh Spur's resin, and again in the late morning. Embryos were then embedded in moulds and baked at 70°C overnight. Embedded embryos were sectioned using an ultramicrotome (Reichert Jung Ultracut E) to 80-100nm and mounted on grids (Electron Microscopy Sciences, Copper, 300 mesh). Grids were stained for 20 minutes in the dark in 4% uranyl acetate/distilled water (room temperature), rinsed in distilled water, and allowed to dry for 5 minutes. Grids were then stained for 7 minutes in lead citrate in a CO_2 free chamber at room temperature. Grids were rinsed again in distilled water, allowed to dry for 5 minutes, and then imaged (TEM Phillips-FEI Morgagni 268 operating at 80kV). Images were captured using a Gatan Orius CCD Camera and Gatan DigitalMicrograph ™ Ver. 1.81.78 software.

2.6 Hematoxilin and Eosin Staining

Hematoxylin and eosin staining was performed at the Advanced Microscopy Unit at the University of Alberta. Embryos were staged, manually dechorionated, and 3-5 were fixed in electron microscopy fixative for at least overnight at room temperature. Embryos were aligned side-by-side in a mould and embedded in a 60°C 2% agar/distilled water solution. Once embryos were aligned satisfactorily, the gel was allowed to cool and solidify. Moulds were trimmed and put in neutral buffered formalin fixative overnight, then transferred to 50% ethanol for 2 hours before processing at room temperature in a Leica Tissue Processor 1020 (Program: 70% ethanol - 1 hourr, 90% ethanol - 1 hour, 100% ethanol - 1.5 hours, 100% ethanol - 1.5 1 hour, 1:1

ethanol/toluene - 1.25 hours, Toluene - 0.5 hour, Toluene - 0.5 hour, wax – 2 hours, wax – 2 hours). Processed agar was embedded into parafin blocks and sectioned using a Leica TP microtome to 10 µm or 5 µm sections. Sections were mounted on glass slides and baked in a 37°C oven overnight.

Once sections were baked onto the slides, they were dewaxed by two 5 minute toluene washes, and then slowly hydrated through a series of ethanol washes (2 minutes each: 100% ethanol, 100% ethanol, 90% ethanol, 70% ethanol, 50% ethanol, 100% distilled water). Slides were stained in hematoxylin (Surgipath/Leica - Gill III, Cat. # 3801542) for 2 minutes, then rinsed in continuously flowing distilled water for 15 minutes. Slides were prepped for eosin staining with a 2 minute wash in 70% ethanol, then stained for 30 seconds in eosin (Surgipath/Leica, Cat. # 3801602). Slides were immediately transferred to 100% ethanol for 2 minutes, then to fresh 100% ethanol for another 2 minutes. Slides underwent two 2 minute washes in toluene and were kept in toluene until they were coverslipped in DPX mounting medium. Coverslipped slides were baked at 37°C overnight and then imaged (Zeiss A1 microscope and SebaView camera).

2.6.1 Myofibril Bundle Numbers & Cross Sectional Area

Two fish per biological replicate were analyzed by ImageJ software from a protocol modified from (Khan et al., 2018). Images with attached scale bars were converted to 8-bit depth and segmented with a threshold range of 0-130. Myofiber bundle numbers were counted by hand for the upper left hand quadrant of the cross section, averaged, and plotted using GraphPad. To calculate myofibril cross sectional area, image scale was set using the line tool to count the number of pixels on the scale bar, and that scale was used to calculate cross sectional area from outlines of myofibril bundles using the analyze particles tool. Five myofibril bundles were

chosen per fish and all were located in the upper left hand quadrant of the cross section. The average of the five myofibril cross sectional areas per fish was plotted using GraphPad.

2.7 Tricaine Treatments

Embryos staged at 18 hpf were exposed to 0.04% tricaine methanesulfonate (MS-222; Sigma Aldrich; #E1052) in embryo media until they reached 24 hpf. Tricaine supplemented solutions were refreshed every 3 hours to account for chemical decay. At 24 hpf, embryos were fixed in 4% paraformaldehyde for immunostaining. In recovery experiments, embryos staged at 18 hpf were exposed to 0.04% tricaine/embryo media until they reached 24 hpf, at which they were switched to fresh plates of embryo media. After 2 hours, the embryos were tested for a touch-evoked response. Control embryos were exposed to only embryo media for the duration of the experiment. Tricaine treated embryos were examined for paralysis by touch stimulus applied to the tail at each solution refresh, and videos recorded using Zeiss Axioskop mot plus microscope and Qcapture program (QImaging). All experiments were performed three times with a minimum of 15 embryos per replicate.

2.8 MG-132 Treatments

Embryos were staged and dosed with either 50 μM MG132 (Sigma Aldrich; # M7449) in embryo media or DMSO in embryo media and grown at 28°C until 48 hpf. 50 μM concentration was chosen based on previous results in zebrafish (Shimizu et al., 2017). Embryos were fixed in 4% paraformaldehyde for immunostaining or in electron microscopy fixative for transmission electron microscopy or hematoxylin and eosin staining. All experiments were performed three times with a minimum of 15 embryos per replicate.

Table 3: *in situ* hybridization primers

Gene	Strand	Forward Primer (5'-3')	Reverse Primer (5'-3')
amhc	cloned		
cmlc2	cloned		
hand2	antisense	TGAAGCAATGAGACTAAAG	TAATACGACTCACTATAGACACAGT GGTTTATTGA
hsp90a1	cloned	TCTTTTGCGCTACTACACTT CAGCTTC	GGATAAAATGCAAGAGCAGACACA CAAGG
nppa	cloned	CATCAGAGAGAGCCGTAGA	TTTTGCCGCTATGCTAGTAAT
smyd1b	antisense	GAAGCTGTATCACCCTAATA	TAATACGACTCACTATAGCACATTC ATCAATCCTGAAA
smyd1b	sense	TAATACGACTCACTATAG GAAGCTGTATCACCCTAATA	CACATTCATCAATCCTGAAA
ttn2	antisense	CCGAATTTAACGGTTATGAA	TAATACGACTCACTATAGTTAATGG CCAGGTGATG
ttn2	sense	TAATACGACTCACTATAG CCGAATTTAACGGTTATGAA	TTAATGGCCAGGTGATG
unc45b	cloned	TGTCGTTAGGTGAAGAGAG	TTTCGCAGGTCAGAGTT
vmhc	cloned		

underlined sequence denotes T7 RNA polymerase promoter

cloned indicates sequences cloned into a plasmid with flanking SP6 and T7 RNA polymerase promoters

cloned probes with no primer sequence listed are probes obtained from previous students where no information was given

Table 4: qPCR primers

Gene	Forward Primer (5'-3')	Reverse Primer (5'-3')	cDNA Dilution
ef1a	CCTTCGTCCCAATTTCAGG	CCTTGAACCAGCCCATGT	matched with target gene
hsf-1	CCATCGACAGCGGTTTAGAA	GACGCCGCTGAAGAGAAA	1/200
hsp70-1	CAGGAGGCTGACAAGTACAAA	GTCGTCTTCCACACTGTTCTT	1/200
hsp90a1	GGATGAGCTGAAGGCCAAATA	GTATGTGCTGGTGACGATACAG	1/200
smyd1a	GTTCATGTTCTGCGTGTCCT	GCCCAGCTGAGCGTTATT	1/200
smyd1b	ATGGAGAAGGCCAGGATAGA	GGTACAACACACACGCAGATA	1/200
stub-1	TCGCATCGCCAAGAAGAAA	CCAGGATGAGTTTGCTGAGATAG	1/40
trim101	CTGGAGACAAGAAGACAG	TCAGCACAAACACGTAA	1/40
trim55b	CCTGCGCAATATTGACTTCATC	TGGCCAAGTAAATCCACTTCT	1/40
trim63a	AGGAGCAGGATGAGAAGGT	TCTGAGAAGCTTTGTCCATCAG	1/40
trim63b	GTTGCTTAACCAGATGGAGGA	CAAGGCTGCATAGAGGGAAT	1/40
ttn2	TGGAAACCACCAAAGGATGAT	CTGAGACAGCCGATGATACAAG	1/200
ube4b	CTTCCCTCGGGCAACATAAT	GTCAGAGGCTGTCTGTTGAAG	1/50
unc45b	ACCTCCTTGCAGCAAACT	AGGATCATGAACAGATCAGACAA	1/200

CHAPTER 3. RESULTS:

3.1 *Steif* mutants fail to form myosin thick filaments, whereas *herzschlag* mutants do form thick filaments, but they become disorganized over time due to contraction induced damage

3.1.1 Introduction and selection of zebrafish mutants

To examine potential differences in myosin quality control when myosin damage occurs at or before the sarcomere assembly stage or after sarcomere assembly is complete, I needed zebrafish that completed myosin thick filament assembly, zebrafish that did not complete myosin thick filament assembly, and zebrafish that complete myosin thick filament assembly, but underwent subsequent myosin damage. I hypothesized that wild-type (AB or sibling) zebrafish would complete normal myosin assembly/maintenance (Figure 13A-B') and that *steif* would represent a myosin thick filament assembly mutant based on their loss of function mutation in the myosin chaperone, *unc45b* (Etard et al., 2007; Figure 13C-D'). For our myosin maintenance mutant, I chose to examine the *herzschlag* line, as *herzschlag* encodes a *titin2* mutation predicted to result in the loss of the titin A-band and C-terminus (Myhre et al., 2014b). How this mutation affects myosin thick filament assembly is less clear as the role of titin in myosin thick filament assembly is still widely debated (reviewed in Myhre and Pilgrim, 2014; Figure 13E-F').

Many hypotheses of the role of titin in sarcomere assembly exist (reviewed in Myhre and Pilgrim, 2014). The molecular ruler hypothesis (Whiting et al., 1989) proposed a dual role of titin in acting as a template for thick filament assembly and regulating the precise spacing of thick filaments. As titin's regularly spaced A-band fibronectin-like domains correlate with the spacing of thick filaments (Labeit and Kolmerer, 1995), this hypothesis provided a simple and elegant explanation of the role of titin in sarcomere assembly. The molecular ruler hypothesis

predicted that sarcomeres lacking titin would show severe defects in assembly, which has been supported by work done in cell culture (van der Ven et al., 2000). More recently, a near-null titin mutation generated in zebrafish, which lacks functional copies of both paralogs of zebrafish titin (*titin2*, previously *titina*, and *titin1*, previously *titinb*), supported a sarcomere assembly role for titin in the maturation of premyofibrils to mature myofibrils (Shih et al., 2016). It is still unclear which domain(s) of Titin2 are directly responsible for its ruler function, as mice with targeted deletions of the titin I-band/A-band junction have normal thick filament length (Granzier et al., 2014), but those with C-terminal interruptions do not (Tonino et al., 2017). A recent atomic force microscopy experiment provided evidence against a role for titin as a template for thick filament assembly, and suggested that titin creates a cap for thick filament length, rather than acting as a ruler (Kellermayer et al., 2018). As such, the molecular role of titin in sarcomere assembly continues to be a hotly debated subject.

Rigorous testing of the above hypotheses has been challenging for many reasons (reviewed in Greaser, 2009). Titin is the largest known protein, with human titin consisting of 363 exons making a protein up to 4200 KDa (Bang et al., 2001). Its immense size has made experimental manipulation and sequencing of the entire gene unfavourable by conventional methods. As next generation sequencing becomes more cost effective, this problem is being overcome, but highlights a new problem: titin's extensive alternative splicing and isoform switching (Greaser et al., 2005). With the development and optimization of genome editing with CRISPR/Cas9, the ability to make unique mutations and test the functions of specific domains of titin are now possible, but homozygous titin mutations can be embryonic lethal. Finally, it is still unclear which domains of titin are most important for sarcomere assembly, maintenance, and overall survival. Mutations in certain titin domains, like the N-terminus and C-terminus, are

underrepresented in humans when compared to A-band mutations (Herman 2012), which led to the initial hypothesis that mutations in these areas are less severe than those in the A-band. More recently, however, an internal promoter encoding a C-terminal portion of titin (dubbed "Cronos") was identified (Zou et al., 2015) which suggests a second interpretation by which A-band and M-line mutations are more severe as they interrupt the function of the full length gene as well as any rescuing function that Cronos could provide.

3.1.2 The *herzschlag* mutation affects the Titin2 A-band and M-line regions

In order for a titin mutation to affect the assembly of the sarcomere, titin must be expressed during the stages of sarcomere assembly. Titin protein has been detected early in sarcomere development in cell culture models (Schultheiss et al., 1990) where N-terminal titin epitopes are detectable with the appearance of α-actinin. However, the increased pace of sarcomerogenesis in culture (van der Ven and Furst, 1997) coupled with the widely reported concern that isolated primary cultures of muscle cells may model sarcomere disassembly rather than sarcomere assembly (Boateng and Goldspink, 2007; Gregorio et al., 2006) leaves the role of titin in sarcomere assembly unaddressed in *in vivo* models. Immunofluorescence performed on sections of whole mount chicken embryos recapitulates the work done in cell culture, with N-terminal titin puncta visible with the appearance of α-actinin puncta (Tokuyasu and Maher, 1987). However, the appearance of the A-band region of this protein, which is most important to thick filament assembly, has still not been examined *in vivo*. As zebrafish are externally fertilized, examination of early sarcomere assembly stages can be done under a microscope without sacrificing the mother. Therefore, zebrafish make an excellent model system to address the role of titin during sarcomere assembly. To determine whether *titin2* was expressed during the periods of sarcomere assembly in zebrafish, we determined when *titin2* mRNA was

expressed in zebrafish by performing qPCR on wild-type embryos at stages before and during sarcomere assembly (Figure 14A). Expression of *titin2* is negligible at 10 hpf, but expression increases at 14 hpf and 17 hpf, which correlates with the onset of slow muscle sarcomere assembly. *titin2* expression increases at 19 hpf and 24 hpf, which correlates with the assembly of fast muscle sarcomeres and the completion of sarcomere assembly. To determine whether this expression was detectable in skeletal muscle, I performed *in situ* hybridization on wild-type zebrafish at these timepoints (Figure 14B-F). Consistent with the qPCR data, the *in situ* hybridization data shows *titin2* expression beginning in the somites at 14 hpf (Figure 14B), and expression remains in skeletal muscle until 48 hpf (Figure 14F). Together this suggests that *titin2* mRNA is present in developing muscle at the time slow and fast sarcomeres are assembling.

Although the above data is consistent with a role for titin in sarcomere assembly, because of titin's enormous size, it is likely that protein synthesis is a time consuming process. Predicted eukaryote translation speed ranges from 2.8 - 10.0 amino acids/second (Karpinets et al., 2006), such that zebrafish *titin2*'s 32 757 amino acids (Accession: ABG48500.1) would require roughly 1-3 hours to translate. Therefore, I wanted to ensure that Titin2 protein, particularly the A-band region, was detectable in skeletal muscle during sarcomere assembly. At the same time, I wanted to characterize the protein consequences of the *herzschlag* mutation in greater detail to determine what portions of the Titin2 protein were present in *herzschlag* mutants during stages of myosin assembly.

Previous work had mapped the *herzschlag* mutation to a ~10Mbp region on chromosome 9 that corresponds to the zebrafish paralogs of titin, including *titin2* (Myhre et al., 2014b). Based on complementation testing with an existing *titin2* mutant, differential antibody staining, and simple sequence length polymorphism marker microsatellite mapping, *herzschlag* was predicted

to have a mutation in *titin2* (Myhre et al., 2014). The consequence of this mutation was shown to affect Titin2 between the I-band and before the A-band region of the protein, suggesting that the mutation exists somewhere in the sequence that encodes this region (Myhre et al., 2014b; see Figure 15A). It is still unknown what the exact *herzshlag* mutation is, and due to the many proposed splice isoforms of human titin (Greaser et al., 2005), and their conservation in zebrafish (Seeley et al., 2007), it remained unclear how this mutation affects the Titin2 protein. To examine the consequences of the *herzschlag* mutation on the Titin2 protein, I performed immunostaining with different titin epitope-specific antibodies, T12 (Fürst et al., 1988; Tskhovrebova and Trinick, 2002) and T11 (Fürst et al., 1988) at timepoints earlier and later than what was previously examined in *herzschlag*. T11 and T12 staining in 30 hpf *herzschlag* and wild-type zebrafish show the presence of T12 at 30 hpf, but a loss of T11 staining in *herzschlag* mutants (Myhre et al., 2014b). I was able to detect T11 staining in wild-type zebrafish skeletal muscle at 17 hpf (Figure 15B), and striations indicating titin incorporation into sarcomeres at 19 hpf (Figure 15D) and 24 hpf (Figure 15H). In contrast, I was unable to detect T11 staining in the muscle fibers of 30% of embryos (n=65 embryos; one biological replicate) in mixed *herzschlag* broods at 17 hpf (Figure 15C&J), 30% at 19 hpf (n= 108 embryos; two biological replicates; Figure 15E&J), and 25% (n=178 embryos) at 24 hpf (Figure 15I&J). However, I was able to detect T12 staining in both *herzschlag* and wild-type zebrafish at 24 hpf (n=183 embryos), which is consistent with the previously reported loss of the A-band of Titin2 throughout the stages of sarcomere assembly (Myhre et al., 2014b). This work was consistent with the *herzschlag* titin mutation resulting in various consequences to the Titin2 protein including: a permanent truncation causing loss of the partial or entire A-band region of the protein, a transient truncation

causing loss of the partial or entire A-band region of the protein, or a mutation that interfered with the T11 epitope domain.

To address these hypotheses, I examined T11 staining later in *herzschlag* development. If the consequence of the *herzschlag* mutation is a permanent truncation of Titin2 before the T11 epitope, then T11 staining should never appear in *herzschlag* embryos. However, by 48 hpf, both T11 and T12 striations were evident in *herzschlag* (Figure 15L&N) and wild-type embryos (Figure 15K&M). While this result eliminated both the possibilities of the *herzschlag* mutation resulting in a permanent truncation beginning before the T11 epitope, or existing within the T11 epitope, it was still consistent with both a transient truncation causing loss of the partial or entire A-band region of the protein, or a mutation that interfered with the T11 epitope domain but existed outside of it. The best method of differentiating between these hypotheses would require protein work, which due to titin's size is something only a handful of labs are capable of performing.

In lieu of a western blot, I chose to examine whether *herzschlag* Titin2 was full length through immunostaining of Titin2's C-terminal end using the generously donated antibody, M8/M9. Due to the limited quantity of M8/M9, I chose to perform this analysis at 48 hpf, when homozygous *herzschlag* mutants could be phenotypically identified. I hypothesized that if Titin2 was full length at 48 hpf, when both T12 and T11 striations are evident, that this was evidence that the *herzshlag* mutation caused the T11 epitope to be occluded early in development, but that the mutation was spliced out or additional exons were spliced in which caused the T11 epitope to be available later in development. At 48 hpf, immunostaining shows that the M8/M9 striations in wild-type fish (Figure 15O&O'), but not *herzschlag* embryos (Figure 15P&P'), which suggested

that either the M8/M9 epitope was also occluded in *herzschlag* embryos, or that the full Titin2 protein is not made in *herzschlag* embryos at this timepoint.

Because *herzschlag* was generated in a N-ethyl-N-nitrosourea mutagenesis screen (Granato et al., 1996), it is likely that the mutation is a single nucleotide polymorphism, although it is not impossible for *herzschlag* to have two mutations in *titin2* which cause both T11 and M8/M9 to be obstructed at various times during development. It is also possible that the *herzshlag* mutation results in a transient truncation of Titin2, where the protein is initially severely truncated before the T11 epitope, and later before the M8/M9 epitope. If this is the case, the *herzschlag* Titin2 protein would represent a novel titin isoform as currently there are no identified titin isoforms reported to contain the T11 epitope but lack the M8/M9 epitope. While M8/M9 staining at 24hpf would help address this question, protein gels will be necessary to absolutely determine the consequences of the *herzschlag* mutation on the Titin2 protein.

Together, this work suggests that Titin2 protein is present in the sarcomere during the stages of sarcomere assembly, which is consistent with the protein playing a role in the proper assembly of the sarcomere. The *herzschlag* mutation results in the loss of the T11 epitope between 17 hpf and 24 hpf, while the M8/M9 epitope is not present at 48 hpf, likely indicating that the A-band region of Titin2 is not fully intact in *herzschlag* embryos during sarcomere assembly stages.

3.1.3 Myosin thick filament assembly is normal in *herzschlag*, but not *steif*

After determining that the A-band region of Titin2 was likely affected throughout *herzschlag* sarcomere assembly stages, I wanted to determine whether the *herzschlag* mutation affected the ability of myosin to assemble into thick filaments. In *herzschlag* embryos, thick and

thin filament striations have been detected in a few sarcomeres at approximately 24 hpf and 30 hpf, in otherwise disorganized muscle tissue (Myhre et al., 2014b). However, as muscle development begins much earlier than 24 hpf, it was not possible from this data to determine whether the disorganized actin and myosin are a result of improper assembly or if damage occurs post-assembly. To differentiate between these hypotheses, I examined the difference in integrity between *herzschlag* and wild-type zebrafish sarcomeres at 18 hpf, when slow muscle thick filaments are forming (Felsenfeld et al., 1990). At 18 hpf, immunostaining of *herzschlag* mixed brood embryos (Figure 16B&B') against slow myosin (F59) and actin (phalloidin) show grossly normal sarcomere assembly in 94% of fish examined (n=321 embryos), indicating that *herzschlag* sarcomeres cannot be differentiated from their wild-type siblings (Figure 16A&A', quantification in Figure 16D). In comparison, *steif* embryos can be identified from wild-type siblings in Mendelian ratios (Figure 16C&C'), as an average of 25% (n=119 embryos) fail to form thick filament myofibrils (Figure 16D). The inability to identify homozygous *herzschlag* embryos from their wild-type or heterozygous siblings suggests that thick filament assembly occurs normally in *herzschlag* embryos. However, *steif* mutants never form myosin thick filaments.

3.1.4 *herzschlag* thick filaments become disorganized over time as a result of contraction induced damage

Our results support a model by which the interruption in the *herzschlag* Titin2 A-band does not affect myosin thick filament assembly. However, other roles for titin in sarcomere assembly and maintenance exist. Titin's immunoglobulin repeats and PEVK domain in the I-band (Labeit and Kolmerer, 1995), as well as the kinase domain near the C-terminus (Krüger and Linke, 2011), suggested roles for titin beyond, or in addition to, a function in sarcomere

assembly. As such, alternative functions of titin have been proposed (reviewed in Myhre and Pilgrim, 2014), such as damage sensing (Krüger and Kötter, 2016) and signalling roles (Krüger and Linke, 2011), bracing the sarcomere during contractions (Shih et al., 2016; Wang et al., 1993), controlling gene expression and forming a link between the sarcomere and the ubiquitin proteasome system (Centner et al., 2001; Lange et al., 2005). These hypotheses, while not necessarily mutually exclusive, implicate titin not only in sarcomere assembly, but also propose roles for titin in regulating the coordinated movement and maintenance functions of the sarcomere. In support of roles for titin beyond sarcomere assembly, sarcomeres with A-band titin mutations show a reduction in slow fiber damage when contractions are inhibited (Shih et al., 2016), supporting a role for titin in sarcomere bracing during contractions.

Previous work shows that *herzschlag* mutants are fully paralyzed by 48 hpf and display significant sarcomere damage (Myhre et al., 2014b). Consistent with these reports, I show that slow myosin staining is almost nonexistent at 48 hpf (Figure 17B) in phenotypically identified *herzschlag* embryos, while wild-type embryos have organized slow muscle myofibrils with repeating striations (Figure 17A). To determine whether an absence of slow myosin staining was common in fish displaying general muscle damage, I examined slow myosin staining in *steif* mutants to find that, while disorganized, slow myosin staining was present (Figure 17C). Fast myosin staining at 48 hpf in wild-type embryos (Figure 17D) showed organized myofibrils with repeating striations indicating fast myosin incorporation into sarcomeres. In contrast to the absence of slow myosin staining observed in *herzschlag*, fast myosin is present in these mutants at 48 hpf, but not organized into sarcomeres (Figure 17E). *steif* mutants also retain fast myosin staining at 48 hpf, but the staining is diffuse and fast myosin is not incorporated into sarcomeres (Figure 17F). By 5 dpf, all sarcomere and myofibril organization observed in wild-type embryos

(Figure 17G) has been lost in *herzschlag* mutants (Figure 17H) and muscle appears to consist of large protein aggregates. *steif* mutants at 5 dpf (Figure 17I) also have lost any sarcomere and myofibril organization, with faint actin and myosin staining present in these mutants.

Because early sarcomere thick filament assembly is grossly normal in *herzschlag* embryos (Figure 16B&B'), I hypothesized that the later thick filament disorganization in *herzschlag* (Figure 17B,E,H) may be a result of contraction induced damage due to interruptions in the A-band of Titin2 during muscle development. Supporting this hypothesis is previous work which showed that *herzschlag* cultured myocytes deprived of contractile signals assembled sarcomeres normally (Myhre et al., 2014b). However, I chose to examine this *in vivo* using the putative sodium channel inhibitor, tricaine (Topic Popovic et al., 2012), as it has been successfully used in zebrafish (Mazelet et al., 2016; Shih et al., 2016). Embryos were paralyzed before initial contractions (18 hpf; Bessarab et al., 2008) to 24 hpf, when sarcomere assembly is complete (Bessarab et al., 2008), and slow myosin and actin integrity was examined via immunofluorescence.

Tricaine treated embryos displayed no response to tactile stimulus (Supplemental Video 1), while untreated controls twitched. After the tricaine was replaced by fresh embryo media and embryos were allowed to recover, a tactile stimulus evoked a response in all embryos, showing that these embryos were paralyzed, but alive (Supplemental Video 2). Untreated *herzschlag* mix brood embryos, exposed to only embryo media from 18-24 hpf, showed a loss of slow myosin staining and disorganized actin in 26% of embryos (n=415 embryos; Figure 17K&K'). This percentage likely reflects *herzschlag* embryos based on Mendelian ratios (Figure 17P), and the remaining 74% of embryos showed normal slow myosin incorporation into sarcomeres (Figure 17J&J').

However, when *herzschlag* mix brood embryos were treated with the paralytic tricaine from 18 hpf-24 hpf, the ability to identify mutants based on slow myosin staining was lost, as 91% of embryos (n=431 embryos; Figure N-N') showed a retention of slow myosin myofibrils (quantification in Figure 17P). Slow myosin sarcomeres were much harder to detect in all fish treated with tricaine, including wild-type (AB) embryos (Figure 17M&M') and a disorganization was apparent in all embryos treated with tricaine as well as a global decrease in actin and myosin staining. As muscle contractions are known to play an important role in muscle development, it is likely that these phenotypes are a consequence of continued muscle development in the absence of contractions, and have been characterized before in tricaine paralyzed embryos and in the paralyzed zebrafish mutant, *relaxed* (Mazelet et al., 2016).

Our inability to differentiate paralyzed *herzschlag* embryos from their paralyzed wild-type siblings supports the hypothesis that *herzschlag* sarcomere damage is contraction induced due to a loss of the bracing function of titin during sarcomere development, as other functions of titin should be uninhibited in the presence of a chemical paralytic. If this hypothesis is correct, I would expect that embryos with muscle damage that is not contraction induced would not show an increase in slow muscle integrity when treated with tricaine. Therefore, I repeated this experiment with *steif* mutants (Figure 17L&L') and found that 26% of untreated mix brood embryos had a loss of slow myosin striations compared to wild-type embryos (n=78 embryos; Figure 17P). When mix brood *steif* embryos were treated with tricaine from 18 hpf to 24 hpf, I was still able to identify 26% of embryos (n=53 embryos; Figure 17P) that did not display slow myosin myofibrils (Figure O&O') which suggests that tricaine treatment did not improve slow myosin integrity in *steif* mutants. Together this data suggests that the slow muscle damage observed in *herzschlag* mutants is contraction induced.

3.1.5 *herzschlag* cardiac sarcomeres assemble normally but impact cardiac function

Due to the necessity of titin function in the developing heart (Seeley et al., 2007) and the diseases that result from its loss (reviewed in Gigli et al., 2016), I wanted to examine the integrity of the heart in *herzschlag* embryos. *in situ* hybridizations against the cardiac myosin light chain, *cmlc2*, show normal D-looping in 34/45 wild-type embryos at 48 hpf (Figure 18A), with a small number of embryos showing reversed S-looping (6/45) or no looping (O-looping; 5/45; quantification in Figure 18C). In contrast, at 48 hpf *herzschlag* hearts are primarily unlooped (33/45; Figure 18B), with only 5/45 embryos undergoing correct looping. DIC imaging of *herzschlag* hearts recapitulate this failure of looping and show pericardial and yolk sac edema (Figure 18E) when compared to wild-type hearts (Figure 18D). *herzschlag* hearts also display increased instances of blood regurgitation (Supplemental Video 3) and show a significant decrease in functionality, with average *herzschlag* heart rate at 71 bpm compared to the wild-type 101 bpm ($p<0.0001$; Figure 18F). By 5 dpf, wild-type hearts are tucked under the chin of the fish (Figure 18G) while severe edema has stretched *herzschlag* hearts, although chambers still remained visible in some fish (Figure 18H). While contractions in *herzschlag* hearts are poor (Supplemental Video 4), they only beat slightly slower than wild-type fish (102 bpm vs 130 bpm), but cardiac function was obviously impaired and blood regurgitation was very pronounced (Supplemental Video 5). The *herzschlag* cardiac phenotype was very similar to homozygous titin A-band zebrafish mutants described in Huttner et al. (2018). To determine whether *herzschlag* heart phenotypes were a result of degeneration of muscle, I examined the integrity of the cardiac Z-disc, I-band, A-band and M-line via immunofluorescence.

At 48 hpf striations in the N-terminus of Titin2, (Figure 18J&K), actin (Figure 18L&M), total myosin (Figure 18N&O), and myomesin (Figure 18P&Q) can be found in *herzschlag*

embryos as well as wild-type siblings suggesting that all parts of the cardiac sarcomere are intact, although sarcomeres appear disorganized in *herzschlag* mutants. As myomesin is never detected in *herzschlag* skeletal sarcomeres (Prill *et al*., in preparation), this suggests that *herzschlag* cardiac titin could be full length. This assay is supported by a previous paper which used the absence of myomesin sarcomere localization as a readout of an interruption in full length titin (Huttner et al., 2018). However, obvious disorganization in the *herzschlag* cardiac myofibrils can be seen which suggests that the *herzschlag* mutation has consequences to cardiac muscle as well as skeletal.

Titin has been shown to affect Serum Response Factor signalling (Lange et al., 2005) and Serum Response Factor can regulate cardiac transcription factors (Evans et al., 2010). Therefore, I wanted to examine whether the *herzschlag* mutation affected cardiac transcriptional networks. Expression of *hand2*, an indirect target of Serum Response Factor (Evans et al., 2010) and a major player in cardiac development (Figure 19C, reviewed in Lu et al., 2016), showed spatial dysregulation in *herzschlag* embryos (Figure 19B) compared to wild-type siblings (Figure 19A). To determine the consequences of *hand2* dysregulation, I examined chamber identity in *herzschlag* and wild-type embryos via expression of the atrial specific myosin, *amhc*, and the ventricle specific myosin, *vmhc*. At 48 hpf, both *amhc* (Figure 19D&E) and *vmhc* (Figure 19F&G) expression is restricted to their proper chamber in the majority of *herzschlag* and wild-type embryos, suggesting that heart chamber specification and maintenance is normal in *herzschlag* mutants. *herzschlag* atria appear slightly enlarged compared to wild-type siblings, which has been previously reported for titin mutants (Radke et al., 2019). As *hand2* is also an upstream factor involved in the proper development of the atrioventricular canal (AVC; Grassini et al., 2018; Laurent et al., 2017), I examined expression of *anf/nppa*, which is excluded from the

AVC when it is properly developed. At 48 hpf, *nppa* is absent from the wild-type AVC in 42/45 of the embryos examined (Figure 19H&J), but present in the AVC in 44/45 of the *herzschlag* embryos examined (Figure 19I&J). As the *nppa* and *nppb* function to restrict the expression of AVC transcription factors (Grassini et al., 2018), expansion of *nppa* into *herzschlag* AVCs is suggestive of improper AVC patterning. AVC defects could explain the regurgitation of blood visible from the *herzschlag* ventricle into the atrium (Supplemental Videos 3&5).

Together, this section suggests that although *herzschlag* cardiac sarcomeres have intact Z-discs, I-bands, A-bands, and M-lines, cardiac function is impaired in *herzschlag* mutants. A possible mechanism of this impairment is cardiac transcriptional dysregulation which results in improper AVC development.

3.2 Different protein quality control systems respond to myosin damage in *steif* and *herzschlag*

The above sections show that *herzschlag* mutants assemble thick filaments that disassemble over time, while *steif* mutants fail to assemble thick filaments. As the thick filament disorganization observed in these fish occur either after myosin has been incorporated into the sarcomere (*herzschlag*), or before myosin has been incorporated into the sarcomere (*steif*), I hypothesized that different quality control systems would recognize and respond to the thick filament disorganization in these embryos. Thus, I predicted that transcriptional differences would exist between *herzschlag* and *steif* mutants in myosin protein quality control systems.

3.2.1 Myosin damage in *steif* is recognized by the misfolded myosin response, but the myosin damage in *herzschlag* is not

We and others have described a phenomenon by which loss of a myosin chaperone (Etard et al., 2015; Etard et al., 2007; Prill et al., 2015) results in strong upregulation of other myosin

chaperones due to an accumulation of misfolded myosin. This response, called the misfolded myosin response, is an excellent candidate to respond to myosin damage in *steif* mutants, however, it has not been reported to occur in *herzschlag* (Etard et al., 2015; Myhre et al., 2014b). Consistent with this, I detected no significant change in myosin chaperones *hsp90a1*, *snyd1b*, *unc45b*, or their regulator, *hsf-1*, in *herzschlag* embryos compared to wild-type (AB) embryos (Figure 20A). However, strong upregulation of all myosin chaperones, except the cognate gene of the *steif* mutation, *unc45b*, was observed between *steif* and wild-type embryos (Figure 20A). As the qPCR was performed on total RNA extractions, I performed *in situ* hybridizations at 48 hpf in wild-type (siblings), *herzschlag*, and *steif* embryos to determine whether the observed upregulation of myosin chaperones in *steif* embryos was due to cardiac or skeletal expression. Consistent with the qPCR data, strongest upregulation was observed in *steif* embryos probed with *hsp90a1* or *smyd1b*, while fainter (*smyd1b*) or zero (*hsp90a1*) staining was observed in *herzschlag* and wild-type embryos (Figure 20B). Also consistent with the qPCR data, staining of *unc45b* in *herzschlag* and wild-type embryos was comparable, while *unc45b* expression in the myosin chaperone mutant, *still heart* (*smyd1b*; Prill et al., 2015) was strongly upregulated (Figure 20B). All three of these genes were expressed in the skeletal muscle.

To determine whether myosin chaperone transcriptional upregulation persisted in *steif* embryos, or whether more severe myosin damage could induce myosin chaperone expression in *herzschlag* embryos, I performed *in situ hybridizations* on 5 dpf embryos of *unc45b* (N=2), *hsp90a1* (N=2), and *smyd1b* (N=1) on 5 dpf embryos (Figure 20C). *hsp90a1* and *smyd1b* was upregulated in *steif* embryos at 5 dpf, compared to a complete absence of staining in wild-type and *herzschlag* embryos. The same trend was found for *unc45b* in *still heart* embryos, and an

absence of staining in wild-type and in the skeletal muscle of *herzschlag* embryos. Interestingly, by 5 dpf, *herzschlag* embryos showed cardiac *unc45b* staining (Figure 20C).

The myosin chaperone upregulation in *steif* and its absence in *herzschlag* raised the question of whether all muscle chaperones were upregulated in *steif*, and whether any were upregulated in *herzschlag*. *smyd1a* and *hsp70-1* made good candidates to investigate this question as *smyd1a* is a paralog of *smyd1b*, a myosin chaperone directly involved in the misfolded myosin response. *hsp70-1* is a ubiquitous chaperone, but is known to respond to muscle damage (reviewed in Senf, 2013). If muscle chaperones globally respond to the absence of a myosin chaperone and the presence of misfolded myosin, I would expect both these genes to be strongly upregulated in *steif*. However, qPCR showed that neither *smyd1a* nor *hsp70-1* were significantly different from wild-type embryos at 48 hpf (Figure 21A). Interestingly, *hsp70-1* was upregulated in *herzschlag* embryos compared to wild-type at 48 hpf, although there was no significant change in *smyd1a* expression. This data suggests that the misfolded myosin response does not cause a global upregulation of muscle chaperones, and that myosin chaperones do not respond to myosin damage when it occurs after sarcomere assembly stages. This raises interesting questions about how a myosin chaperone would recognize and differentiate a 'misfolded' protein (a protein that never reached its proper conformation after synthesis) from a 'damaged' protein (a protein that was initially folded properly and but lost structural integrity over time) as current models suggest detection is via exposure of hydrophobic amino acids, which would occur in both cases. *hsp70-1* upregulation in *herzschlag* was also unexpected, but as *hsp70-1* is linked to protein turnover mechanisms (Senf, 2013), this upregulation could suggest increased protein turnover in *herzschlag* embryos.

3.2.2 *herzschlag* undergoes an early, slow myosin specific, skeletal muscle atrophy while atrophy in *steif* is global and occurs later

There is an apparent difference in slow myosin immunostaining intensity between *herzschlag* embryos and wild-type or *steif* embryos (see Figure 17A-C), which may suggest an additional consequence of the titin mutation. I hypothesized that this lack of slow myosin staining was due to either: 1) sarcomere disarray to such an extreme extent that the antibody's epitope is occluded, or 2) myosin is being removed from the sarcomere, resulting in a gradual loss of staining. To test these hypotheses, I used transmission electron microscopy (TEM) to examine the sarcomere ultrastructure in greater detail. TEM of longitudinal sections show intact fast muscle sarcomeres in wild-type embryos at 48 hpf (Figure 22A), while only residual sarcomere structures with identifiable Z-discs and I-bands remain in *herzschlag* (Figure 22B) and *steif* mutants (Figure 22C). TEM cross sections imaged in the slow muscle layer show intact bundles of myofibrils surrounded by sarcolemma in wild-type embryos at 48 hpf (Figure 22D). Disorganization of these bundles is evident in both *herzschlag* (Figure 22E) and *steif* embryos (Figure 22F), however, there is a marked loss of tissue accompanied by a breaking apart of the myofibril bundling that is present only in the *herzschlag* embryos (Figure 22E). These data are suggestive of a selective atrophy in the slow muscle layer of *herzschlag* embryos. In order to image both layers at the same time, I performed Hematoxilin and Eosin (H&E) staining of cross sectioned wild-type, *herzschlag*, and *steif* embryos at 48 hpf. Both wild-type (Figure 22G) and *steif* (Figure 22I) embryos show tissue retention in both the peripheral slow muscle layer (insets; black arrowheads) and central fast muscle layer (inset; white arrowhead). However, *herzschlag* embryos (Figure 22H) show a loss of staining in slow muscle layer (inset; black arrowhead), but not fast muscle layer (inset; white arrowhead). Together, the immunofluorescence staining,

TEM, and H&E suggested to a slow muscle atrophy specific to *herzschlag* embryos. As this atrophy is not seen in *steif* mutants, it can be determined that the consequences to slow muscle is a result of the *herzschlag* titin mutation, and not a defect associated with general muscle damage.

I was interested in whether fast myosin would follow the same trend in *herzschlag* if damage was allowed to progress. TEM examination of the cross sections and longitudinal sections in the fast muscle layer show intact sarcomeres in wild-type embryos at 5 dpf (Figure 23A&D). In *herzschlag* (Figure 23B&E) and *steif* (Figure 23C&F) longitudinal sections, large aggregates of proteins exist, which is similar to what is observed in 5 dpf immunofluorescence of fast myosin (see Figure 17H). Residual sarcomere structures are still identifiable in the protein aggregates, including Z-discs (black arrowheads) and I-bands. To better examine the tissue integrity, I performed H&E staining on 5 dpf *herzschlag*, *steif*, and wild-type siblings. While wild-type 5 dpf embryos show organized staining and maintained integrity of fast and slow muscle (Figure 23G), both *herzschlag* (Figure 23H) and *steif* (Figure 23I) embryos had undergone severe muscle atrophy. Both *herzschlag* and *steif* embryos exhibited fewer myofibril bundles (Figure 23J) as well as smaller cross sectional area of those myofibril bundles (Figure 23K), both of which were consistent with muscle atrophy.

I considered that the *herzschlag* slow muscle atrophy evident at 48 hpf might suggest that the *herzschlag titin2* mutation sensitizes slow muscle to atrophy. As the *steif unc45b* mutation affects both slow muscle and fast muscle (Etard et al., 2007), both tissues might be equally sensitized to atrophy and an unnoticed reduction in both tissues is occurring. To address this, I examined H&E cross sections of a second muscle mutant, *still heart*. *Still heart* encodes a mutation in the myosin chaperone *smyd1b*, which affects fast muscle but leaves slow muscle intact (Prill et al., 2015). I hypothesized that if the *still heart* mutation sensitizes fast muscle for

degradation, I would see a reduction in fast muscle in these mutants. However, at 48 hpf, *still heart* fast muscle staining (Figure 24B) was comparable to wild-type siblings (Figure 24A). By 5 dpf, *still heart* cross sections (Figure 24D) display a severe muscle atrophy in both fast and slow muscle (Figure 24D) that does not occur in wild-type siblings (Figure 24C). 5 dpf *still heart* cross sections resemble *steif* and *herzschlag* cross sections (Figure 23I&H), suggesting that the global muscle atrophy observed in these mutants at older stages is a consequence of general muscle damage and not due to a specific mutation.

A third muscle mutant, *jam*, carries an unknown mutation that is believed to affect slow muscle (Cappellano, unpublished). To determine whether the *jam* mutation sensitizes slow muscle for degradation, I performed H&E staining on 7 dpf *jam* mutants when they can be phenotypically identified from wild-type siblings. At 7 dpf, *jam* embryos (Figure 24F) are quite small compared to wild-type (AB) embryos (Figure 24E), with a substantial increase in the size of the notochord. Interestingly, a similar gap in the slow muscle layer is present in *jam* embryos as in *herzschlag* embryos, suggesting that the *jam* mutation may indeed influence the maintenance of this tissue. However, more work is needed in *jam* mutants to determine whether slow muscle development is initially normal in these fish.

From this work, I concluded that the *herzschlag* titin mutation causes a degenerating muscle disease that preferentially affects slow muscle but eventually progresses to fast muscle. However, muscle damage in general, as represented by all 5 dpf mutants, will cause a global muscle atrophy if allowed to progress.

3.2.3 Different E3 ligases are upregulated in *herzschlag* and in *steif* throughout developmental stages

The specific loss of the slow muscle layer in *herzschlag* mutants suggests a titin-related mechanism that sensitizes this tissue for degradation. Although many protein turnover and quality control mechanisms exist, they are often understudied in striated muscle (reviewed in Carlisle et al., 2018). However, based on the previously published link between the C-terminal titin kinase domain and the ubiquitin proteasome system (Centner et al., 2001; Lange et al., 2005), I hypothesized that the slow muscle in *herzschlag* was being targeted for removal by the UPS. I used qPCR to screen through E3 ligases known to be expressed in striated muscle in both *herzschlag* and *steif* mutants with comparison to wild-type at time before (19 hpf), during (24 hpf), and after (48 hpf) slow muscle atrophy had occurred in *herzschlag* mutants (Figure 25A-C).

The MuRF Family of E3 ligases were excellent candidates to examine due to their muscle specificity (Centner et al., 2001; Spencer et al., 2000) and implication in titin signalling (Centner et al., 2001; Lange et al., 2005). At 19 hpf, during sarcomere assembly, there is a high degree of variation in the mutant samples likely due to them being mix broods (Figure 25A). Unsurprisingly, *steif* mix broods show elevated expression of Unc45b quality control genes, *ube4b* and *stub1* (Hoppe et al., 2004), that is significantly different from wild-type embryos. As this is a period where myosin transcription is very strong (Prill, unpublished), accumulation of misfolded myosin in *steif* will be occurring. The strong upregulation of the MuRF family E3 ligase, *trim63a*, (MuRF1a) observed in *steif* could be responding to this myosin damage. Expression of *trim63b* (data not shown) may also be elevated in *steif* mutants. This expression data would support a model where chaperones and E3 ligases cooperate to degrade damaged proteins, or whether they exist as separate, competing, entities.

In *herzschlag* mix broods at 19 hpf, I observed upregulation of MuRF family E3 ligases *trim55b*, (MuRF2b), *trim63a*, and *trim63b* compared to wild-type embryos (Figure 25A). As myosin thick filament sarcomere assembly appears normal in *herzschlag* mutants at 18 hpf (Figure 16B&B'), this upregulation was surprising and suggests that sarcomere damage exists and is being recognized by 19 hpf. As muscle contractions begin between 18 hpf and 19 hpf, this damage could be a consequence of initial muscle contractions. Interestingly, expression of the Unc45b quality control genes, *ube4b* and *stub1* were slightly, but still significantly, upregulated in *herzschlag* mix broods at 19 hpf. Together these data suggest that E3 ligase and UPS activity is occurring in both *steif* and *herzschlag* mutants during periods of sarcomere assembly. However, the contributions of specific E3 ligases to protein turnover are likely different between these mutants at this timepoint.

At 24 hpf, immunofluorescence of slow myosin shows a loss of staining in *herzschlag* mutants (Figure 17K&K'). At this same timepoint, qPCR of E3 ligases shows only significant differences between *herzschlag* mix broods and wild-type embryos in two of the five genes examined (Figure 25B), as opposed to the upregulation of 5/6 seen at 19 hpf (Figure 25A). As sarcomere assembly is complete by 24 hpf, upregulation at or after this time period could reflect genes involved in protein turnover associated with sarcomere maintenance. In mix brood *herzschlag* embryos, *trim63b* remains slightly elevated at 24 hpf and upregulation of the uncharacterized, teleost specific, *trim101* (MuRF4) is observed. A similar trend is shown in *steif* mix broods at this timepoint, where only *trim63b* remains statistically different from wild-type embryos. These data are consistent with the idea that different E3 ligases respond to myosin damage at the sarcomere assembly stages than those that respond to damage at the sarcomere maintenance stages.

I continued this analysis to 48 hpf, when fast myosin is disorganized in *herzschlag* mutants (Figure 22B) and slow muscle has been almost entirely lost (Figure 22E). At 48 hpf, the E3 ligases that were upregulated during the stages of slow muscle atrophy, *trim63b* and *trim101*, have either returned to baseline in *herzschlag* mutants or are significantly downregulated compared to wild-type animals (Figure 25C). In *steif* mutants at 48 hpf, I also see a return to baseline of *trim63b* and subsequent upregulation of *trim55b* and *trim63a* in comparison to wild-type (Figure 25C). Together these data suggest that differential E3 ligases respond to muscle damage in *herzschlag* and *steif* as well as during different stages of muscle development.

3.2.4 Slow muscle atrophy in *herzschlag* is dependent on the ubiquitin proteasome system, but ubiquitin proteasome system inhibition in *steif* exacerbates skeletal muscle atrophy

The E3 ligase expression data is consistent with UPS activity in *herzschlag* and *steif*, so I hypothesized that the loss of slow muscle tissue in *herzschlag* embryos was due to UPS mediated degradation. To test this hypothesis, I utilized the commonly used UPS inhibitor, MG132, to block proteasomal degradation from 22 hpf (before slow muscle is lost) to 48 hpf (when *herzschlag* embryos can be phenotypically identified from wild-type siblings). Various concentrations of MG132 (2 μM, 10 μM, 40 μM and 50 μM) were tested, with 50 μM being the lowest dose that affected the integrity of wild-type skeletal muscle. MG132 has previously been used in zebrafish to inhibit the proteasome at this concentration (Shimizu et al., 2017), therefore, 50 μM MG132 was used for the remainder of the experiments.

At 48 hpf, immunofluorescence of both DMSO treated wild-type controls and 50 μM MG132 treated wild-type fish show myofibrils with repeating striations (Figure 26A&B, insets A' and B'). DMSO treated *herzschlag* embryos (Figure 26C&C') and DMSO treated *steif* embryos (Figure 26E&E') both show diffuse staining of slow myosin, which appears faint in

herzschlag emrbyos. MG132 treated *herzschlag* embryos (Figure 26D) show an improvement in slow muscle integrity with an identifiable, intact, striated myofibril (inset D'). Interestingly, in MG132 treated *steif* mutants (Figure 26F&F'), slow muscle integrity is not improved and staining appears fainter than DMSO treated controls. To better examine muscle ultrastructure in these embryos, I examined MG132 and DMSO treated control embryos by H&E staining and Transmission Electron Microscopy.

H&E stained wild-type zebrafish treated with DMSO (Figure 26G) or MG132 (Figure 26H) appear mostly normal with some muscle disorganization occurring in MG132 treated embryos. Black arrowheads mark the slow muscle layer which looks comparable in both fish. In *herzschlag* H&E stained embryos treated with DMSO (Figure 26I), the loss of tissue in the peripheral slow muscle layer can again be seen (black arrowhead). MG132 treatment of *herzschlag* embryos (Figure 26J) does not appear to fully rescue this loss of tissue, but the gaps in staining appear less regular along the slow muscle layer (black arrowheads). MG132 treatment of *steif* embryos (Figure 26L) appears to have resulted in a global decrease in tissue staining (compare purple intensity between Figure 26K & Figure 26L) compared to DMSO treated controls (Figure 26K). This loss of staining appears uniform throughout slow and fast muscle, with black arrowheads marking the slow muscle layer.

To examine slow muscle integrity at a higher magnification, I took DMSO treated controls and MG132 treated embryos for TEM. Wild-type embryos treated with DMSO (Figure 26M) or MG132 (Figure 26N) both show organized bundles of myofibrils (yellow outline) in the slow muscle layer although the sarcolemma appears more disorganized in MG132 treated embryos (white coating around myofibril bundles). In contrast, DMSO treated *herzschlag* embryos have undergone a severe loss of slow muscle by 48 hpf (Figure 26O) with few to no

myofibril bundles remaining. When treated with MG132 (Figure 26P), these embryos have a dramatic retention of slow muscle proteins (Figure 26P) with some visible myofibrils (yellow circles). However, the tissue is still quite disorganized when compared to wild-type embryos, likely due to continually occurring contraction-induced muscle damage. DMSO treated *steif* embryos retain slow muscle into bundles (Figure 26Q; yellow circle) although the muscle is not organized properly in the myofibril likely due to a failure of the sarcomere to assemble normally. When treated with MG132, gaps in the bundled myofibrils appear (Figure 26R; yellow circles) as well as an increased number of abnormal mitochondria. In rat ventricular myocytes, MG132 treatment enhanced autophagy (Zheng et al., 2011), which is consistent with the appearance of abnormal mitochondria and absence of slow muscle tissue in MG132 treated *steif* mutants. Together, these data support the hypothesis that the *herzschlag titin2* mutation increases slow muscle degradation through the UPS, while the *steif* mutation sensitizes the fish to proteasome inhibition.

The combined results suggest that different mechanisms respond to myosin damage when it occurs during or before sarcomere assembly and when it occurs after sarcomere thick filament assembly is complete. *steif* represents a model system where myosin damage occurs before myosin thick filament assembly occurs, and the misfolded myosin response as well as specific E3 ligases respond to this myosin damage. In contrast, when myosin damage occurs after myosin is folded and incorporated into the sarcomere, as shown in *herzschlag* mutants, myosin chaperones do not respond to this damage, but specific E3 ligases do. Response to proteasome inhibition also differs in these mutants, with *steif* being more sensitive to muscle loss through other mechanisms when the proteasome is inhibited, when compared to *herzschlag* and wild-type embryos.

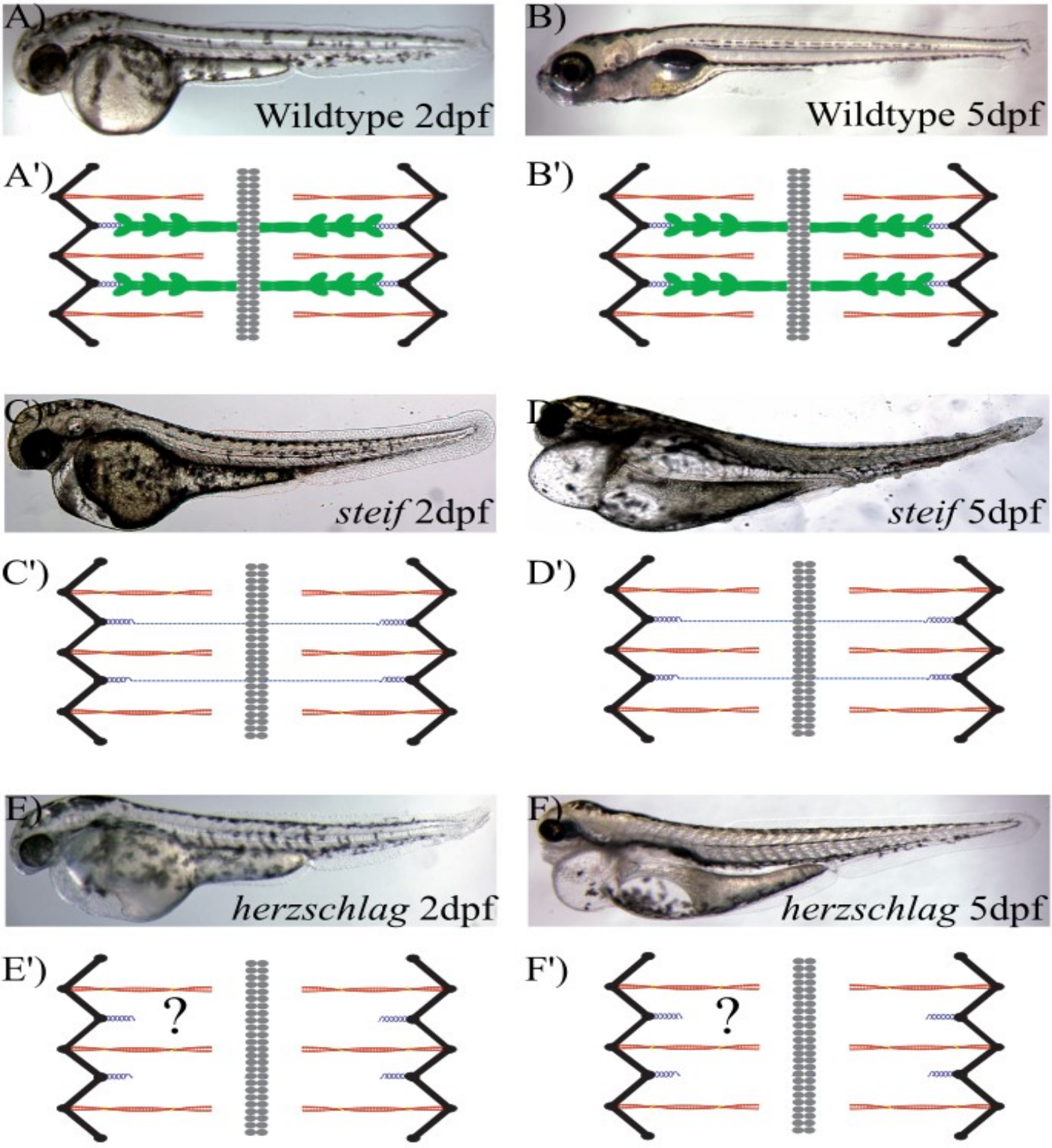
A)
Wildtype 2dpf
B)
Wildtype 5dpf
A')
B')
C)
steif 2dpf
D)
steif 5dpf
C')
D')
E)
herzschlag 2dpf
F)
herzschlag 5dpf
E')
?
F')
?

Figure 13: Selection of zebrafish muscle mutants to examine myosin thick filament quality control during sarcomere assembly and maintenance.

A) Wild-type zebrafish at 2 dpf with a schematic of the sarcomere (A') showing myosin assembled into thick filaments. B) Wild-type zebrafish at 5 dpf with a schematic of the sarcomere (B') showing myosin maintained into thick filaments. C) *Steif* mutant zebrafish at 2 dpf with a schematic of the sarcomere (C') showing a predicted failure of myosin thick filament assembly into the sarcomere. D) *Steif* mutant zebrafish at 5 dpf with a schematic of the sarcomere (D') showing a continuation of failure of myosin thick filament assembly into the sarcomere. E) *herzschlag* mutant zebrafish at 2 dpf and 5 dpf (F) with a schematic of the sarcomere (E'&F') showing truncated Titin2 and a question mark representing whether myosin thick filaments will assemble into the sarcomere and be maintained.

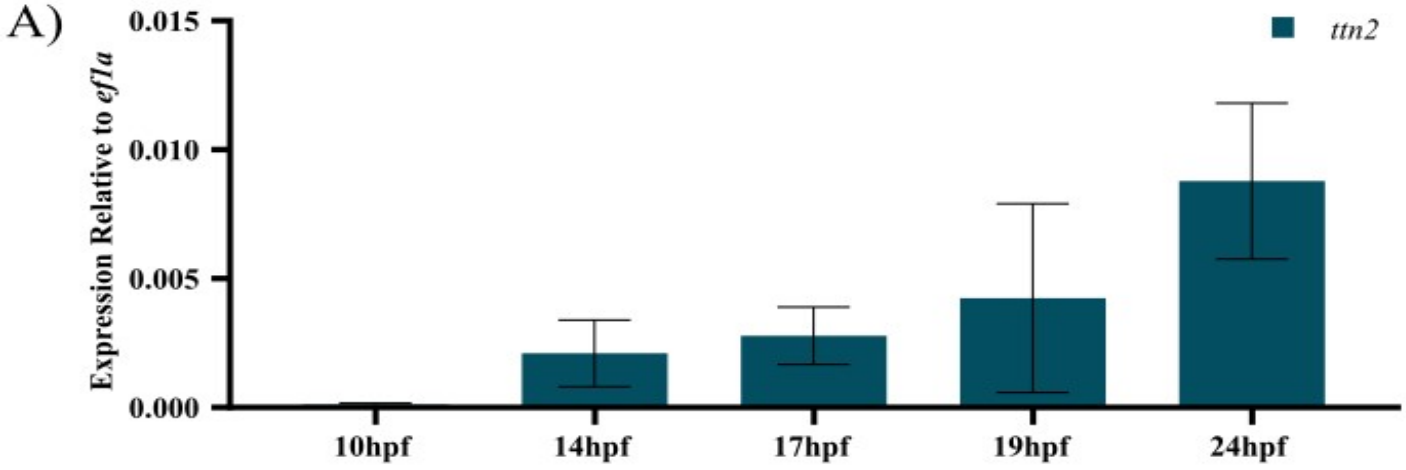
A)
0.015
0.010
0.005
0.000
Expression Relative to ef1a
ttn2
10hpf
14hpf
17hpf
19hpf
24hpf

ttn2

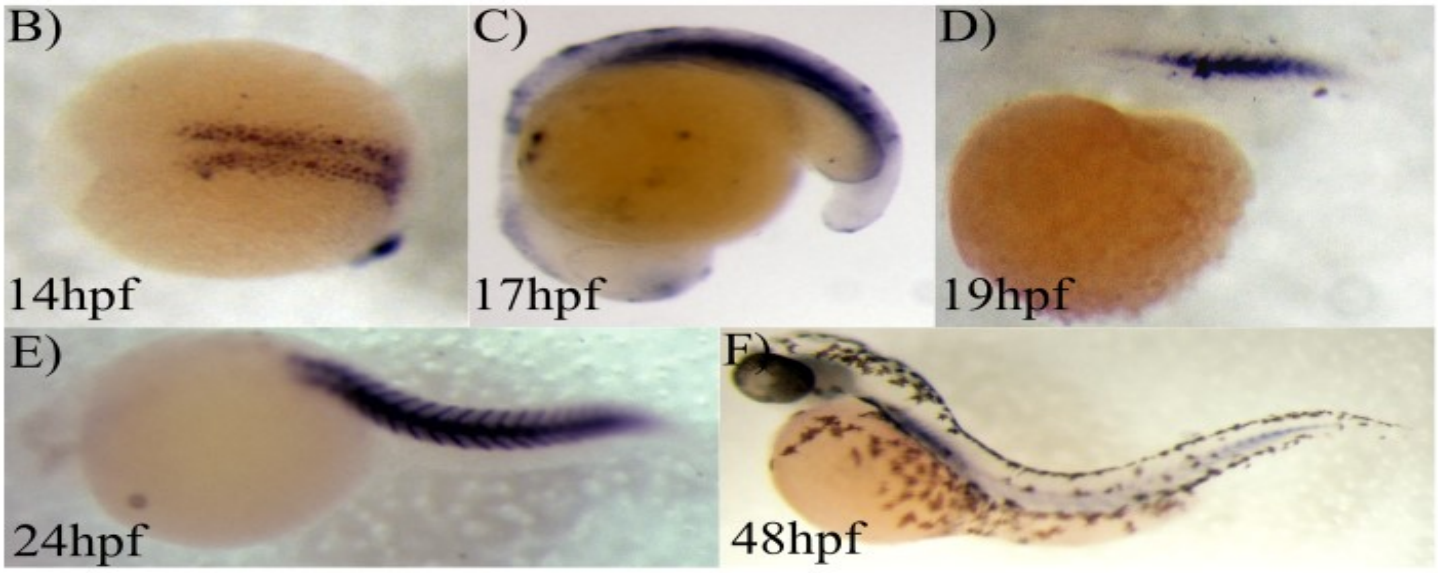
B)
14hpf
C)
17hpf
D)
19hpf
E)
24hpf
F)
48hpf

Figure 14: *titin2* is expressed in skeletal muscle during sarcomere assembly stages.

A) qPCR of *titin2* in wild-type zebrafish at 10 hpf, 14 hpf, 17 hpf, 19 hpf, and 24 hpf. Values plotted were determined by ΔCT relative to the housekeeping gene, *ef1a*. *titin2* is not expressed at 10 hpf in wild-type zebrafish, after which expression increases at timepoints that correlate with muscle specification and sarcomere assembly. B-F) *In situ* hybridization of *titin2* shows expression in somites and skeletal muscle at 14 hpf (B), 17 hpf (C), 19 hpf (D), 24 hpf (E), and 48 hpf (F).

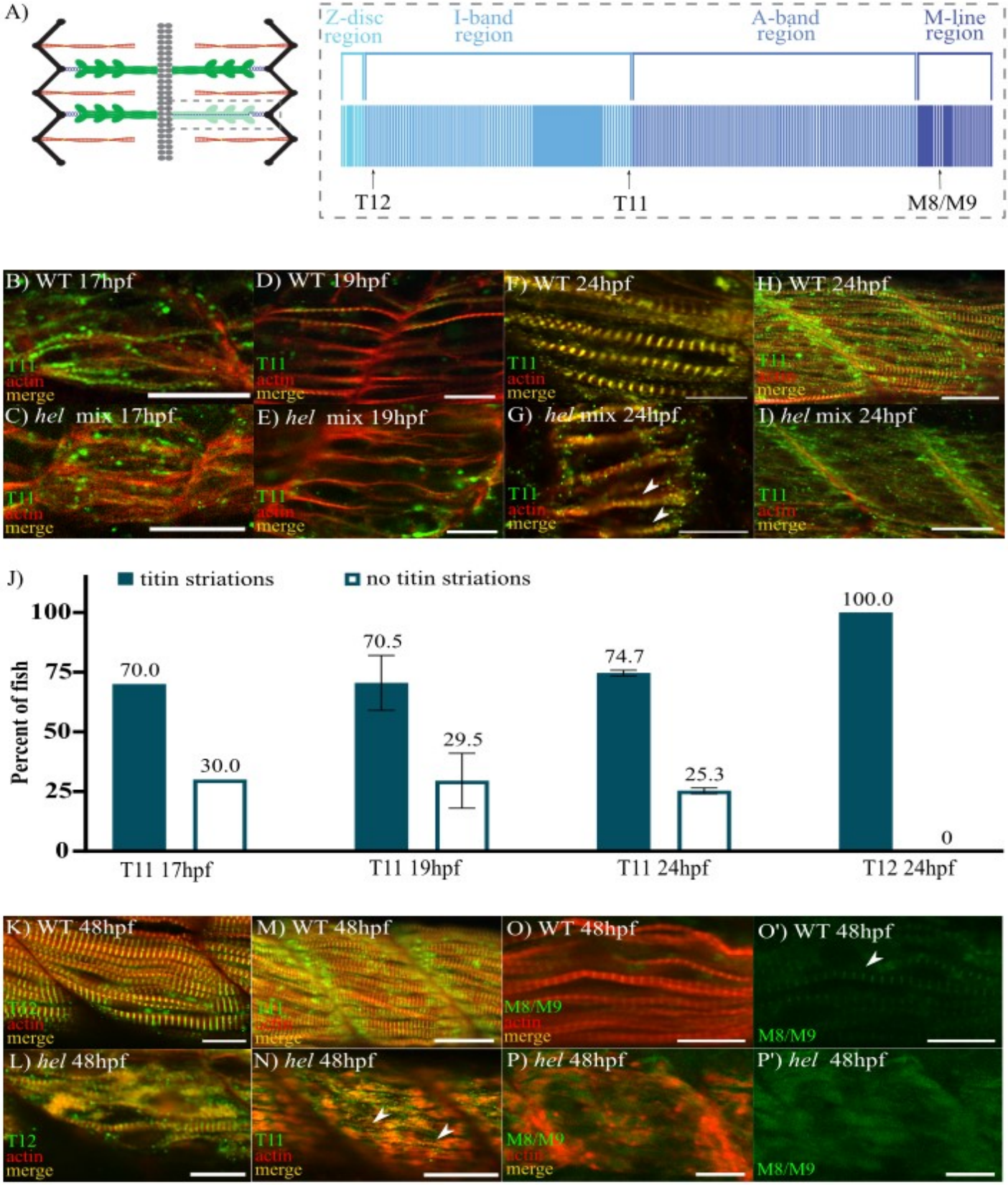
A)
Z-disc region
I-band region
A-band region
M-line region
T12
T11
M8/M9
B) WT 17hpf
C) hel mix 17hpf
D) WT 19hpf
E) hel mix 19hpf
F) WT 24hpf
G) hel mix 24hpf
H) WT 24hpf
I) hel mix 24hpf
T11
actin
merge
J)
titin striations
no titin striations
Percent of fish
100
75
50
25
0
70.0
30.0
70.5
29.5
74.7
25.3
100.0
0
T11 17hpf
T11 19hpf
T11 24hpf
T12 24hpf
K) WT 48hpf
L) hel 48hpf
M) WT 48hpf
N) hel 48hpf
O) WT 48hpf
P) hel 48hpf
O') WT 48hpf
P') hel 48hpf
T12
T11
M8/M9

Figure 15: The *titin2* mutation in *herzschlag* results in an interruption of the A-band region of the Titin2 protein.

A) Schematic of the sarcomere with Titin2 (inset) magnified. Antibody binding sites are indicated with arrows. B-E) Immunofluorescence of T11 (green) and actin (phalloidin; red) in wild-type embryos at 17 hpf (B) shows colocalization of green and red staining some myofibers fibers indicating presence of A-band Titin2. This colocalization is not apparent in a subset of *herzschlag* mix brood embryos at 17 hpf (C). Scale bars are 20 μm. Wild-type embryos at 19 hpf (D) show striated staining indicating incorporation of the Titin2 A-band into sarcomeres. This striated staining is absent in a subset of *herzschlag* mix brood embryos at 19 hpf (E). Scale bars are 10 μm. F-G) Immunofluorescence of T12 (green) and actin (phalloidin; red) in wild-type embryos at 24 hpf (F) shows striated staining indicating incorporation of the Titin2 Z-disc region into sarcomeres. Striations (arrowheads) are also detectable in *herzschlag* mix brood embryos (G). Scale bars are 10 μm. H-I) Immunofluorescence of T11 (green) and actin (phalloidin; red) in wild-type embryos at 24 hpf (H) shows striated staining indicating incorporation of the Titin2 Z-disc region into sarcomeres. Striated staining is not detectable in a subset of *herzschlag* mix brood embryos at 24 hpf (I). (J) Quantification of embryos showing in presence or absence of striated Titin2 staining. Error bars represent standard error. K-L) Immunofluorescence of T12 (green) and actin (phalloidin; red) in wild-type embryos at 48 hpf (K) shows striated staining indicating incorporation of the Titin2 Z-disc region into sarcomeres. Striations are also detectable in *herzschlag* embryos (L). Scale bars are 10 μm. (M-N) Immunofluorescence of T11 (green) and actin (phalloidin; red) in wild-type embryos at 48 hpf (M) shows striated staining indicating incorporation of the Titin2 Z-disc region into sarcomeres. Striations are also detectable in *herzschlag* embryos (N). Scale bars are 20 μm. (O-P') Immunofluorescence of

M8/M9 (green) and actin (phalloidin; red) in wild-type embryos at 48 hpf (O) shows striated staining indicating incorporation of the Titin2 Z-disc region into sarcomeres. (O') shows only the green channel with striations marked by an arrowhead. Striations are not detectable in *herzschlag* embryos (P, green only channel P'). Scale bars are 10 μm.

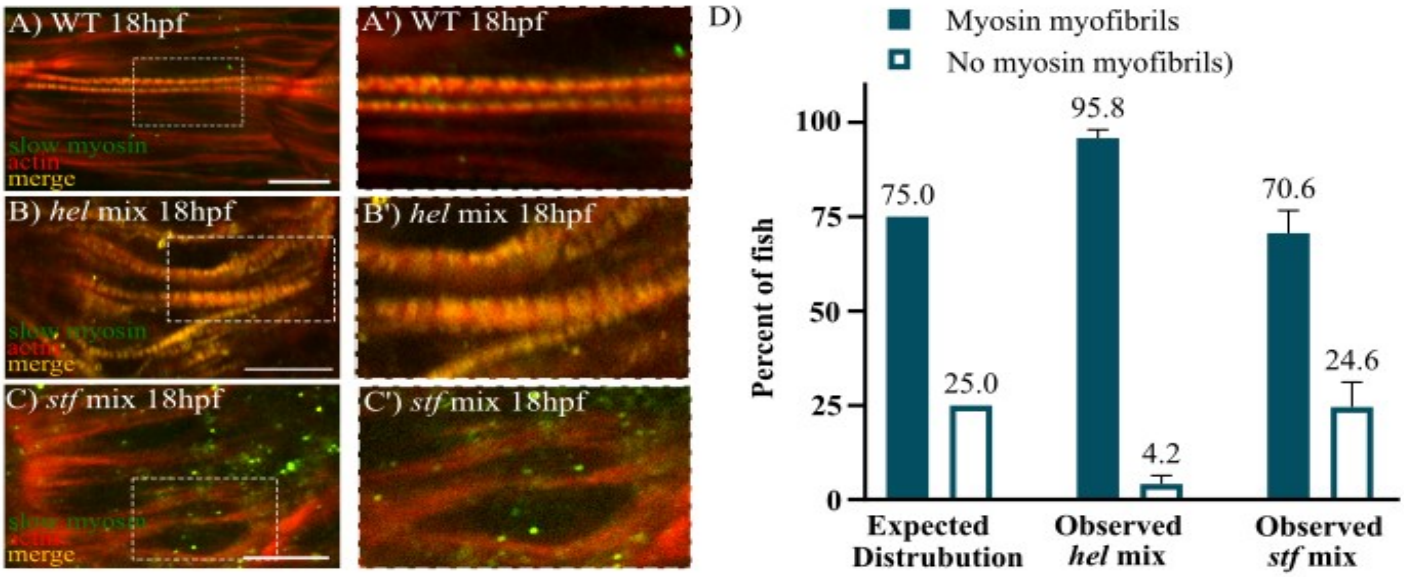
A) WT 18hpf
slow myosin
actin
merge
A') WT 18hpf
B) hel mix 18hpf
slow myosin
actin
merge
B') hel mix 18hpf
C) stf mix 18hpf
slow myosin
actin
merge
C') stf mix 18hpf
D)
Myosin myofibrils
No myosin myofibrils)
Percent of fish
100
75
50
25
0
75.0
25.0
95.8
4.2
70.6
24.6
Expected Distrubution
Observed hel mix
Observed stf mix

Figure 16: Myosin thick filament assembly is normal in *herzschlag*, but not *steif* mutants.

(A&A') Immunofluorescence of slow myosin (F59) and actin (phalloidin) in 18 hpf wild-type zebrafish shows normal incorporation of myosin into sarcomeres. Myosin thick filaments also form in 95% of *herzschlag* mix brood embryos (B&B'). In *steif* mix brood embryos, 25% of the embryos fail to incorporate myosin into developing myofibrils (C&C', quantification in D). Scale bars are 10 μm. Error bars represent standard error.

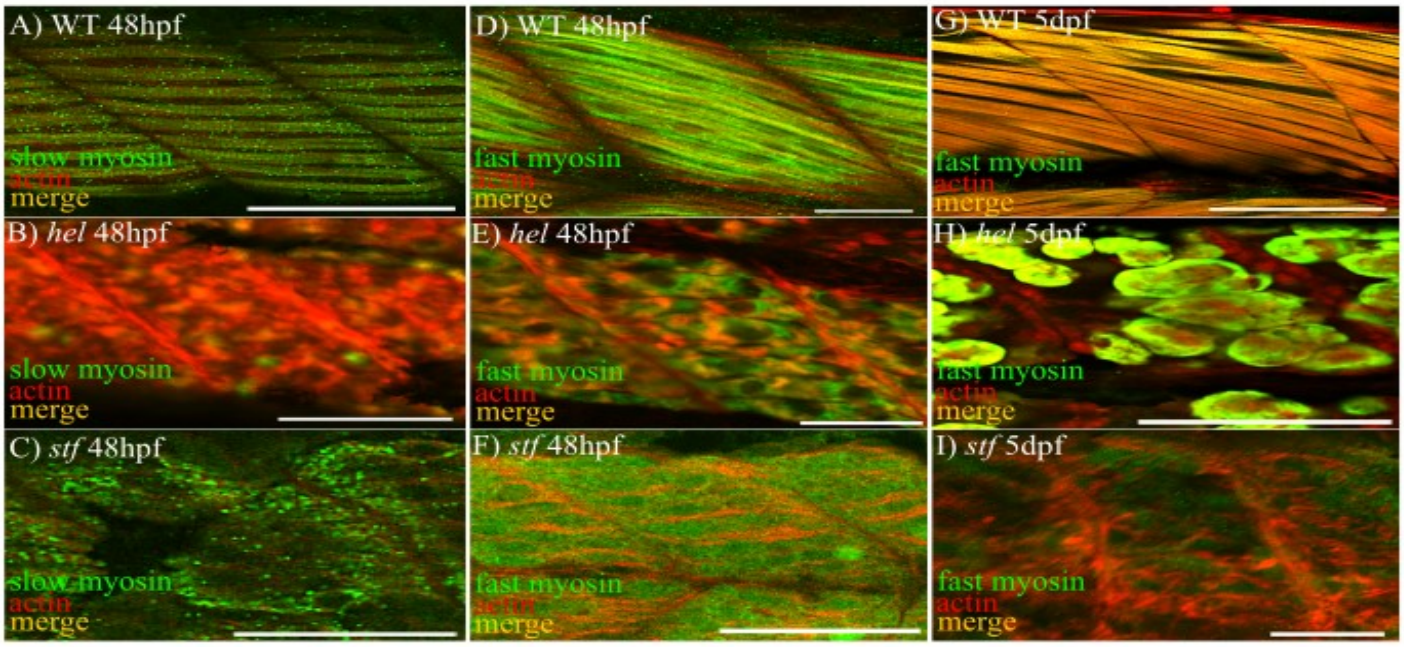
A) WT 48hpf
slow myosin
actin
merge
D) WT 48hpf
fast myosin
actin
merge
G) WT 5dpf
fast myosin
actin
merge
B) hel 48hpf
slow myosin
actin
merge
E) hel 48hpf
fast myosin
actin
merge
H) hel 5dpf
fast myosin
actin
merge
C) stf 48hpf
slow myosin
actin
merge
F) stf 48hpf
fast myosin
actin
merge
I) stf 5dpf
fast myosin
actin
merge

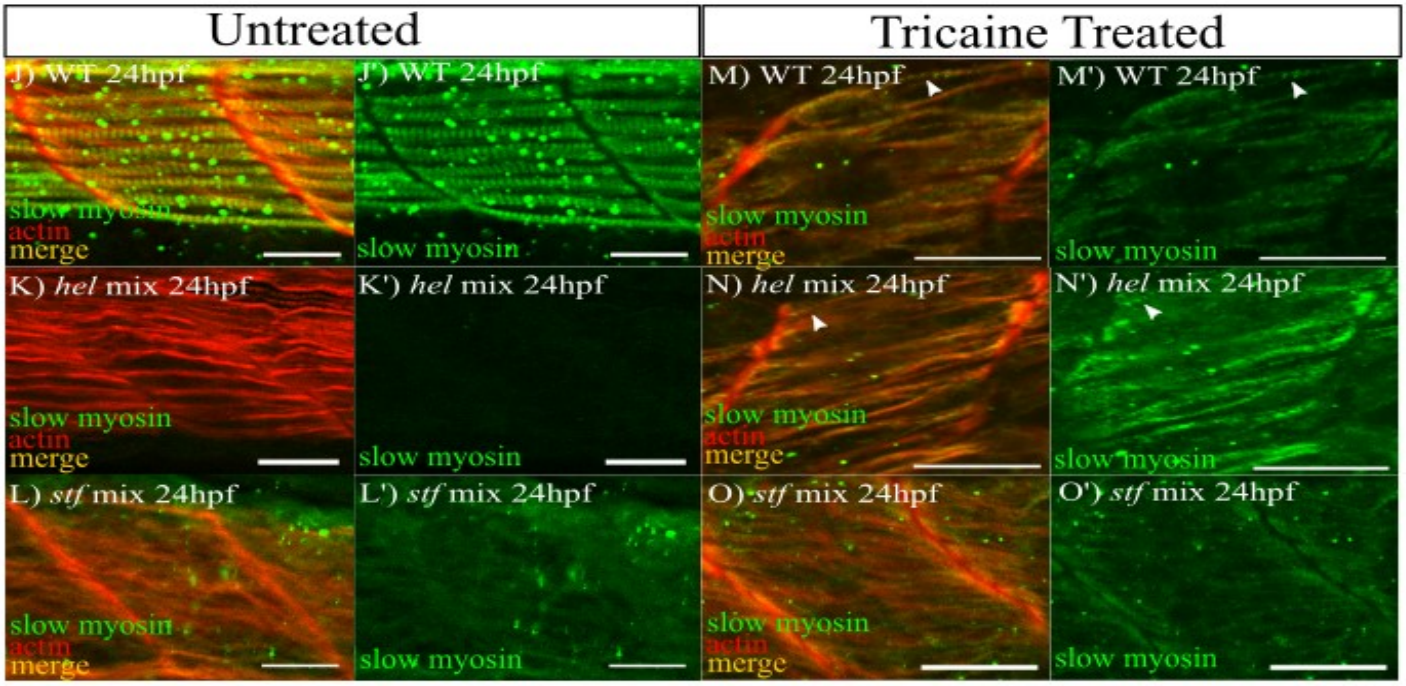
Untreated
Tricaine Treated
J) WT 24hpf
slow myosin
actin
merge
J') WT 24hpf
slow myosin
M) WT 24hpf
slow myosin
actin
merge
M') WT 24hpf
slow myosin
K) hel mix 24hpf
slow myosin
actin
merge
K') hel mix 24hpf
slow myosin
N) hel mix 24hpf
slow myosin
actin
merge
N') hel mix 24hpf
slow myosin
L) stf mix 24hpf
slow myosin
actin
merge
L') stf mix 24hpf
slow myosin
O) stf mix 24hpf
slow myosin
actin
merge
O') stf mix 24hpf
slow myosin

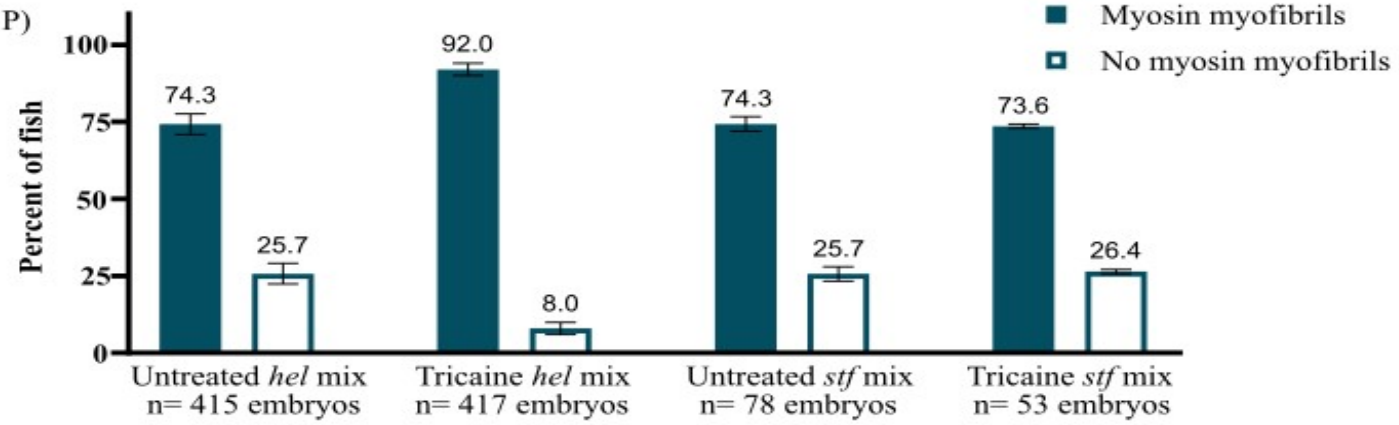
P)
Myosin myofibrils
No myosin myofibrils
Percent of fish
100
75
50
25
0
74.3
25.7
92.0
8.0
74.3
25.7
73.6
26.4
Untreated hel mix
n= 415 embryos
Tricaine hel mix
n= 417 embryos
Untreated stf mix
n= 78 embryos
Tricaine stf mix
n= 53 embryos

Figure 17: Slow myosin damage in *herzschlag* is contraction induced.

A-C) Immunofluorescence of slow myosin (green) and actin (phalloidin; red) in wild-type embryos at 48 hpf (A) shows striated staining indicating slow myosin incorporation into sarcomeres. This organization is lost in *herzschlag* mutants (B) and *steif* mutants (C), although *herzschlag* slow myosin staining appears much fainter. D-I) Immunofluorescence of fast myosin (green) and actin (phalloidin; red) in wild-type embryos at 48 hpf (D) shows striated staining indicating fast myosin incorporation into sarcomeres. This organization is lost in both *herzschlag* mutants (E) and *steif* mutants (F). Immunofluorescence of fast myosin (green) and actin (phalloidin; red) in wild-type embryos at 5 dpf (G) shows striated staining indicating fast myosin incorporation into sarcomeres. Large protein aggregates appear in *herzschlag* embryos (H) instead of myofibrils while *steif* embryos show a general lack of staining (I). Scale bars are 50μm. Immunofluorescence of slow myosin (green) and actin (phalloidin; red) in untreated wild-type embryos at 24 hpf (J) show striated staining indicating slow myosin incorporation into sarcomeres. (J') shows green channel only. In *herzschlag* mix brood embryos, a subset of embryos display faint or no slow myosin staining (K&K'), while a subset of *steif* mix brood embryos (L&L') show diffuse slow myosin staining and an absence of slow myosin striations. Immunofluorescence of slow myosin (green) and actin (phalloidin; red) in embryos treated with tricaine from 17 hpf to 24 hpf shows global reduction in staining and general disorganization of muscle tissue in all embryos examined. In wild-type embryos (M&M') slow myosin sarcomeres are visible in a few fibers (arrowheads) as well as in the majority of *herzschlag* mix brood embryos (N&N'; arrowheads). However, myosin myofibrils still do not form in a subset of *steif* mix brood embryos (O&O'). Scale bars are 20μm. (P) Quantification of myosin myofibrils in untreated and tricaine treated embryos. Error bars represent standard error.

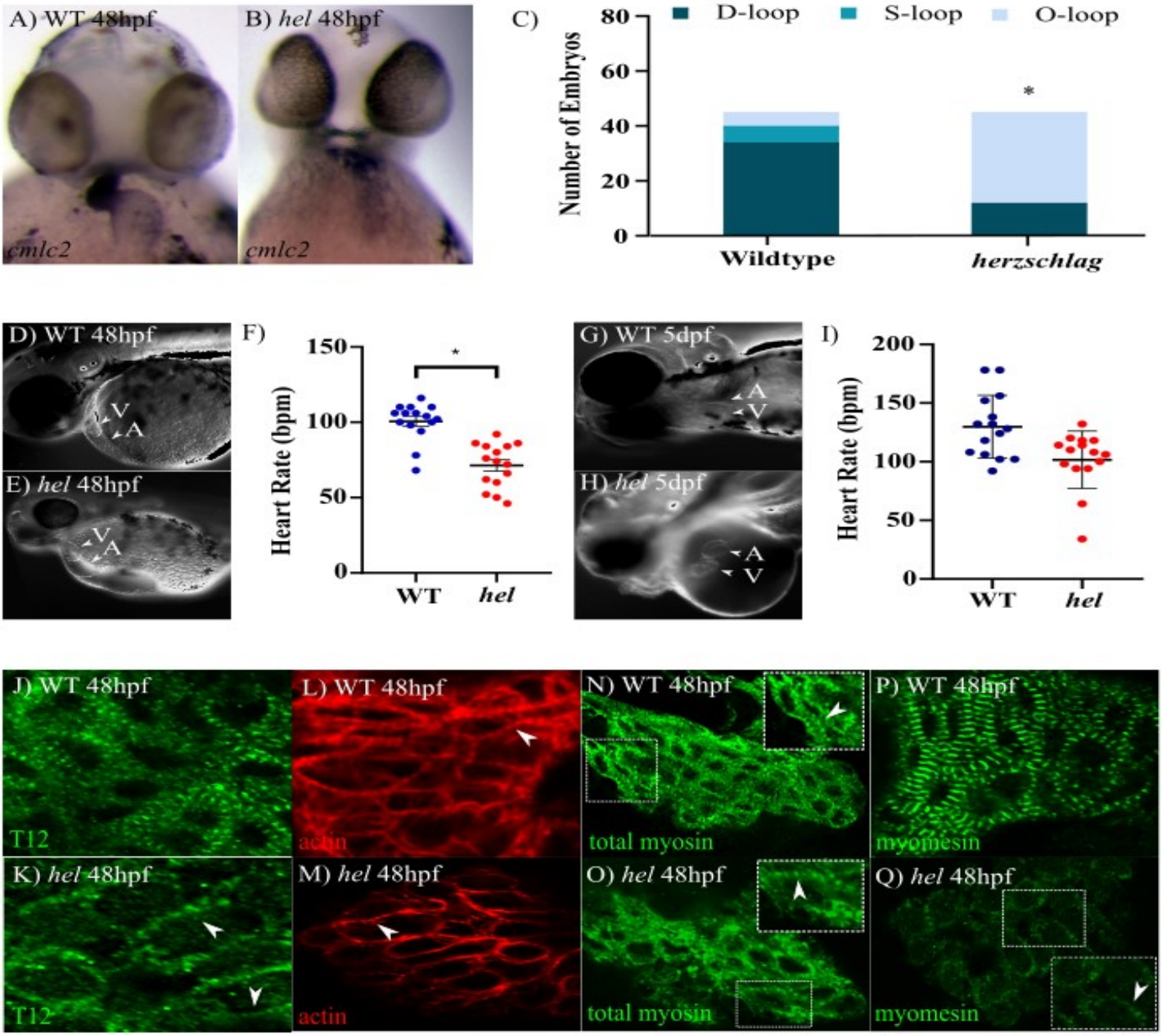
A) WT 48hpf
cmlc2
B) hel 48hpf
cmlc2
C)
D-loop
S-loop
O-loop
Number of Embryos
80
60
40
20
0
*
Wildtype
herzschlag
D) WT 48hpf
V
A
E) hel 48hpf
V
A
F)
Heart Rate (bpm)
150
100
50
0
*
WT
hel
G) WT 5dpf
A
V
H) hel 5dpf
A
V
I)
Heart Rate (bpm)
200
150
100
50
0
WT
hel
J) WT 48hpf
T12
K) hel 48hpf
T12
L) WT 48hpf
actin
M) hel 48hpf
actin
N) WT 48hpf
total myosin
O) hel 48hpf
total myosin
P) WT 48hpf
myomesin
Q) hel 48hpf
myomesin

Figure 18: Heart morphology is abnormal and heart function is decreased in *herzschlag* embryos although cardiac sarcomeres are intact.

cmlc2 in situ hybridization of wild-type hearts at 48 hpf (A) and *herzschlag* hearts at 48 hpf (B) show normal D-looping in the majority of wild-type hearts, while most *herzschlag* hearts are unlooped (C; $p<0.05$). DIC optical images of wild-type hearts (D) and *herzschlag* hearts (E) at 48 hpf show looping defects and pericardial and yolk sac edema in *herzschlag* embryos. F) Heart function measured as beats per minute (bpm) is significantly decreased in *herzschlag* embryos at 48 hpf compared to wild-type siblings ($p<0.0005$). Wild-type hearts (G) and *herzschlag* mutant hearts (H) at 5 dpf show severe changes to cardiac morphology and pronounced edema in *herzschlag* embryos. (I) Heart function measured as beats per minute shows a reduction in *herzschlag* embryos, although it is not statistically significant ($p=0.056$). J-K) Z disc integrity, measured by immunofluorescence of an epitope at the Titin2 N-terminus (T12; green) shows striations (arrowheads) in wild-type and *herzschlag* hearts. L-M) Immunofluorescence of actin (phalloidin; red) shows striations (arrowheads) in wild-type and *herzschlag* embryos. N-O) Immunofluorescence of total myosin (MF20; green) shows striations (arrowheads) in wild-type and *herzschlag* embryos, although *herzschlag* thick filaments are disorganized. P-Q) Immunofluorescence of myomesin (green) shows striations in wild-type embryos and faintly in *herzschlag* embryos (arrowhead).

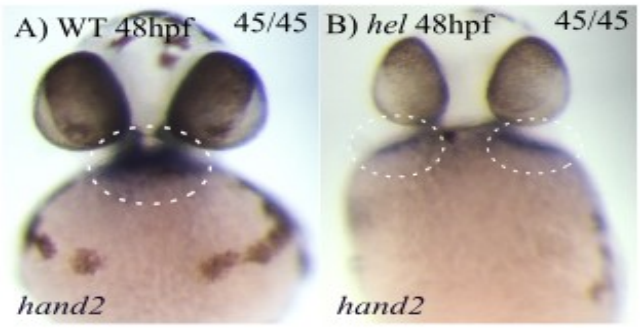
A) WT 48hpf
45/45
B) hel 48hpf
45/45
hand2
hand2

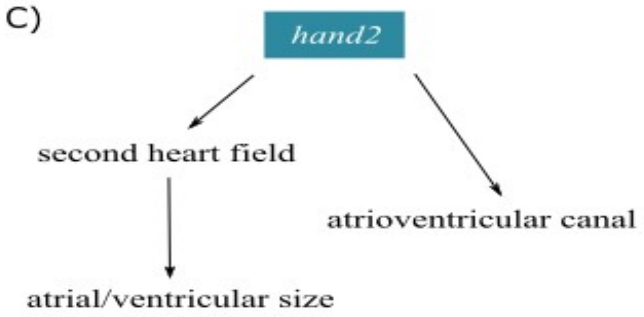
C)
hand2
second heart field
atrioventricular canal
atrial/ventricular size

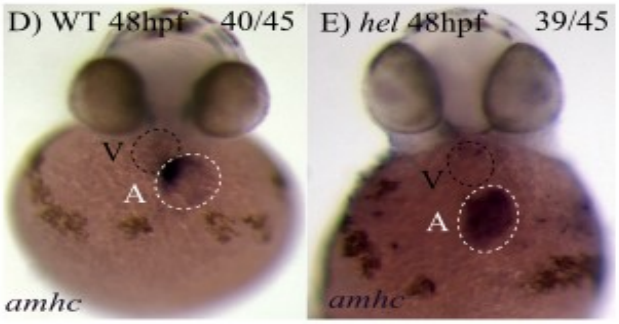
D) WT 48hpf
40/45
E) hel 48hpf
39/45
V
A
V
A
amhc
amhc

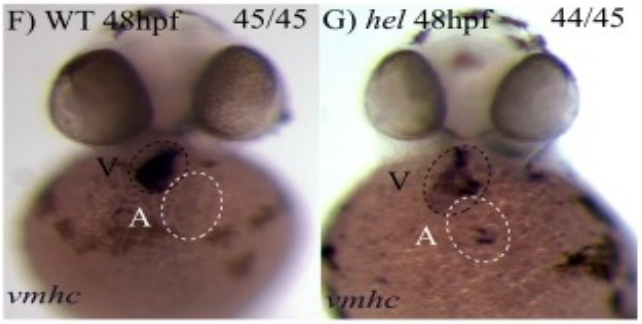
F) WT 48hpf
45/45
G) hel 48hpf
44/45
V
A
V
A
vmhc
vmhc

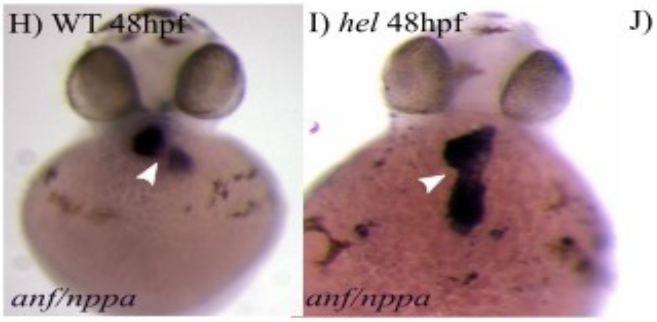
H) WT 48hpf
I) hel 48hpf
anf/nppa
anf/nppa

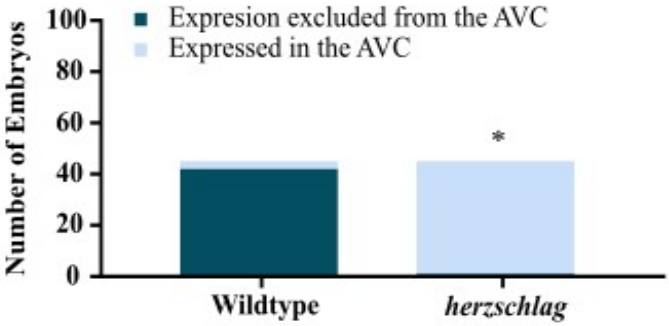
J)
Expresion excluded from the AVC
Expressed in the AVC
Number of Embryos
100
80
60
40
20
0
*
Wildtype
herzschlag

Figure 19: Changes in *hand2* expression in *herzschlag* embryos correlates with AVC patterning defects.

A-B) *In situ* hybridization of *hand2* RNA probe shows spatial changes in expression in *herzschlag* embryos compared to wild-type siblings (white circles). C) Simplified schematic of *hand2* regulation of cardiac development. D-E*) In situ* hybridization of atrial myosin shows expression restricted to the atrium in *herzschlag* and wild-type siblings. F-G) *In situ* hybridization of ventricular myosin shows expression restricted to the ventricle in *herzschlag* and wild-type siblings. H-I) *In situ* hybridization of *anf*/*nppa* shows expression is excluded from the atrioventricular canal (AVC) in wild-type siblings, but not *herzschlag* embryos (white arrowheads in H and I). Quantification of *nppa* expression is shown in (J), $p<0.05$ (Fisher's exact test). V – ventricle; A – atrium.

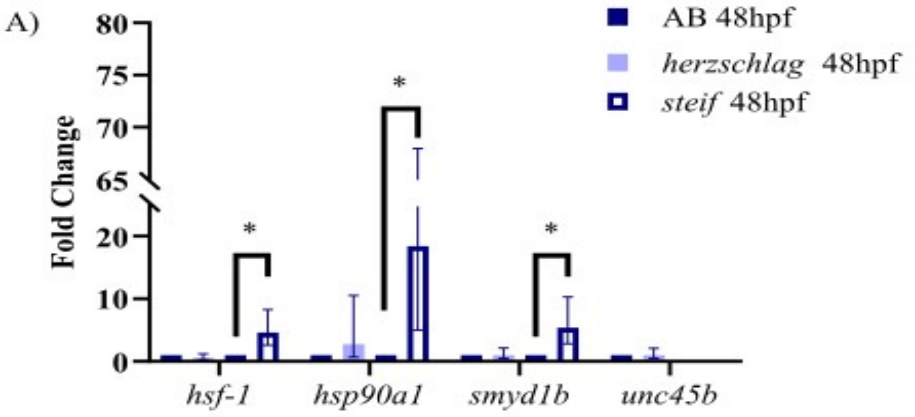
A)
AB 48hpf
herzschlag 48hpf
steif 48hpf
Fold Change
80
75
70
65
20
10
0
*
*
*
hsf-1
hsp90a1
smyd1b
unc45b

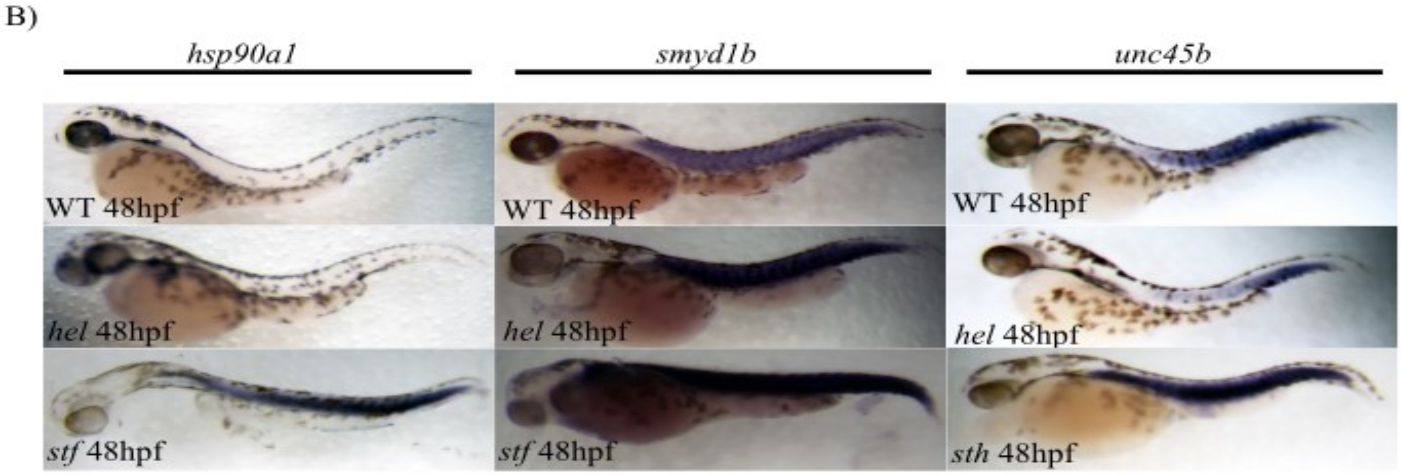
B)
hsp90a1
smyd1b
unc45b
WT 48hpf
WT 48hpf
WT 48hpf
hel 48hpf
hel 48hpf
hel 48hpf
stf 48hpf
stf 48hpf
sth 48hpf

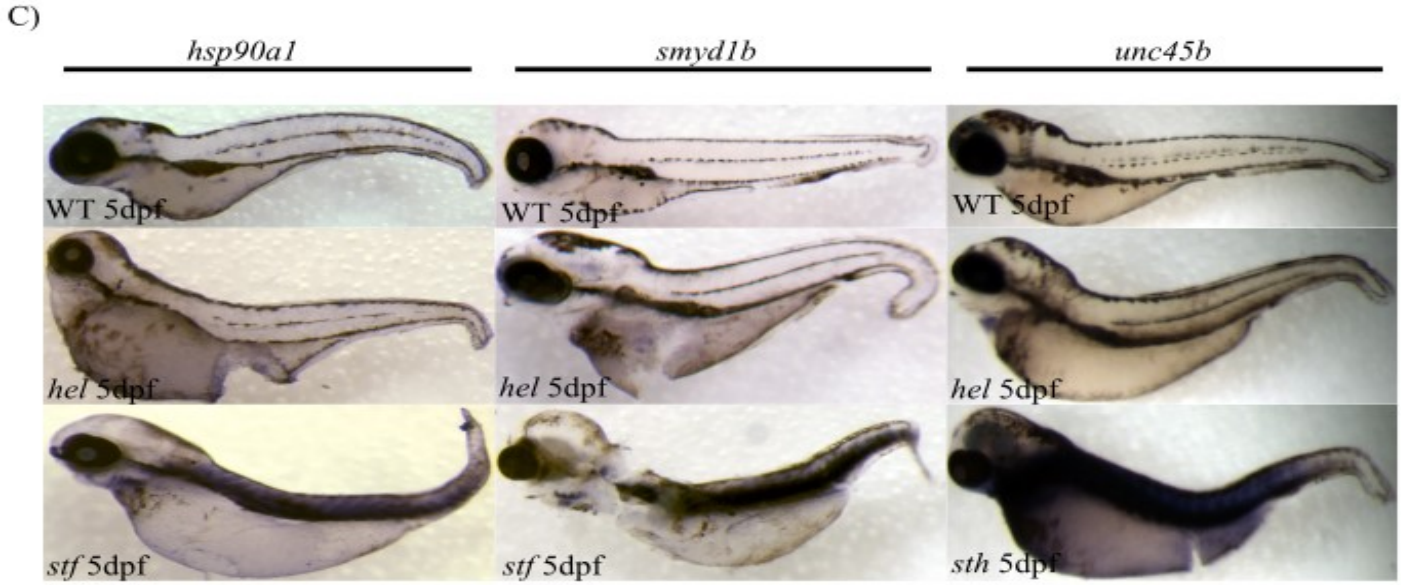
C)
hsp90a1
smyd1b
unc45b
WT 5dpf
WT 5dpf
WT 5dpf
hel 5dpf
hel 5dpf
hel 5dpf
stf 5dpf
stf 5dpf
sth 5dpf

Figure 20: The Misfolded Myosin Response does not occur in *herzschlag* mutants.

A) qPCR of genes involved in the misfolded myosin response: *hsf-1*, *hsp90a1*, *smyd1b*, and *unc45b* were compared between 48 hpf wild-type (AB) zebrafish and 48 hpf *herzschlag* mutants, or 48 hpf wild-type (AB) zebrafish and 48 hpf *steif* mutants. Fold change from wild-type is plotted with error bars representing standard deviation and accounting for propagation of error and linear transformation of data. These genes are strongly upregulated in *steif* mutants compared to wild-type controls (p= 0.02; 0.02; 0.01 for *hsf-1*, *hsp90a1*, and *smyd1b* as determined by a t-test on ddCT values). Expression of *unc45b* in *steif* mutants was not calculated because the *steif* mutation is in this gene. No statistically significant upregulation of these genes occur in *herzschlag* mutants (p= 0.27; 0.26; 0.97; 0.96 for *hsf-1*, *hsp90a1*, *smyd1b*, and *unc45b* as determined by a t-test on ddCT values). B) *in situ* hybridization of *hsp90a1*, *smyd1b*, and *unc45b* at 48 hpf. Probe staining (purple) is limited to skeletal muscle and appears darker in *steif* embryos for *hsp90a1* and *smyd1b* compared to wild-type and *herschlag* embryos, although *herzschlag smyd1b* embryos show darker staining than wild-type. *unc45b* staining is darker in *still heart* embryos compared to wild-type or *herzschlag* embryos. C) *in situ* hybridization of *hsp90a1*, *smyd1b*, and *unc45b* at 5 dpf. No staining is apparent in *herzschlag* or wild-type embryos, but strong upregulation of *hsp90a1* and *smyd1b* is present in *steif* skeletal muscle, and *unc45b* is strongly upregulated in *still heart* skeletal muscle. *unc45b* staining appears in the 5 dpf *herzschlag* heart.

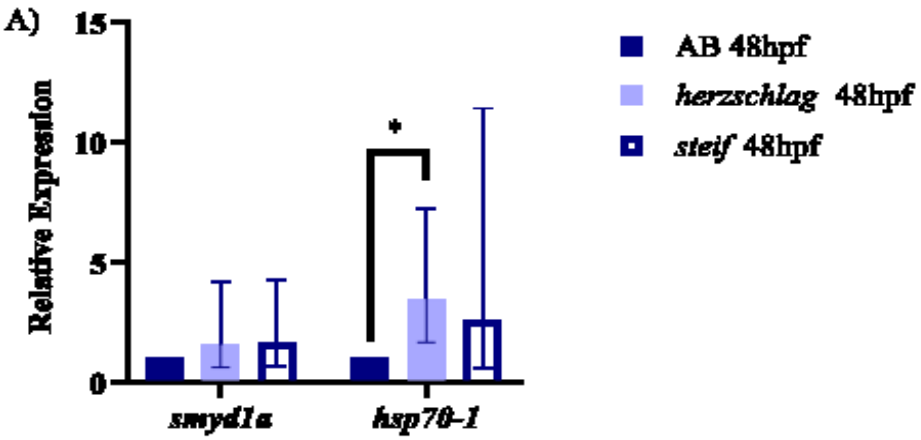
A)
15
10
5
0
Relative Expression
*
smyd1a
hsp70-1
AB 48hpf
herzschlag 48hpf
steif 48hpf

Figure 21: Muscle chaperones are not globally upregulated in *steif* mutants and *hsp70-1* is upregulated in *herzschlag*.

A) qPCR of chaperones *smyd1a* and *hsp70-1* were compared between 48 hpf wild-type (AB) zebrafish and 48 hpf *herzschlag* mutants, or 48 hpf wild-type (AB) zebrafish and 48 hpf *steif* mutants. Fold change from wild-type is plotted with error bars representing standard deviation and accounting for propagation of error and linear transformation of data. *smyd1a* is not upregulated significantly from wild-type in either *steif* or *herzschlag* ($p=0.41$ and $p=0.21$ as determined by a t-test on ddCT values). Expression of *hsp70-1* is upregulated in *herzschlag* mutants compared to wild-type ($p=0.042$), but expression is not significantly different between *steif* mutants and wild-type ($p=0.33$).

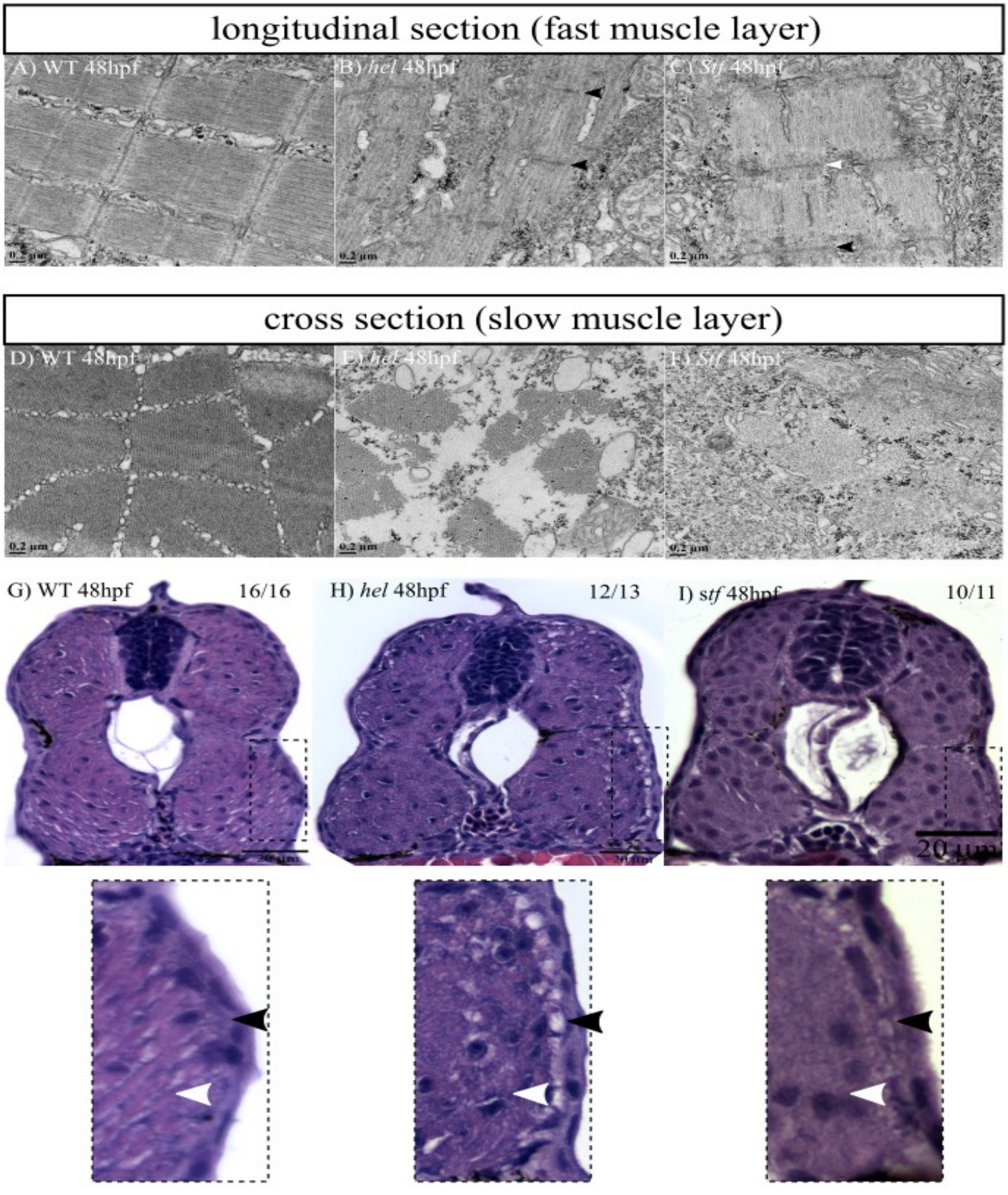
longitudinal section (fast muscle layer)
A) WT 48hpf
B) hel 48hpf
C) Stf 48hpf
0.2 μm
cross section (slow muscle layer)
D) WT 48hpf
E) hel 48hpf
F) Stf 48hpf
0.2 μm
G) WT 48hpf 16/16
H) hel 48hpf 12/13
I) stf 48hpf 10/11
20 μm

Figure 22: *herzschlag* embryos display a slow-muscle-specific atrophy at 48 hpf.

A-C) Transmission electron microscopy (TEM) of longitudinal sections into the fast muscle layer of the zebrafish embryo show aligned sarcomeres in WT siblings (A) but this organization is lost in *herzschlag* (B) and *steif* (C) embryos. Z-discs are still visible in some sarcomeres in these mutants (arrowheads). D-F) TEM of cross sections in the slow muscle layer of WT siblings (D) show bundled myofibrils. Myofibril bundling is lost in *herzschlag* (E) and *steif* (F) embryos, with an additional loss of tissue noticeable in the *herzschlag* embryos. G-I) H&E-stained cross sections of *herzschlag* embryos show a loss of slow muscle tissue that is not present in *steif* embryos or in WT siblings. Insets show black arrowheads marking the slow muscle layer while white arrowheads are in fast muscle tissue.

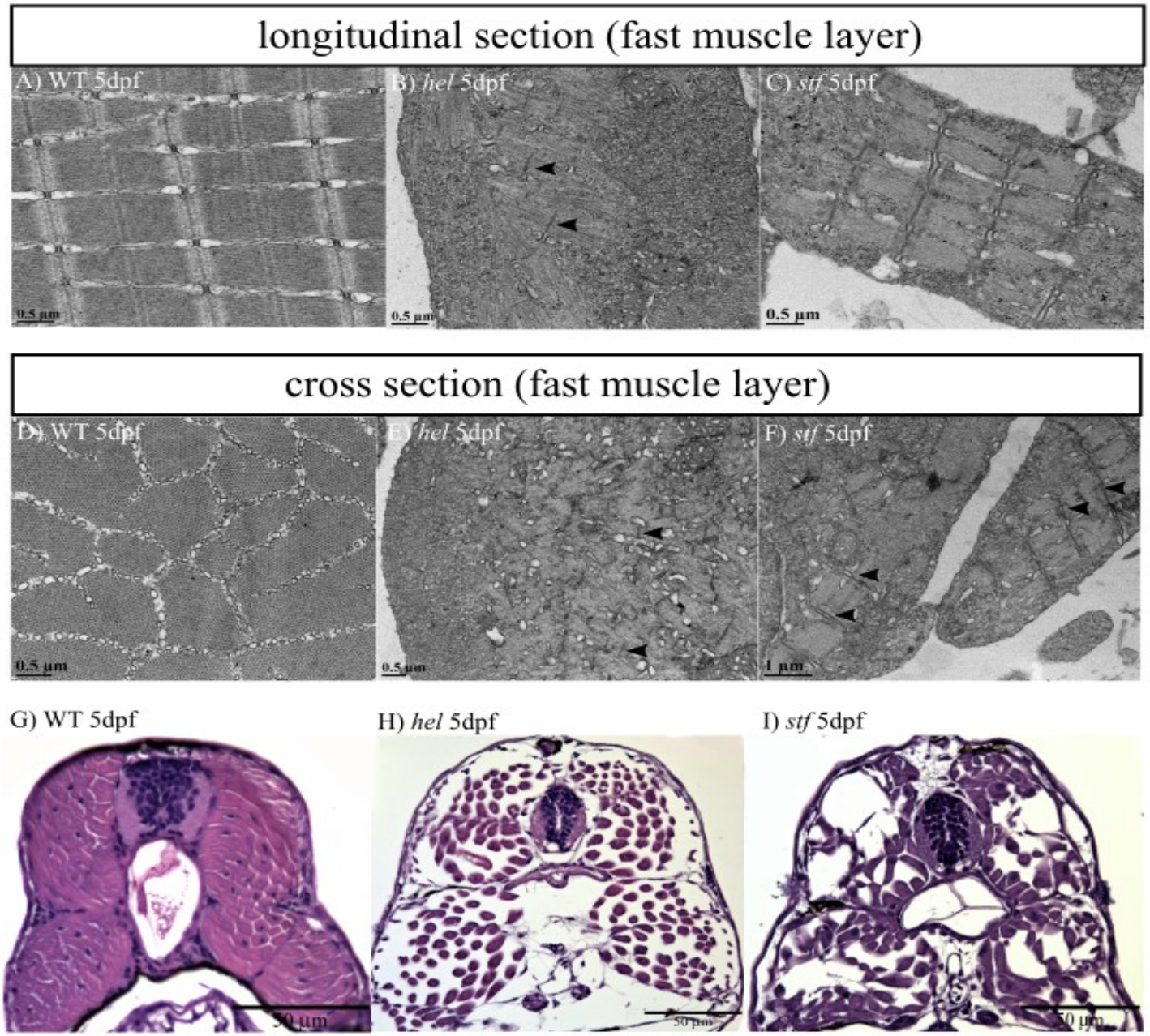
longitudinal section (fast muscle layer)
A) WT 5dpf
B) hel 5dpf
C) stf 5dpf
0.5 µm
cross section (fast muscle layer)
D) WT 5dpf
E) hel 5dpf
F) stf 5dpf
0.5 µm
1 µm
G) WT 5dpf
H) hel 5dpf
I) stf 5dpf
50 µm
J)
Number of Myofibril Bundles
0
20
40
60
80
WT
hel
stf
*
K)
Cross Sectional Area (um2)
0
50
100
150
200
WT
hel
stf
*

Figure 23: *herzschlag* and *steif* embryos show severe muscle atrophy by 5 dpf.

A-C) TEM of longitudinal sections of *herzschlag* (B) and *Stf* (C) embryos show a loss of sarcomere alignment compared to Wild-type siblings (A). Z-discs appear in both mutants (see arrowheads in *herzschlag*) as well as I-bands, but A-band and M-line structures are lost. D-F) TEM of cross sections of *herzschlag* (E) and *steif* (F) show a jumble of sarcomere components with some residual Z-discs (arrowheads) and a complete loss of myofibril bundling compared to Wild-type siblings (D). G-I) H&E staining of *herzschlag* (H) and *steif* (I) embryos show a complete loss of the slow muscle layer and severe atrophy in the interior fast muscle layer compared to Wild-type siblings (G). J) Quantification of myofibril bundles counted in the top left hand quadrant of the cross sectioned embryos show a significant reduction in *herzschlag* ($p< 0.0001$; One-Way ANOVA with Dunnett's multiple comparison test) and in *steif* embryos ($p<0.0001$; One-Way ANOVA with Dunnett's multiple comparison test) when compared to wild-type embryos. K) Cross sectional area of myofibril bundles was calculated using ImageJ. The average cross sectional area of five myofibril bundles is plotted for each embryo examined. *herzschlag* and *steif* embryos both show a significant reduction in myofibril bundle cross sectional area compared to wild-type embryos ($p=0.016$; $p=0.003$; One-Way ANOVA with Dunnett's multiple comparison test).

A) WT 48hpf

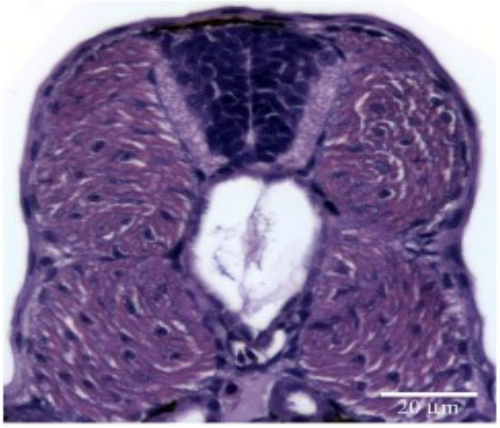

B) *sth* 48hpf

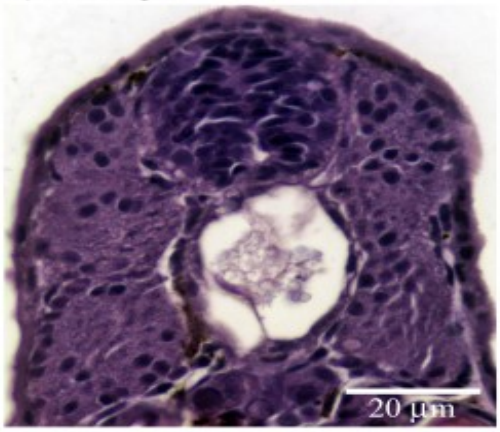

C) WT 5dpf

D) *sth* 5dpf

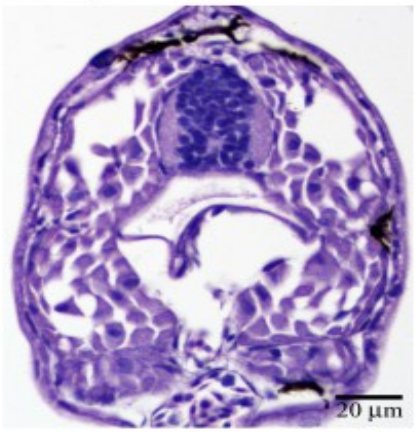

E) WT 7dpf

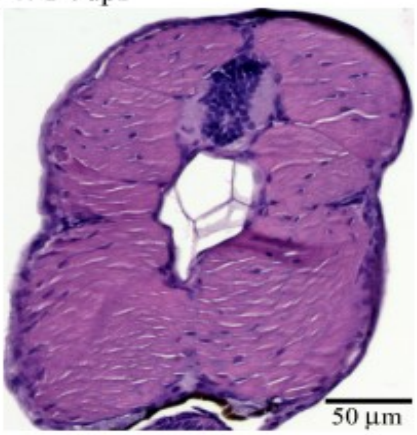

F) *jam* 7dpf

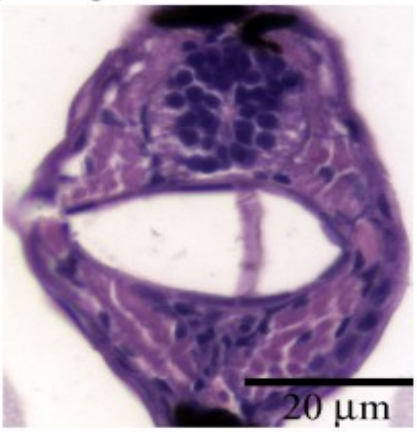

Figure 24: Differential tissue loss in slow and fast muscle mutants.

H&E cross sections of wild-type (sibling) embryos (A) and *still heart* embryos (B) at 48 hpf show normal fast and slow muscle staining. By 5 dpf wild-type siblings (C) still retain this organization, but a severe muscle atrophy is occurring in both slow and fast muscle in *still heart* embryos (D). At 7 dpf, wild-type (AB) embryos show normal fast and slow muscle organization. *Jam* mutants (F) are much smaller at 7 dpf and have increased notochord sizes as well as a decrease in muscle tissue area. *Jam* mutants also appear to have a loss of tissue in the slow muscle area.

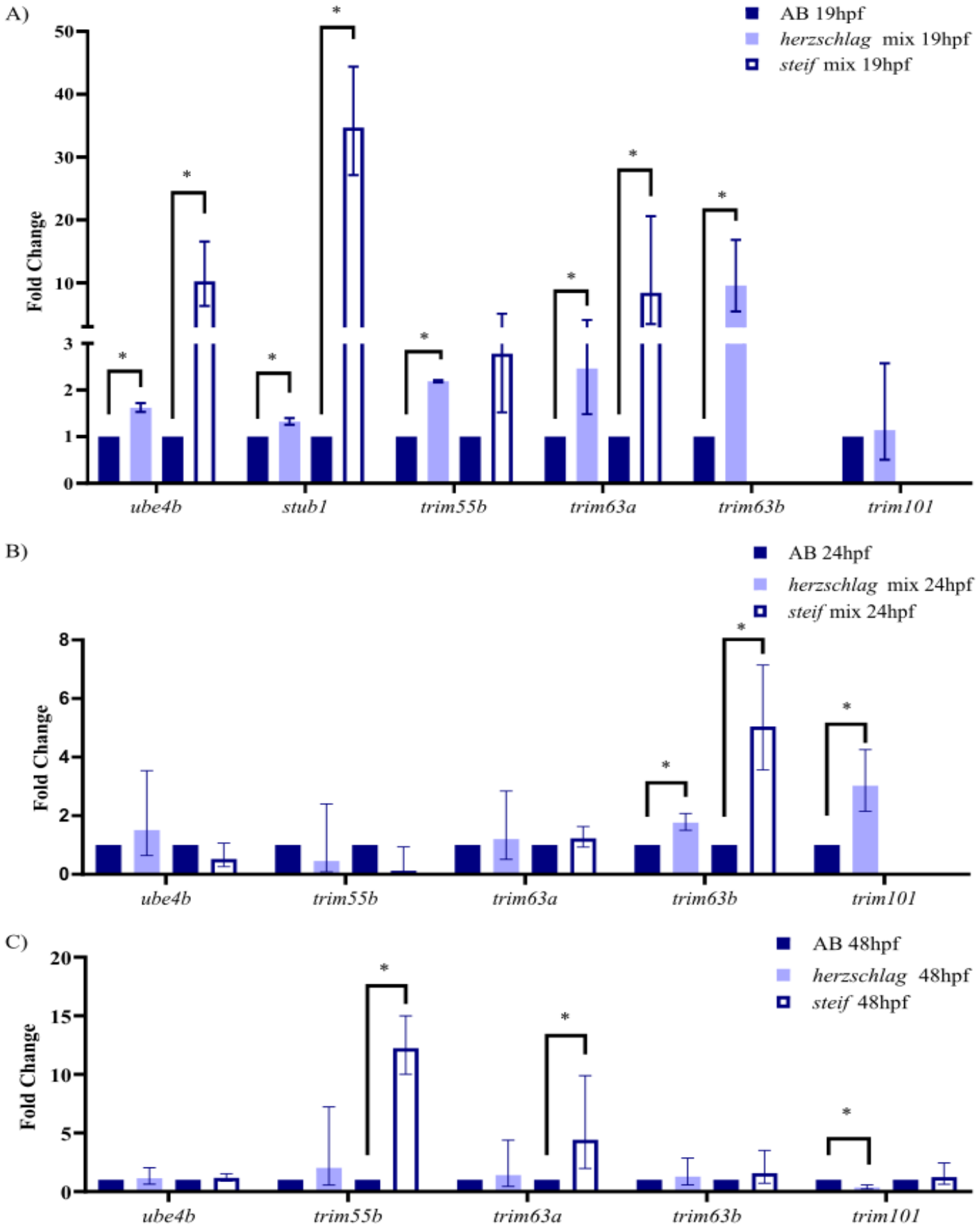
A)
AB 19hpf
herzschlag mix 19hpf
steif mix 19hpf
Fold Change
50
40
30
20
10
3
2
1
0
ube4b
stub1
trim55b
trim63a
trim63b
trim101
B)
AB 24hpf
herzschlag mix 24hpf
steif mix 24hpf
Fold Change
8
6
4
2
0
ube4b
trim55b
trim63a
trim63b
trim101
C)
AB 48hpf
herzschlag 48hpf
steif 48hpf
Fold Change
20
15
10
5
0
ube4b
trim55b
trim63a
trim63b
trim101

Figure 25: Different E3 ligases are upregulated in *herzschlag* and *steif* mutants throughout muscle developmental stages.

A) qPCR of E3 ligases at 19 hpf compared between wild-type (AB) zebrafish and *herzschlag* mix broods, or wild-type (AB) zebrafish and *steif* mix broods. Fold change from wild-type is plotted with error bars representing standard deviation and accounting for propagation of error and linear transformation of data. *ube4b* is upregulated in both *herzschlag* mix broods and *steif* mix brood mutants compared to wild-type ($p=0.007$; $p=0.02$; Student's t-test; N=2), as is *stub1* ($p=0.02$; $p=0.002$; N=2), and *trim63a* ($p=0.04$; $p=0.02$; N=2 for *steif* mix broods). The E3 ligases *trim55b* (N=2) and *trim63b* are also upregulated in *herzschlag* mix broods at 19 hpf ($p<0.001$; $p=0.04$), but *trim55b* is not significantly upregulated in *steif* mix broods ($p=0.14$; N=2). *trim101* is not significantly upregulated in *herzschlag* mix broods at this timepoint ($p=0.84$; N=2). B) qPCR of E3 ligases at 24 hpf compared between wild-type (AB) zebrafish and *herzschlag* mix broods, or wild-type (AB) zebrafish and *steif* mix broods. Fold change from wild-type is plotted with error bars representing standard deviation and accounting for propagation of error and linear transformation of data. Upregulation of *trim63b* is observed in both *herzschlag* and *steif* mix broods (N=2) in comparison to wild-type embryos ($p=0.004$; $p=0.003$) and *trim101* is upregulated in *herzschlag* mix broods ($p=0.005$). C) qPCR of E3 ligases at 48 hpf compared between wild-type (AB) zebrafish and *herzschlag* mutants, or wild-type (AB) zebrafish and *steif* mutants. Fold change from wild-type is plotted with error bars representing standard deviation and accounting for propagation of error and linear transformation of data. *trim55b* and *trim63a* are upregulated in *steif* mutants compared to wild-type ($p<0.001$; $p=0.03$; N=2) and *trim101* is significantly downregulated in *herzschlag* mutants ($p=0.02$).

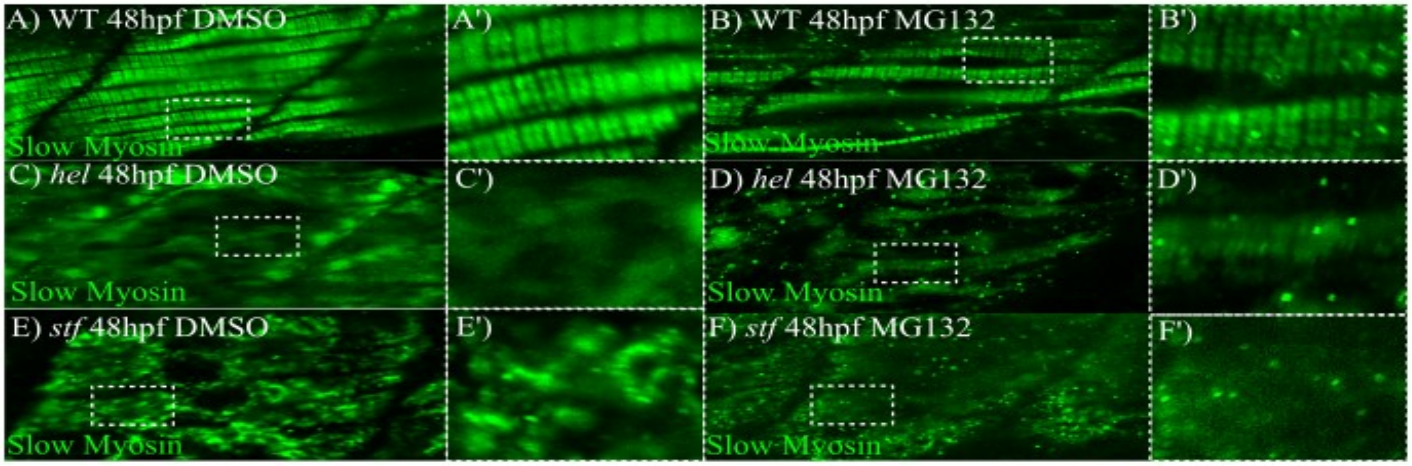
A) WT 48hpf DMSO
A')
B) WT 48hpf MG132
B')
Slow Myosin
C) hel 48hpf DMSO
C')
D) hel 48hpf MG132
D')
Slow Myosin
E) stf 48hpf DMSO
E')
F) stf 48hpf MG132
F')
Slow Myosin

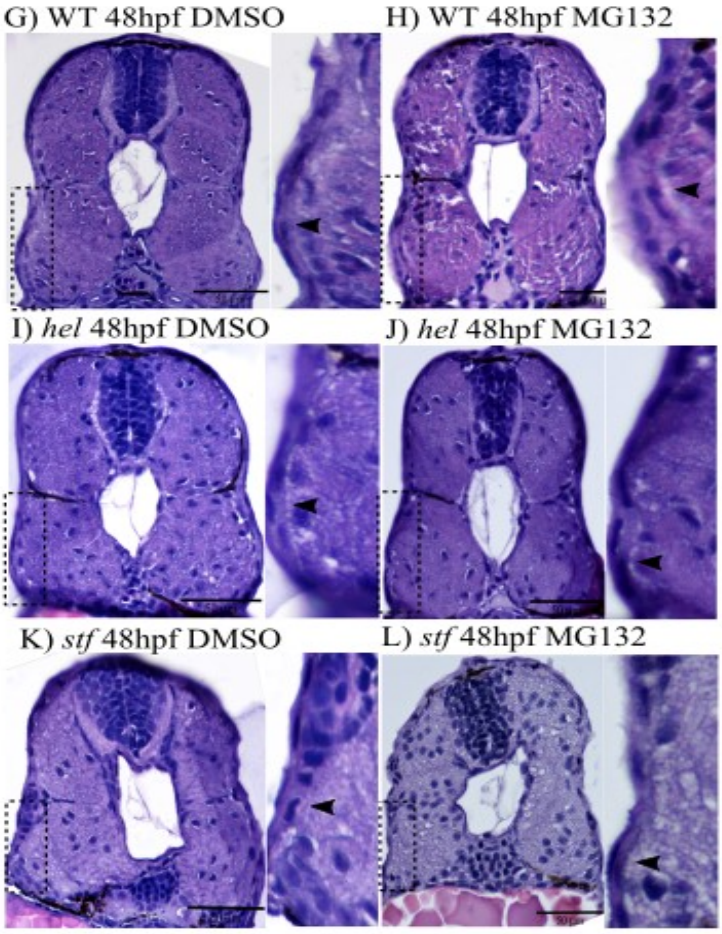
G) WT 48hpf DMSO
H) WT 48hpf MG132
I) hel 48hpf DMSO
J) hel 48hpf MG132
K) stf 48hpf DMSO
L) stf 48hpf MG132

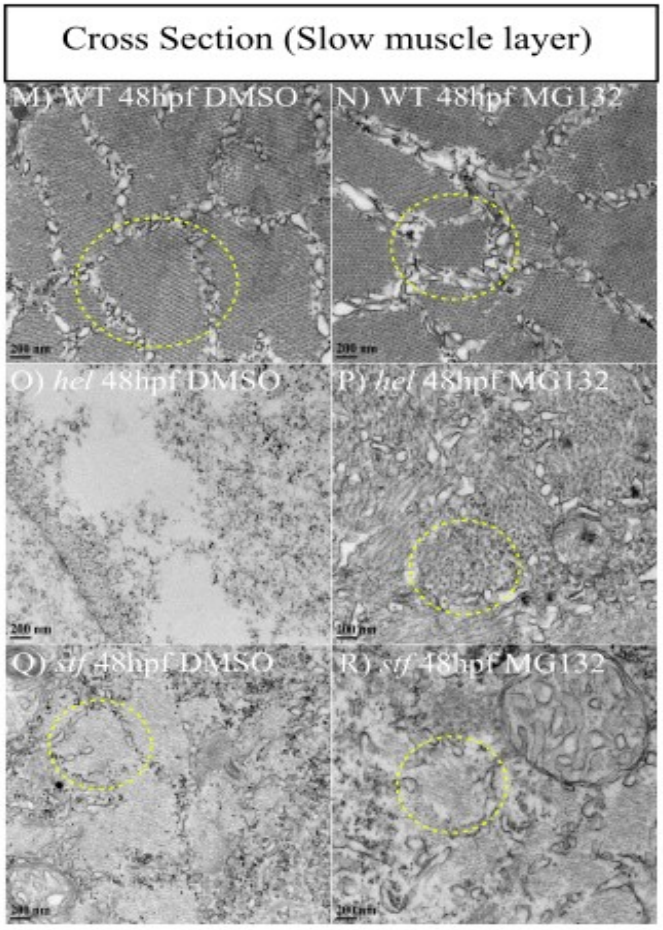
Cross Section (Slow muscle layer)
M) WT 48hpf DMSO
N) WT 48hpf MG132
O) hel 48hpf DMSO
P) hel 48hpf MG132
Q) stf 48hpf DMSO
R) stf 48hpf MG132

Figure 26: UPS inhibition causes slow muscle retention in *herzschlag*, but increases muscle atrophy in *steif*.

Immunofluorescence of slow myosin (F59) in wild-type embryos treated with 50μM DMSO from 22-48 hpf (A; inset A') shows normal slow muscle myofibres with repeating striations. This organization is retained in wild-type embryos treated with 50 μM MG132 (B; inset B'). *herzschlag* embryos treated with DMSO do not have slow myosin myofibers or slow myosin sarcomeres (C; inset C') but those treated with MG132 (D; inset D') show increased organization of slow muscle, with detectable myofibrils and sarcomeres. *steif* embryos treated with DMSO show a diffuse staining of myosin, but no detectable sarcomeres (E; inset E'). *steif* embryos treated with MG132 also do not have myosin myofibrils or myosin sarcomeres (F; inset F'). H&E stained cross-sections of wild-type embryos treated with DMSO (G) show normal organization in the slow muscle layer (black arrowhead). Wild-type embryos treated with MG132 (H) have fainter staining in the slow muscle layer (black arrowhead). H&E stained cross-sections of *herzschlag* embryos treated with DMSO (I) show gaps in staining in the slow muscle layer (black arrowhead), which is less pronounced in MG132 treated embryos (J; black arrowhead). H&E stained cross-sections of *steif* embryos treated with DMSO (K) show no discernable differences in the slow muscle layer (black arrowhead) but *steif* embryos treated with MG132 (L) show a global reduction in staining, not limited to the slow muscle layer. TEM cross sections of wild-type embryos treated with DMSO (M) show organized bundling of myofibrils (yellow outline) while those exposed to 50 μM MG132 (N) still show some organization, but have disruptions to the sarcolemma (yellow outline). TEM cross sections of *herzschlag* embryos treated with DMSO (O) show advanced muscle atrophy in the slow muscle layer. Proteasome inhibition via MG132 in *herzschlag* embryos causes a retention of protein (P) with discernable

myofibril bundles (yellow outline), although general protein organization is still poor. Myofibril bundles with poor general organization (yellow outline) are seen in *steif* embryos treated with DMSO (Q) as well as those treated with MG132 (R), but gaps in the myofibril bundles are evident in MG132 treated embryos as well as increased mitochondrial number and size.

CHAPTER 4. DISCUSSION:

Despite the importance of sarcomere assembly and maintenance to skeletal and cardiac function, mechanisms of protein quality control during sarcomere assembly and maintenance has been understudied (reviewed in Carlisle et al., 2018). The goal of this thesis was to examine zebrafish protein quality control networks in sarcomere assembly mutants and sarcomere maintenance mutants with the hypothesis that separate components would respond to myosin damage respective to when it occurs. Identifying mechanisms of protein quality control and determining the stages of muscle development when they are active is a critical step in identifying possible therapies for myopathies as well as to treat muscle atrophy that results from aging or diseases such as diabetes and cancer. Early detection of muscle atrophy may also lead to early detection of chronic diseases (reviewed in Farkas et al., 2013), and a need for the identification and development of screenable markers of muscle atrophies exists.

While the sarcomere consists of hundreds of proteins and associated factors whose turnover must be regulated, I chose to focus on the thick filament protein, myosin. Myosins are important disease genes, with various myosinopathies existing in the population (reviewed in Goebel and Laing, 2009; Tajsharghi and Oldfors, 2013). Additionally, myosin thick filaments appear to be preferentially lost over actin thin filaments in muscle atrophies associated with critical illness myopathies (Stibler et al., 2003).

In order to examine protein quality control mechanisms with respect to myosin, I sought to identify zebrafish with mutations affecting myosin assembly into the sarcomere and myosin maintenance in the sarcomere. The *unc45b* mutant, *steif*, failed to form myosin thick filaments as anticipated, while I show that the *titin2* mutant, *herzschlag*, forms thick filaments that become disorganized over time as a consequence of muscle contractions. The *titin2* mutation causes a

preferential degeneration of slow myosin over fast myosin that is dependent on the activity of the ubiquitin proteasome system. In contrast, *steif* animals show no preference in myosin fiber degradation, and inhibition of the proteasome increases muscle atrophy in these fish.

With its unparalleled size and central location in the sarcomere, it is unsurprising that the cognate gene of the *herzschlag* mutation, *titin2*, has been implicated as a major human disease gene. Mutations in titin are now linked to both cardiac (reviewed in Kellermayer et al., 2019; LeWinter and Granzier, 2013), and skeletal myopathies (reviewed in Savarese et al., 2016), collectively called titinopathies. However, the mechanisms behind why titin mutations cause disease are still being uncovered. The idea of a molecular spring role for titin was first proposed in 1993 (Wang et al., 1993), and has been widely supported by domain sequencing, revealing a spring-like PEVK domain and stretchy Ig domains in the I-band of titin (Labeit and Kolmerer, 1995), and single molecule force studies (Granzier and Labeit, 2006; Linke and Grützner, 2008). However, we and others show that while anesthetizing zebrafish with titin mutations does improve their slow muscle morphology, it does not completely rescue slow muscle disorganization (Shih et al., 2016), suggesting additional roles for titin beyond sarcomere assembly and contraction bracing. The loss of slow muscle tissue in *herzschlag* mutants suggests that a second consequence of titin mutations can be UPS mediated slow muscle atrophy.

Links between the titin C-terminus and the UPS have been established through the MuRF family of E3 ligases (Centner et al., 2001; Lange et al., 2005), which are muscle specific (Centner et al., 2001; Spencer et al., 2000) and known to target myosin, along with other sarcomere proteins, for polyubiquitination and degradation (Witt et al., 2005). Titin mutations have also been shown to cause skeletal and cardiac muscle atrophy in mice models, where protein expression of MuRF family E3 ligases are unchanged and loss of the titin M-line is

thought to dysregulate FHL2/ERK2 signalling (Radke et al., 2019). In rat hearts, titin truncations have been shown to decrease autophagy through dysregulation of the mTOR pathway (Zhou et al., 2019). Because of the size of titin and its numerous interacting partners, it is likely that numerous protein quality control systems are affected by titin mutations.

Although UPS inhibition has been shown to increase autophagic activity in rat myocytes (Zheng et al., 2011), it is unclear why *steif* embryos would be more sensitive to increased autophagic activity than *herzschlag* or wild-type embryos. However, myosin chaperone expression is extremely high in *steif* mutants (Etard et al., 2015; Prill et al., 2015), a mechanism that has been dubbed the 'misfolded myosin response' (Etard et al., 2015). While this response occurs in other myosin chaperone mutants (Prill et al., 2015), it does not occur in *herzschlag* (Myhre et al., 2014b) or other fish where initial myofibril assembly is grossly normal (Behra et al., 2002; Etard et al., 2005b). As connections between chaperones and protein turnover exist (reviewed in Carlisle et al., 2018) as well as connections between the UPS and autophagy (reviewed in Wang and Wang, 2015), it is possible that increased myosin chaperone expression sensitizes *steif* to autophagy, possibly through chaperone-mediated autophagy, chaperone-assisted selective autophagy, or chaperone-assisted proteasomal degradation. Although this hypothesis remains untested, it could be conceivably similar to connections between the UPS and autophagy in controlling the unfolded protein response during endoplasmic reticulum-associated degradation, by which inhibition of the proteasome increases misfolded protein aggregation and subsequently autophagy (Wang and Wang, 2015). As *hsf-1* is necessary for myosin chaperone upregulation during the misfolded myosin response (Etard et al., 2015), examination of UPS inhibited *steif* embryos with knockdown of *hsf-1* would be an interesting experiment to test the

hypothesis that the muscle atrophy in UPS inhibited *steif* embryos is due to elevated expression of chaperones downstream of *hsf-1*.

Inhibition of the unfolded protein response in mouse models of cancer cachexia has been shown to cause upregulation of UPS components and autophagy markers (Bohnert et al., 2016). Therefore, it is possible that prolonged endoplasmic reticulum/sarcoplasmic reticulum stress in *steif* embryos caused by aggregation of misfolded myosin is responsible for the increase in muscle atrophy observed in UPS inhibited *steif* embryos and that this mechanism occurs independently of myosin chaperone upregulation. In this case, it would likely be downstream consequences of endoplasmic reticulum stress that are responsible for the increased atrophy in these mutants. In HeLa cells, Hsp70 and Bag3 have also been shown to respond to protein aggregation induced by proteasome inhibition (Meriin et al., 2018), and it is likely that many of these signalling axes are affected in *steif* mutants. Further work is required to tease out the mechanisms behind muscle atrophy in UPS inhibited *steif* mutants.

Protein chaperones constitute one of the major protein quality control systems, with the heat shock protein, hsp70, a central component of this system (reviewed in Senf, 2013). Like the myosin chaperones involved in the misfolded myosin response, *hsp70* is also induced by *hsf-1* (Tsukamoto et al., 2019), but rather than recognizing misfolded myosin, *hsp70* chaperones respond to heat, oxidative, and ischemic stress in addition to protein aggregates (reviewed in Daugaard et al., 2007). Both *steif* and *herzschlag* embryos likely undergo hypoxic and oxidative stress due to their poor cardiac function. Although *hsp70-1* is a known stress response gene, I would expect it to be equally expressed in *herzschlag* and *steif* embryos if it was responding to oxidative stress. However, I saw that *hsp70-1* is slightly upregulated only in *herzschlag* mutants by 48 hpf, and previous work shows strong *hsp70-1* upregulation by 19 hpf in *herzschlag* mix

brood embryos (Prill, unpublished). However, I could not detect significantly upregulated *hsp70-1* in *steif* embryos at 48 hpf. Together, this suggests that *hsp70-1* upregulation in *herzschlag* embryos at 48 hpf is not a response to oxidative stress. Other oxidative stress triggered genes, such as MMP2, require further examination in these mutants.

In *mdx* mice, a murine model of Duchenne's muscular dystrophy (reviewed in Partridge, 2013), *hsp70-1* and *hsp70-3* (collectively called *hsp72*) appear to protect against increased intracellular calcium by improving sarco/endoplasmic reticulum Ca^{2+}-ATPase function (Gehrig et al., 2012). As I have shown that *herzschlag* undergoes contraction induced muscle damage, it is possible that the upregulation of *hsp70-1* observed is a result of increased intracellular calcium. This upregulation would not be expected to occur in *steif* embryos as they never undergo muscle contractions. Further examination of sarcolemma integrity in *herzschlag* embryos will be critical to testing this hypothesis, but other hypotheses regarding *hsp70-1* upregulation in *herzschlag* exist in parallel to this one including collaboration with *bag-3* to promote protein clearance through autophagy (Minoia et al., 2014).

Together, this work suggests that different protein quality control mechanisms respond to myosin damage depending on whether it occurs during sarcomere assembly or sarcomere maintenance stages. A lingering question remains as to how myosin damage is detected by these systems, and how these systems are segregated but still able to communicate. Current models of protein triage and protein turnover are unable to answer this question, indicating there is a need for future research in these areas. A thorough understanding of where and when protein quality control systems act on damaged proteins, and mechanisms of communication between systems, will be vital to developing therapies to treat striated muscle myopathies.

CHAPTER 5. CONCLUSIONS:

My hypothesis was that different molecular mechanisms respond to myosin damage when it occurs during sarcomere assembly than those that respond to myosin damage when it occurs after the sarcomere has been properly assembled. While certain mechanisms like the misfolded myosin response did not occur in our myosin maintenance mutant, it is not possible to determine from our data whether this is an assembly specific response, or a response that only occurs upon the loss of a myosin chaperone. I also note that the ubiquitin proteasome system functions during both sarcomere assembly and sarcomere maintenance, but that different E3 ligases are upregulated during sarcomere assembly and during sarcomere maintenance stages which may support our hypothesis. Conditional, inducible, knockout models of specific E3 ligases would help separate sarcomere assembly and sarcomere maintenance functions of these proteins such that their roles in these respective processes can be analyzed in more depth.

Cross talk between chaperones, autophagy, proteases, and the ubiquitin proteasome system makes analysis of protein quality control mechanisms difficult to tease apart. However, our work suggests that certain mutations may sensitize individuals to inhibition of one system by subsequently activating another. As UPS inhibitors are being used as therapies (reviewed in Xolalpa et al., 2013), this could be relevant as personalized medicine becomes more commonplace.

While many titinopathies have already been identified, with the increasing availability of next generation sequencing techniques, it is likely that diagnosis of titin mutations will increase. In order to understand the role of this protein in sarcomere development and disease, a thorough understanding of titin domains, splicing, post-translational modifications, and their consequences to skeletal and cardiac health will be required. Further study of titin binding proteins (calpain-1,

calpain-3, and MMP2) is also warranted, as the same titin mutation has been shown to cause different phenotypes in different patients (Udd et al., 2005) due to their secondary effects. Our work suggests that even transient interruptions in the A-band of titin can have severe consequences to the sarcomere, especially if the C-terminal domains are absent. As genome editing becomes a reality, this may have clinical significance as it suggests to a critical window of development where titin mutations have the most significant effects on survival. In human patients with C-terminal titin mutations, I suggest monitoring of muscles with mixed fast and slow muscle fibers, as our results suggest a degeneration of these muscles may be occurring.

REFERENCES:

Aguzzi, A., O'Connor, T., 2010. Protein aggregation diseases: pathogenicity and therapeutic perspectives. Nature Reviews Drug Discovery 9, 237.

Ali, M.A., Cho, W.J., Hudson, B., Kassiri, Z., Granzier, H., Schulz, R., 2010. Titin is a target of matrix metalloproteinase-2: implications in myocardial ischemia/reperfusion injury. Circulation 122, 2039-2047.

Alvarado, D.M., Buchan, J.G., Gurnett, C.A., Dobbs, M.B., 2011. Exome sequencing identifies an MYH3 mutation in a family with distal arthrogryposis type 1. The Journal of Bone and Joint Surgery 93, 1045-1050.

Amerik, A.Y., Hochstrasser, M., 2004. Mechanism and function of deubiquitinating enzymes. Biochimica et Biophysica Acta 1695, 189-207.

Arndt, V., Dick, N., Tawo, R., Dreiseidler, M., Wenzel, D., Hesse, M., Fürst, D.O., Saftig, P., Saint, R., Fleischmann, B.K., Hoch, M., Höhfeld, J., 2010. Chaperone-assisted selective autophagy is essential for muscle maintenance. Current Biology 20, 143-148.

Arndt, V., Rogon, C., Höhfeld, J., 2007. To be, or not to be — molecular chaperones in protein degradation. Cellular and Molecular Life Sciences 64, 2525-2541.

Bachmair, A., Finley, D., Varshavsky, A., 1986. In vivo half-life of a protein is a function of its amino-terminal residue. Science 234, 179-186.

Bang, M.L., Centner, T., Fornoff, F., Geach, A.J., Gotthardt, M., McNabb, M., Witt, C.C., Labeit, D., Gregorio, C.C., Granzier, H., Labeit, S., 2001. The complete gene sequence of titin, expression of an unusual ≈700-kDa titin isoform, and its interaction with obscurin identify a novel Z-line to I-band linking system. Circulation Research 89, 1065-1072.

Barral, J.M., Hutagalung, A.H., Brinker, A., Hartl, F.U., Epstein, H.F., 2002. Role of the myosin assembly protein UNC-45 as a molecular chaperone for myosin. Science 295, 669-671.

Bassett, D.I., Currie, P.D., 2003. The zebrafish as a model for muscular dystrophy and congenital myopathy. Human Molecular Genetics 12, R265-R270.

Beck, A.E., McMillin, M.J., Gildersleeve, H.I.S., Kezele, P.R., Shively, K.M., Carey, J.C., Regnier, M., Bamshad, M.J., 2013. Spectrum of mutations that cause distal arthrogryposis types 1 and 2B. American Journal of Medical Genetics 161A, 550-555.

Beckmann, J.S., Spencer, M., 2008. Calpain 3, the "gatekeeper" of proper sarcomere assembly, turnover and maintenance. Neuromuscular Disorders 18, 913-921.

Behl, C., 2016. Breaking BAG: The co-chaperone BAG3 in health and disease. Trends in Pharmacological Sciences 37, 672-688.

Behra, M., Cousin, X., Bertrand, C., Vonesch, J.-L., Biellmann, D., Chatonnet, A., Strähle, U., 2002. Acetylcholinesterase is required for neuronal and muscular development in the zebrafish embryo. Nature Neuroscience 5, 111-118.

Berardo, A., DiMauro, S., Hirano, M., 2010. A diagnostic algorithm for metabolic myopathies. Current neurology and neuroscience reports 10, 118-126.

Bercovich, B., Stancovski, I., Mayer, A., Blumenfeld, N., Ciechanover, A., Laszlo, A., Schwartz, A.L., 1997. Ubiquitin-dependent degradation of certain protein substrates in vitro requires the molecular chaperone Hsc70. Journal of Biological Chemistry 272, 9002-9010.

Bernick, E.P., Zhang, P.-J., Du, S., 2010. Knockdown and overexpression of Unc-45b result in defective myofibril organization in skeletal muscles of zebrafish embryos. BMC Cell Biology 11.

Bessarab, D.A., Chong, S.-W., Srinivas, B.P., Korzh, V., 2008. Six1a is required for the onset of fast muscle differentiation in zebrafish. Developmental Biology 323, 216-228.

Bilodeau, P.A., Coyne, E.S., Wing, S.S., 2016. The ubiquitin proteasome system in atrophying skeletal muscle: roles and regulation. American Journal of Physiology - Cell Physiology 311, C392-C403.

Blagden, C.S., Currie, P.D., Ingham, P.W., Hughes, S.M., 1997. Notochord induction of zebrafish slow muscle mediated by Sonic hedgehog. Genes & Development 11, 2163-2175.

Boateng, S.Y., Goldspink, P.H., 2007. Assembly and maintenance of the sarcomere night and day. Cardiovascular Research 77, 667-675.

Bodine, S.C., Latres, E., Baumhueter, S., Lai, V.K.-M., Nunez, L., Clarke, B.A., Poueymirou, W.T., Panaro, F.J., Na, E., Dharmarajan, K., Pan, Z.-Q., Valenzuela, D.M., DeChiara, T.M., Stitt, T.N., Yancopoulos, G.D., Glass, D.J., 2001. Identification of ubiquitin ligases required for skeletal muscle atrophy. Science 294, 1704-1708.

Bohnert, K.R., Gallot, Y.S., Sato, S., Xiong, G., Hindi, S.M., Kumar, A., 2016. Inhibition of ER stress and unfolding protein response pathways causes skeletal muscle wasting during cancer cachexia. Federation of American Societies for Experimental Biology 30, 3053-3068.

Bohnert, K.R., McMillan, J.D., Kumar, A., 2018. Emerging roles of ER stress and unfolded protein response pathways in skeletal muscle health and disease. Journal of Cellular Physiology 233, 67-78.

Bonaldo, P., Sandri, M., 2013. Cellular and molecular mechanisms of muscle atrophy. Disease Models & Mechanisms 6, 25-39.

Buckingham, M., Rigby, Peter W.J., 2014. Gene regulatory networks and transcriptional mechanisms that control myogenesis. Developmental Cell 28, 225-238.

Cai, D., Frantz, J.D., Tawa, N.E., Melendez, P.A., Oh, B.-C., Lidov, H.G.W., Hasselgren, P.-O., Frontera, W.R., Lee, J., Glass, D.J., Shoelson, S.E., 2004. IKKβ/NF-κB activation causes severe muscle wasting in mice. Cell 119, 285-298.

Carapito, R., Goldenberg, A., Paul, N., Pichot, A., David, A., Hamel, A., Dumant-Forest, C., Leroux, J., Ory, B., Isidor, B., Bahram, S., 2016. Protein-altering MYH3 variants are associated with a spectrum of phenotypes extending to spondylocarpotarsal synostosis syndrome. European Journal of Human Genetics 24, 1746-1751.

Carlisle, C., Prill, K., Pilgrim, D., 2018. Chaperones and the proteasome system: regulating the construction and demolition of striated muscle. International Journal of Molecular Sciences 19.

Carmignac, V., Salih, M.A.M., Quijano-Roy, S., Marchand, S., Al Rayess, M.M., Mukhtar, M.M., Urtizberea, J.A., Labeit, S., Guicheney, P., Leturcq, F., Gautel, M., Fardeau, M., Campbell, K.P., Richard, I., Estournet, B., Ferreiro, A., 2007. C-terminal titin deletions cause a novel early-onset myopathy with fatal cardiomyopathy. Annals of Neurology 61, 340-351.

Carniel, E., Taylor, M.R.G., Sinagra, G., Lenarda, A.D., Ku, L., Fain, P.R., Boucek, M.M., Cavanaugh, J., Miocic, S., Slavov, D., Graw, S.L., Feiger, J., Zhu, X.Z., Dao, D., Ferguson, D.A., Bristow, M.R., Mestroni, L., 2005. Alpha-myosin heavy chain: a sarcomeric gene associated with dilated and hypertrophic phenotypes of cardiomyopathy. Circulation 112, 54-59.

Carrara, M., Prischi, F., Nowak, P.R., Kopp, M.C., Ali, M.M.U., 2015. Noncanonical binding of BiP ATPase domain to Ire1 and Perk is dissociated by unfolded protein CH1 to initiate ER stress signaling. eLife 4.

Centner, T., Yano, J., Kimura, E., McElhinny, A.S., Pelin, K., Witt, C.C., Bang, M.-L., Trombitas, K., Granzier, H., Gregorio, C.C., Sorimachi, H., Labeit, S., 2001. Identification of muscle specific ring finger proteins as potential regulators of the titin kinase domain11Edited by J. Karn. Journal of Molecular Biology 306, 717-726.

Ceyhan-Birsoy, O., Agrawal, P.B., Shur, N., Dennison, J.M., Lawlor, M.W., Laporte, J., Markianos, K., Fairbrother, W.G., Granzier, H., Beggs, A.H., Hidalgo, C., Schmitz-Abe, K., Dechene, E.T., Swanson, L.C., Soemedi, R., Vasli, N., Iannaccone, S.T., Shieh, P.B., 2013. Recessive truncating titin gene, TTN, mutations presenting as centronuclear myopathy. Neurology, 1205-1214.

Chal, J., Pourquié, O., 2017. Making muscle: skeletal myogenesis in vivo and in vitro. Development 144, 2104-2122.

Charton, K., Danièle, N., Vihola, A., Roudaut, C., Gicquel, E., Monjaret, F., Tarrade, A., Sarparanta, J., Udd, B., Richard, I., 2010. Removal of the calpain 3 protease reverses the myopathology in a mouse model for titinopathies. Human Molecular Genetics 19, 4608-4624.

Chau, V., Tobias, J., Bachmair, A., Marriott, D., Ecker, D., Gonda, D., Varshavsky, A., 1989. A multiubiquitin chain is confined to specific lysine in a targeted short-lived protein. Science 243, 1576-1583.

Chauveau, C., Rowell, J., Ferreiro, A., 2014. A Rising Titan: TTN Review and Mutation Update. Human Mutation 35, 1046-1059.

Chelly, J., Desguerre, I., 2013. Chapter 141 - Progressive muscular dystrophies, in: Dulac, O., Lassonde, M., Sarnat, H.B. (Eds.), Handbook of Clinical Neurology. Elsevier, pp. 1343-1366.

Chen, J.N., Haffter, P., Odenthal, J., Vogelsang, E., Brand, M., Eeden, F.J., 1996. Mutations affecting the cardiovascular system and other internal organs in zebrafish. Development. 123, 293-302.

Chiang, H., Terlecky, Plant, C., Dice, J., 1989. A role for a 70-kilodalton heat shock protein in lysosomal degradation of intracellular proteins. Science 246, 382-385.

Ching, Y.-H., Ghosh, T.K., Cross, S.J., Packham, E.A., Honeyman, L., Loughna, S., Robinson, T.E., Dearlove, A.M., Ribas, G., Bonser, A.J., Thomas, N.R., Scotter, A.J., Caves, L.S.D., Tyrrell, G.P., Newbury-Ecob, R.A., Munnich, A., Bonnet, D., Brook, J.D., 2005. Mutation in myosin heavy chain 6 causes atrial septal defect. Nature Genetics 37, 423-428.

Chong, J.X., Burrage, L.C., Beck, A.E., Marvin, C.T., McMillin, M.J., Shively, K.M., Harrell, T.M., Buckingham, K.J., Bacino, C.A., Jain, M., Alanay, Y., Berry, S.A., Carey, J.C., Gibbs, R.A., Lee, B.H., Krakow, D., Shendure, J., Nickerson, D.A., University of Washington Center for Mendelian, G., Bamshad, M.J., 2015. Autosomal-dominant multiple pterygium syndrome is caused by mutations in MYH3. American Journal of Human Genetics 96, 841-849.

Ciechanover, A., 1994. The ubiquitin-proteasome proteolytic pathway. Cell 79, 13-21.

Clark, I.M., Swingler, T.E., Sampieri, C.L., Edwards, D.R., 2008. The regulation of matrix metalloproteinases and their inhibitors. The International Journal of Biochemistry & Cell Biology 40, 1362-1378.

Clarke, B.A., Drujan, D., Willis, M.S., Murphy, L.O., Corpina, R.A., Burova, E., Rakhilin, S.V., Stitt, T.N., Patterson, C., Latres, E., Glass, D.J., 2007. The E3 ligase MuRF1 degrades myosin heavy chain protein in dexamethasone-treated skeletal muscle. Cell Metabolism 6, 376-385.

Cohen, S., Brault, J.J., Gygi, S.P., Glass, D.J., Valenzuela, D.M., Gartner, C., Latres, E., Goldberg, A.L., 2009. During muscle atrophy, thick, but not thin, filament components are degraded by MuRF1-dependent ubiquitylation. The Journal of Cell Biology 185, 1083-1095.

Connell, P., Ballinger, C.A., Jiang, J., Wu, Y., Thompson, L.J., Hohfeld, J., Patterson, C., 2001. The co-chaperone CHIP regulates protein triage decisions mediated by heat-shock proteins. Nature Cell Biology 3, 93-96.

Cooper, G., 2000. The cell: a molecular approach, 2nd edition ed. Sinauer Associates, Sunderland (MA).

Costa, M.L., Escaleira, R.C., Rodrigues, V.B., Manasfi, M., Mermelstein, C.S., 2002. Some distinctive features of zebrafish myogenesis based on unexpected distributions of the muscle cytoskeletal proteins actin, myosin, desmin, α-actinin, troponin and titin. Mechanisms of Development 116, 95-104.

Coux, O., Tanaka, K., Goldberg, A.L., 1996. Structure and functions of the 20S and 26S proteasomes. Annual Review of Biochemistry 65, 801-847.

da Silva Lopes, K., Pietas, A., Radke, M.H., Gotthardt, M., 2011. Titin visualization in real time reveals an unexpected level of mobility within and between sarcomeres. The Journal of Cell Biology 193, 785-798.

Dai, Q., Zhang, C., Wu, Y., McDonough, H., Whaley, R.A., Godfrey, V., Li, H.-H., Madamanchi, N., Xu, W., Neckers, L., Cyr, D., Patterson, C., 2003. CHIP activates HSF1 and confers protection against apoptosis and cellular stress. The EMBO Journal 22, 5446-5458.

Danon, M.J., Oh, S.J., DiMauro, S., Manaligod, J.R., Eastwood, A., Naidu, S., Schliselfeld, L.H., 1981. Lysosomal glycogen storage disease with normal acid maltase. Neurology 31, 51-51.

Daugaard, M., Rohde, M., Jäättelä, M., 2007. The heat shock protein 70 family: highly homologous proteins with overlapping and distinct functions. FEBS Letters 581, 3702-3710.

De Cid, R., Ben Yaou, R., Roudaut, C., Charton, K., Baulande, S., Leturcq, F., Romero, N.B., Malfatti, E., Beuvin, M., Vihola, A., Criqui, A., Nelson, I., Nectoux, J., Ben Aim, L., Caloustian, C., Olaso, R., Udd, B., Bonne, G., Eymard, B., Richard, I., 2015. A new titinopathy: Childhood-juvenile onset Emery-Dreifuss-like phenotype without cardiomyopathy. Neurology 85, 2126-2135.

Deldicque, L., 2013. Endoplasmic reticulum stress in human skeletal muscle: any contribution to sarcopenia? Frontiers in physiology 4, 236-236.

Demand, J., Alberti, S., Patterson, C., Höhfeld, J., 2001. Cooperation of a ubiquitin domain protein and an E3 ubiquitin ligase during chaperone/proteasome coupling. Current Biology 11, 1569-1577.

Devoto, S.H., Melançon, E., Eisen, J.S., Westerfield, M., 1996. Identification of separate slow and fast muscle precursor cells in vivo, prior to somite formation. Development 122, 3371-3380.

Dimachkie, M.M., Barohn, R.J., 2014. Distal myopathies. Neurologic clinics 32.

Ding, W.-X., Ni, H.-M., Gao, W., Yoshimori, T., Stolz, D.B., Ron, D., Yin, X.-M., 2007. Linking of autophagy to ubiquitin-proteasome system is important for the regulation of endoplasmic reticulum stress and cell viability. The American Journal of Pathology 171, 513-524.

Du, S.J., Li, H.Q., Bian, Y., Zhong, Y., 2008. Heat-shock Protein 90a1 is required for organized myofibril assembly in skeletal muscles of zebrafish embryos. Proceedings of the National Academy of Sciences of the United States of America 105, 554–559.

Echeverría, P.C., Briand, P.-A., Picard, D., 2016. A remodeled Hsp90 molecular chaperone ensemble with the novel cochaperone Aarsd1 is required for muscle differentiation. Molecular And Cellular Biology 36, 1310-1321.

Edström, L., Thornell, L.-E., Albo, J., Landin, S., Samuelsson, M., 1990. Myopathy with respiratory failure and typical myofibrillar lesions. Journal of the Neurological Sciences 96, 211-228.

Eldeeb, M.A., Leitao, L.C.A., Fahlman, R.P., 2017. Emerging branches of the N-end rule pathways are revealing the sequence complexities of N-termini dependent protein degradation. Biochemistry and Cell Biology 96, 289-294.

Ellis, R.J., 2006. Molecular chaperones: assisting assembly in addition to folding. Trends in Biochemical Sciences 31, 395-401.

Esser, C., Alberti, S., Höhfeld, J., 2004. Cooperation of molecular chaperones with the ubiquitin/proteasome system. Biochimica et Biophysica Acta 1695, 171-188.

Etard, C., Armant, O., Roostalu, U., Gourain, V., Ferg, M., Strähle, U., 2015. Loss of function of myosin chaperones triggers Hsf1-mediated transcriptional response in skeletal muscle cells. Genome Biology 16.

Etard, C., Behra, M., Ertzer, R., Fischer, N., Jesuthasan, S., Blader, P., 2005a. Mutation in the delta-subunit of the nAChR suppresses the muscle defects caused by lack of Dystrophin. Dev Dyn. 234.

Etard, C., Behra, M., Ertzer, R., Fischer, N., Jesuthasan, S., Blader, P., Geisler, R., Strähle, U., 2005b. Mutation in the δ-subunit of the nAChR suppresses the muscle defects caused by lack of dystrophin. Developmental Dynamics 234, 1016-1025.

Etard, C., Behra, M., Fischer, N., Hutcheson, D., Geisler, R., Strähle, U., 2007. The UCS factor Steif/Unc-45b interacts with the heat shock protein Hsp90a during myofibrillogenesis. Developmental Biology 308, 133-143.

Evans, S.M., Yelon, D., Conlon, F.L., Kirby, M.L., 2010. Myocardial lineage development. Circulation research 107, 1428-1444.

Evilä, A., Palmio, J., Vihola, A., Savarese, M., Tasca, G., Penttilä, S., Lehtinen, S., Jonson, P.H., De Bleecker, J., Rainer, P., Auer-Grumbach, M., Pouget, J., Salort-Campana, E., Vilchez, J.J., Muelas, N., Olive, M., Hackman, P., Udd, B., 2017. Targeted next-generation sequencing reveals novel TTN mutations causing recessive distal titinopathy. Molecular Neurobiology 54, 7212-7223.

Evila, A., Vihola, A., Sarparanta, J., Raheem, O., Palmio, J., Sandell, S., Eymard, B., Illa, I., Rojas-Garcia, R., Hankiewicz, K., Negrao, L., Lopponen, T., Nokelainen, P., Karppa, M., Penttila, S., Screen, M., Suominen, T., Richard, I., Hackman, P., Udd, B., 2014. Atypical phenotypes in titinopathies explained by second titin mutations. Annals of Neurology 75, 230-240.

Eytan, E., Ganoth, D., Armon, T., Hershko, A., 1989. ATP-dependent incorporation of 20S protease into the 26S complex that degrades proteins conjugated to ubiquitin. Proceedings of the National Academy of Sciences of the United States of America 86, 7751-7755.

Falsaperla, R., Praticò, A.D., Ruggieri, M., Parano, E., Rizzo, R., Corsello, G., Vitaliti, G., Pavone, P., 2016. Congenital muscular dystrophy: from muscle to brain. Italian Journal of Pediatrics 42, 78-78.

Farkas, J., von Haehling, S., Kalantar-Zadeh, K., Morley, J.E., Anker, S.D., Lainscak, M., 2013. Cachexia as a major public health problem: frequent, costly, and deadly. Journal of Cachexia, Sarcopenia and Muscle 4, 173-178.

Fattori, F., Maggi, L., Bruno, C., Cassandrini, D., Codemo, V., Catteruccia, M., Tasca, G., Berardinelli, A., Magri, F., Pane, M., Rubegni, A., Santoro, L., Ruggiero, L., Fiorini, P., Pini, A., Mongini, T., Messina, S., Brisca, G., Colombo, I., Astrea, G., Fiorillo, C., Bragato, C., Moroni, I., Pegoraro, E., D'Apice, M.R., Alfei, E., Mora, M., Morandi, L., Donati, A., Evilä, A., Vihola, A., Udd, B., Bernansconi, P., Mercuri, E., Santorelli, F.M., Bertini, E., D'Amico, A., 2015. Centronuclear myopathies: genotype–phenotype correlation and frequency of defined genetic forms in an Italian cohort. Journal of Neurology 262, 1728-1740.

Felsenfeld, A.L., Walker, C., Westerfield, M., Kimmel, C., Streisinger, G., 1990. Mutations affecting skeletal muscle myofibril structure in the zebrafish. Development 108, 443-459.

Fougerousse, F., Anderson, L.V.B., Delezoide, A.-L., Suel, L., Durand, M., Beckmann, J.S., 2000. Calpain3 expression during human cardiogenesis. Neuromuscular Disorders 10, 251-256.

Frey, N., Luedde, M., Katus, H.A., 2011. Mechanisms of disease: hypertrophic cardiomyopathy. Nature Reviews Cardiology 9, 91-100.

Fürst, D.O., Osborn, M., Nave, R., Weber, K., 1988. The organization of titin filaments in the half-sarcomere revealed by monoclonal antibodies in immunoelectron microscopy: a map of ten nonrepetitive epitopes starting at the Z line extends close to the M line. The Journal of Cell Biology 106, 1563-1572.

Ganoth, D., Leshinsky, E., Eytan, E., Hershko, A., 1988. A multicomponent system that degrades proteins conjugated to ubiquitin. Resolution of factors and evidence for ATP-dependent complex formation. Journal of Biological Chemistry 263, 12412-12419.

Gao, Q.Q., McNally, E.M., 2015. The dystrophin complex: structure, function, and implications for therapy. Comprehensive Physiology 5, 1223-1239.

Gautel, M., 2011. Cytoskeletal protein kinases: titin and its relations in mechanosensing. Pflugers Archiv 462, 119-134.

Gehrig, S.M., van der Poel, C., Sayer, T.A., Schertzer, J.D., Henstridge, D.C., Church, J.E., Lamon, S., Russell, A.P., Davies, K.E., Febbraio, M.A., Lynch, G.S., 2012. Hsp72 preserves muscle function and slows progression of severe muscular dystrophy. Nature 484, 394-398.

Gigli, M., Begay, R.L., Morea, G., Graw, S.L., Sinagra, G., Taylor, M.R.G., Granzier, H., Mestroni, L., 2016. A review of the giant protein titin in clinical molecular diagnostics of cardiomyopathies. Frontiers in Cardiovascular Medicine 3.

Goebel, H.H., Laing, N.G., 2009. Actinopathies and myosinopathies. Brain Pathology 19, 516-522.

Goldberg, A.L., 2012. Development of proteasome inhibitors as research tools and cancer drugs. The Journal of Cell Biology 199, 583-588.

Goldstein, J.A., McNally, E.M., 2010. Mechanisms of muscle weakness in muscular dystrophy. The Journal of General Physiology 136, 29-34.

Gottesman, S., Wickner, S., Maurizi, M.R., 1997. Protein quality control: triage by chaperones and proteases. Genes & Development 11, 815-823.

Granato, M., van Eeden, F.J., Schach, U., Trowe, T., Brand, M., Furutani-Seiki, M., Haffter, P., Hammerschmidt, M., Heisenberg, C.P., Jiang, Y.J., Kane, D.A., Kelsh, R.N., Mullins, M.C., Odenthal, J., Nusslein-Volhard, C., 1996. Genes controlling and mediating locomotion behavior of the zebrafish embryo and larva. Development 123, 399-413.

Granzier, H.L., Hutchinson, K.R., Tonino, P., Methawasin, M., Li, F.W., Slater, R.E., Bull, M.M., Saripalli, C., Pappas, C.T., Gregorio, C.C., Smith, J.E., 2014. Deleting titin's I-band/A-band junction reveals critical roles for titin in biomechanical sensing and cardiac function. Proceedings of the National Academy of Sciences 111, 14589-14594.

Granzier, H.L., Labeit, S., 2004. The giant protein titin: a major player in myocardial mechanics, signaling, and disease. Circulation Research 94, 284-295.

Granzier, H.L., Labeit, S., 2006. The giant muscle protein titin is an adjustable molecular spring. Exercise and Sport Sciences Reviews 34, 50-53.

Grassini, D.R., Lagendijk, A.K., De Angelis, J.E., Da Silva, J., Jeanes, A., Zettler, N., Bower, N.I., Hogan, B.M., Smith, K.A., 2018. Nppa and Nppb act redundantly during zebrafish cardiac development to confine AVC marker expression and reduce cardiac jelly volume. Development 145, dev160739.

Greaser, M.L., 2009. Stressing the giant: a new approach to understanding dilated cardiomyopathy. Journal of Molecular and Cellular Cardiology 47, 347-349.

Greaser, M.L., Krzesinski, P.R., Warren, C.M., Kirkpatrick, B., Campbell, K.S., Moss, R.L., 2005. Developmental changes in rat cardiac titin/connectin: transitions in normal animals and in mutants with a delayed pattern of isoform transition. Journal of Muscle Research & Cell Motility 26, 325-332.

Gregorio, C.C., Granzier, H., Sorimachi, H., Labeit, S., 1999. Muscle assembly: a titanic achievement? Current Opinion in Cell Biology 11, 18-25.

Gregorio, C.C., Perry, C.N., McElhinny, A.S., 2006. Functional properties of the titin/connectin-associated proteins, the muscle-specific RING finger proteins (MURFs), in striated muscle. Journal of Muscle Research & Cell Motility 26, 389-400.

Hackman, P., Marchand, S., Sarparanta, J., Vihola, A., Penisson-Besnier, I., Eymard, B., Pardal-Fernandez, J.M., Hammouda el, H., Richard, I., Illa, I., Udd, B., 2008. Truncating mutations in C-terminal titin may cause more severe tibial muscular dystrophy (TMD). Neuromuscular Disorders 18, 922-928.

Hackman, P., Vihola, A., Haravuori, H., Marchand, S., Sarparanta, J., de Seze, J., Labeit, S., Witt, C., Peltonen, L., Richard, I., Udd, B., 2002. Tibial muscular dystrophy is a titinopathy caused by mutations in TTN, the gene encoding the giant skeletal-muscle protein Titin. The American Journal of Human Genetics 71, 492-500.

Halpern, M.E., Ho, R.K., Walker, C., Kimmel, C.B., 1993. Induction of muscle pioneers and floor plate is distinguished by the zebrafish no tail mutation. Cell 75, 99-111.

Hanneman, E., Westerfield, M., 1989. Early expression of acetylcholinesterase activity in functionally distinct neurons of the zebrafish. Journal of Comparative Neurology 284, 350-361.

Hanpude, P., Bhattacharya, S., Dey, A.K., Maiti, T.K., 2015. Deubiquitinating enzymes in cellular signaling and disease regulation. IUBMB Life 67, 544-555.

Hartman, M.A., Spudich, J.A., 2012. The myosin superfamily at a glance. Journal of Cell Science 125, 1627-1632.

Hawkins, T.A., Haramis, A.P., Etard, C., Prodromou, C., Vaughn, C.K., Ashworth, R., Ray, W., Behra, M., Holder, N., Talbot, W.S., Pearl, L.H., Strähle, U., Wilson, S.W., 2008. The ATP-ase dependent chaperoning activity of Hsp90a regulates thick filament formation and integration during skeletal muscle myofibrillogenesis. Development 135, 1147-1156.

Heidenhain, M., 1913. Über die Entstehung der quergestreiften Muskelsubstanz bei der Forelle. Archiv für mikroskopische Anatomie 83, A427-A447.

Hellerschmied, D., Clausen, T., 2014. Myosin chaperones. Current Opinion in Structural Biology 25, 9-15.

Herman, D.S., Lam, L., Taylor, M.R.G., Wang, L., Teekakirikul, P., Christodoulou, D., Conner, L., DePalma, S.R., McDonough, B., Sparks, E., Teodorescu, D.L., Cirino, A.L., Banner, N.R., Pennell, D.J., Graw, S., Merlo, M., Di Lenarda, A., Sinagra, G., Bos, J.M., Ackerman, M.J., Mitchell, R.N., Murry, C.E., Lakdawala, N.K., Ho, C.Y., Barton, P.J.R., Cook, S.A., Mestroni, L., Seidman, J.G., Seidman, C.E., 2012. Truncations of titin causing dilated cardiomyopathy. The New England Journal Of Medicine 366, 619-628.

Hershko, A., 1996. Lessons from the discovery ofthe ubiquitin system. Trends in Biochemical Sciences 21, 445-449.

Hershko, A., Ciechanover, A., 1998. The ubiquitin system. Annual Review of Biochemistry 67, 425-479.

Hershko, A., Ciechanover, A., Rose, I.A., 1979. Resolution of the ATP-dependent proteolytic system from reticulocytes: a component that interacts with ATP. Proceedings of the National Academy of Sciences of the United States of America 76, 3107-3110.

Hochstrasser, M., 1996. Ubiquitin-dependent protein degradation. Annual review of genetics, 405.

Holtzer, H., Hijikata, T., Lin, Z.X., Zhang, Z.Q., Holtzer, S., Protasi, F., Franzini-Armstrong, C., Sweeney, H.L., 1997. Independent assembly of 1.6 micron long bipolar MHC filaments and I-Z-I bodies. Cell Structure and Function 22, 83-93.

Homma, S., Iwasaki, M., Shelton, G.D., Engvall, E., Reed, J.C., Takayama, S., 2006. BAG3 deficiency results in fulminant myopathy and early lethality. The American Journal of Pathology 169, 761-773.

Hoppe, T., 2005. Multiubiquitylation by E4 enzymes: ‘one size’ doesn't fit all. Trends in Biochemical Sciences 30, 183-187.

Hoppe, T., Cassata, G., Barral, J.M., Springer, W., Hutagalung, A.H., Epstein, H.F., Baumseister, R., 2004. Regulation of the myosin directed chaperone UNC-45 by a novel E3/E4-Multiubiquitylation Complex in C. elegans. Cell 118, 337-349.

Hough, R., Pratt, G., Rechsteiner, M., 1986. Ubiquitin-lysozyme conjugates. Identification and characterization of an ATP-dependent protease from rabbit reticulocyte lysates. Journal of Biological Chemistry 261, 2400-2408.

Huttner, I.G., Wang, L.W., Santiago, C.F., Horvat, C., Johnson, R., Cheng, D., Frieling-Salewsky, M.v., Hillcoat, K., Bemand, T.J., Trivedi, G., Braet, F., Hesselson, D., Alford, K., Hayward, C.S., Seidman, J.G., Seidman, C.E., Feneley, M.P., Linke, W.A., Fatkin, D., 2018. A-Band Titin Truncation in Zebrafish Causes Dilated Cardiomyopathy and Hemodynamic Stress Intolerance. Circulation: Genomic and Precision Medicine 11, e002135.

Jackson, H.E., Ingham, P.W., 2013. Control of muscle fibre-type diversity during embryonic development: the zebrafish paradigm. Mechanisms of Development 130, 447-457.

Janeisch, P.C., Kim, J., Mouysset, J., Barikbin, R., Lochmüller, H., Cassata, G., Krause, S., Hoppe, T., 2007. The ubiquitin sensitive chaperone CDC-48/p97 links myosin assembly to human myopathy. Nature Cell Biology 9, 379-390.

Johnson, E.K., Li, B., Yoon, J.H., Flanigan, K.M., Martin, P.T., Ervasti, J., Montanaro, F., 2013. Identification of new dystroglycan complexes in skeletal muscle. PLOS ONE 8.

Just, S., Meder, B., Berger, I.M., Etard, C., Trano, N., Patzel, E., 2011a. The myosin-interacting protein SMYD1 is essential for sarcomere organization. J Cell Sci. 124.

Just, S., Meder, B., Berger, I.M., Etard, C., Trano, N., Patzel, E., Hassel, D., Marquart, S., Dahme, T., Vogel, B., Fishman, M.C., Katus, H.A., Strähle, U., Rottbauer, W., 2011b. The myosin-interacting protein SMYD1 is essential for sarcomere organization. Journal of Cell Science 124, 3127-3136.

Kanelakis, K.C., Morishima, Y., Dittmar, K.D., Galigniana, M.D., Takayama, S., Reed, J.C., Pratt, W.B., 2000. Differential effects of the hsp70-binding protein BAG-1 on glucocorticoid receptor folding by the hsp90-based chaperone machinery. Journal of Biological Chemistry 274, 34134-34140.

Karpinets, T.V., Greenwood, D.J., Sams, C.E., Ammons, J.T., 2006. RNA:protein ratio of the unicellular organism as a characteristic of phosphorous and nitrogen stoichiometry and of the cellular requirement of ribosomes for protein synthesis. BMC Biology 4.

Kaushik, S., Cuervo, A.M., 2012a. Chaperone-mediated autophagy: a unique way to enter the lysosome world. Trends in Cell Biology 22, 407-417.

Kaushik, S., Cuervo, A.M., 2012b. Chaperones in autophagy. Pharmacological Research 66, 484-493.

Keira, Y., Noguchi, S., Minami, N., Hayashi, Y.K., Nishino, I., 2003. Localization of calpain 3 in human skeletal muscle and Its alteration in limb-girdle muscular dystrophy 2A muscle. Journal of Biochemistry 133, 659-664.

Kellermayer, D., Smith, J.E., Granzier, H., 2019. Titin mutations and muscle disease. European Journal of Physiology 471, 673-682.

Kellermayer, M., Sziklai, D., Papp, Z., Decker, B., Lakatos, E., Mártonfalvi, Z., 2018. Topology of interaction between titin and myosin thick filaments. Journal of Structural Biology 203, 46-53.

Kettern, N., Dreiseidler, M., Tawo, R., Höhfeld, J., 2010. Chaperone-assisted degradation: multiple paths to destruction, Biological Chemistry, pp. 481-489.

Khairallah, R.J., Shi, G., Sbrana, F., Prosser, B.L., Borroto, C., Mazaitis, M.J., Hoffman, E.P., Mahurkar, A., Sachs, F., Sun, Y., Chen, Y.-W., Raiteri, R., Lederer, W.J., Dorsey, S.G., Ward, C.W., 2012. Microtubules underlie dysfunction in duchenne muscular dystrophy. Science signaling 5, ra56-ra56.

Khan, M.F.J., Little, J., Abelli, L., Mossey, P.A., Autelitano, L., Nag, T.C., Rubini, M., 2018. Muscle fiber diameter assessment in cleft lip using image processing. Oral diseases 24, 476-481.

Kim, J., Löwe, T., Hoppe, T., 2008. Protein quality control gets muscle into shape. Trends in Cell Biology 18, 264-272.

Kirschner, J., 2013. Chapter 143 - Congenital muscular dystrophies, in: Dulac, O., Lassonde, M., Sarnat, H.B. (Eds.), Handbook of Clinical Neurology. Elsevier, pp. 1377-1385.

Koegl, M., Hoppe, T., Schlenker, S., Ulrich, H.D., Mayer, T.U., Jentsch, S., 1999. A novel ubiquitination factor, E4, is involved in multiubiquitin chain assembly. Cell 96, 635-644.

Korolchuk, V.I., Menzies, F.M., Rubinsztein, D.C., 2010. Mechanisms of cross-talk between the ubiquitin-proteasome and autophagy-lysosome systems. FEBS Letters 584, 1393-1398.

Kriegenburg, F., Ellgaard, L., Hartmann-Petersen, R., 2012. Molecular chaperones in targeting misfolded proteins for ubiquitin-dependent degradation. FEBS Journal 279, 532-542.

Krüger, M., Kötter, S., 2016. Titin, a central mediator for hypertrophic signaling, exercise-induced mechanosignaling and skeletal muscle remodeling. Frontiers in Physiology 7, 1-8.

Krüger, M., Linke, W.A., 2011. The giant protein titin: a regulatory node that integrates myocyte signaling pathways. The Journal Of Biological Chemistry 286, 9905-9912.

Kukreti, H., Amuthavalli, K., Harikumar, A., Sathiyamoorthy, S., Feng, P.Z., Anantharaj, R., Tan, S.L., Lokireddy, S., Bonala, S., Sriram, S., McFarlane, C., Kambadur, R., Sharma, M., 2013. Muscle-specific microRNA1 (miR1) targets heat shock protein 70 (HSP70) during dexamethasone-mediated atrophy. Journal Biological Chemistry 288, 6663-6678.

Labeit, S., Kolmerer, B., 1995. Titins: giant proteins in charge of muscle ultrastructure and elasticity. Science 270, 293-296.

Laing, N.G., Ceuterick-de Groote, C., Dye, D.E., Liyanage, K., Duff, R.M., Dubois, B., Robberecht, W., Sciot, R., Martin, J.J., Goebel, H.H., 2005. Myosin storage myopathy: slow skeletal myosin (MYH7) mutation in two isolated cases. Neurology 64, 527-529.

Laing, N.G., Laing, B.A., Meredith, C., Wilton, S.D., Robbins, P., Honeyman, K., Dorosz, S., Kozman, H., Mastaglia, F.L., Kakulas, B.A., 1995. Autosomal dominant distal myopathy: linkage to chromosome 14. American Journal of Human Genetics 56, 422-427.

Lange, S., Xiang, F., Yakovenko, A., Vihola, A., Hackman, P., Rostkova, E., Kristensen, J., Brandmeier, B., Franzen, G., Hedberg, B., Gunnarsson, L.G., Hughes, S.M., Marchand, S., Sejersen, T., Richard, I., Edström, L., Ehler, E., Udd, B., Gautel, M., 2005. The kinase domain of titin controls muscle gene expression and protein turnover. Science 308, 1599-1603.

Laskey, R.A., Honda, B.M., Mills, A.D., Finch, J.T., 1978. Nucleosomes are assembled by an acidic protein which binds histones and transfers them to DNA. Nature 275, 416-420.

Laurent, F., Girdziusaite, A., Gamart, J., Barozzi, I., Osterwalder, M., Akiyama, J.A., Lincoln, J., Lopez-Rios, J., Visel, A., Zuniga, A., Zeller, R., 2017. HAND2 target gene regulatory networks control atrioventricular canal and cardiac valve development. Cell reports 19, 1602-1613.

LeWinter, M.M., Granzier, H.L., 2013. Titin is a major human disease gene. Circulation 127, 938-944.

Li, H., Malhotra, S., Kumar, A., 2008. Nuclear factor-kappa B signaling in skeletal muscle atrophy. Journal of Molecular Medicine 86, 1113-1126.

Li, H., Zhong, Y., Wang, Z., Gao, J., Xu, J., Chu, W., 2013. Smyd1b is required for skeletal and cardiac muscle function in zebrafish. Molecular Biology of the Cell 24, 3511–3521.

Lieschke, G.J., Currie, P.D., 2007. Animal models of human disease: zebrafish swim into view. Nature Reviews Genetics 8, 353-367.

Linke, W.A., 2008. Sense and stretchability: The role of titin and titin-associated proteins in myocardial stress-sensing and mechanical dysfunction†. Cardiovascular Research 77, 637-648.

Linke, W.A., Grützner, A., 2008. Pulling single molecules of titin by AFM—recent advances and physiological implications. European Journal of Physiology 456, 101-115.

Liu, C.Y., Kaufman, R.J., 2003. The unfolded protein response. Journal of Cell Science 116, 1861-1862.

Liu, L., Srikakulam, R., Winkelmann, D.A., 2008. Unc-45 activates Hsp90-dependent folding of the myosin motor domain. Journal of Biological Chemistry 283, 13185-13193.

Livak, K.J., Schmittgen, T.D., 2001. Analysis of relative gene expression data using real-time quantitative PCR and the 2(-Delta Delta C(T)) Method. Nature Methods 25, 402-408.

Lodka, D., Pahuja, A., Geers-Knörr, C., Scheibe, R.J., Nowak, M., Hamati, J., Köhncke, C., Purfürst, B., Kanashova, T., Schmidt, S., Glass, D.J., Morano, I., Heuser, A., Kraft, T.,

Bassel-Duby, R., Olson, E.N., Dittmar, G., Sommer, T., Fielitz, J., 2016. Muscle RING-finger 2 and 3 maintain striated-muscle structure and function. Journal of Cachexia, Sarcopenia and Muscle 7, 165-180.

Lu, F., Langenbacher, A.D., Chen, J.-N., 2016. Transcriptional regulation of heart development in zebrafish. Journal of Cardiovascular Development and Disease 3.

Lu, M., DiLullo, C., Schultheiss, T., Holtzer, S., Murray, J., Choi, J., Fischman, D., Holtzer, H., 1992. The vinculin/sarcomeric-alpha-actinin/alpha-actin nexus in cultured cardiac myocytes. The Journal of Cell Biology 117, 1007-1022.

Luders, J., Demand, J., Hohfeld, J., 2000. The ubiquitin-related BAG-1 provides a link between the molecular chaperones Hsc70/Hsp70 and the proteasome. Journal of Biological Chemistry 275, 4613-4617.

Macqueen, D.J., Fuentes, E.N., Valdés, J.A., Molina, A., Martin, S.A.M., 2014. The vertebrate muscle-specific RING finger protein family includes MuRF4 – A novel, conserved E3-ubiquitin ligase. FEBS Letters 588, 4390-4397.

Mankodi, A., Udd, B., Griggs, R.C., 2015. Chapter 94 - The Distal Myopathies, in: Rosenberg, R.N., Pascual, J.M. (Eds.), Rosenberg's Molecular and Genetic Basis of Neurological and Psychiatric Disease (Fifth Edition). Academic Press, Boston, pp. 1131-1143.

Maron, B.J., Maron, M.S., 2013. Hypertrophic cardiomyopathy. The Lancet 381, 242-255.

Martinsson, T., Oldfors, A., Darin, N., Berg, K., Tajsharghi, H., Kyllerman, M., Wahlstrom, J., 2000. Autosomal dominant myopathy: missense mutation (Glu-706 --> Lys) in the myosin heavy chain IIa gene. Proceedings of the National Academy of Sciences of the United States of America 97, 14614-14619.

Matsumoto, M., Yada, M., Hatakeyama, S., Ishimoto, H., Tanimura, T., Tsuji, S., Kakizuka, A., Kitagawa, M., Nakayama, K.I., 2004. Molecular clearance of ataxin-3 is regulated by a mammalian E4. The EMBO journal 23, 659-669.

Matsumoto, Y., Hayashi, T., Inagaki, N., Takahashi, M., Hiroi, S., Nakamura, T., Arimura, T., Nakamura, K., Ashizawa, N., Yasunami, M., Ohe, T., Yano, K., Kimura, A., 2005. Functional analysis of titin/connectin N2-B mutations found in cardiomyopathy. Journal of Muscle Research and Cell Motility 26, 367-374.

Matthews, E., Fialho, D., Tan, S.V., Venance, S.L., Cannon, S.C., Sternberg, D., Fontaine, B., Amato, A.A., Barohn, R.J., Griggs, R.C., Hanna, M.G., Investigators, C., 2010. The non-dystrophic myotonias: molecular pathogenesis, diagnosis and treatment. Brain 133, 9-22.

Mazelet, L., Parker, M.O., Li, M., Arner, A., Ashworth, R., 2016. Role of active contraction and tropomodulins in regulating actin filament length and sarcomere structure in developing zebrafish skeletal muscle. Frontiers in Physiology 7.

Meriin, A.B., Narayanan, A., Meng, L., Alexandrov, I., Varelas, X., Cissé, I.I., Sherman, M.Y., 2018. Hsp70-Bag3 complex is a hub for proteotoxicity-induced signaling that controls protein aggregation. Proceedings of the National Academy of Sciences of the United States of America 115, E7043-E7052.

Minoia, M., Boncoraglio, A., Vinet, J., Morelli, F.F., Brunsting, J.F., Poletti, A., Krom, S., Reits, E., Kampinga, H.H., Carra, S., 2014. BAG3 induces the sequestration of proteasomal clients into cytoplasmic puncta: implications for a proteasome-to-autophagy switch. Autophagy 10, 1603-1621.

Mittal, A., Bhatnagar, S., Kumar, A., Lach-Trifilieff, E., Wauters, S., Li, H., Makonchuk, D.Y., Glass, D.J., Kumar, A., 2010. The TWEAK-Fn14 system is a critical regulator of denervation-induced skeletal muscle atrophy in mice. Journal of Cell Biology 188, 833-849.

Moriscot, A., Baptista, I.L., Bogomolovas, J., Krohne, C., Hirner, S., Granzier, H., Labeit, S., 2010. MuRF1 is a muscle fiber type II associated factor and together with MuRF2 regulates type II fiber trophicity and maintenance. Journal of Structural Biology 170, 344-353.

Morrison, B.M., 2016. Neuromuscular Diseases. Seminars in neurology 36, 409-418.

Mrosek, M., Labeit, D., Witt, S., Heerklotz, H., von Castelmur, E., Labeit, S., Mayans, O., 2007. Molecular determinants for the recruitment of the ubiquitin-ligase MuRF-1 onto M-line titin. The FASEB Journal 21, 1383-1392.

Murata, S., Minami, Y., Minami, M., Chiba, T., Tanaka, K., 2001. CHIP is a chaperone-dependent E3 ligase that ubiquitylates unfolded protein. EMBO Reports 2, 1133-1138.

Myhre, J.L., Hills, J.A., Jean, F., Pilgrim, D.B., 2014a. Unc45b is essential for early myofibrillogenesis and costamere formation in zebrafish. Developmental Biology 390, 26-40.

Myhre, J.L., Hills, J.A., Prill, K., Wohlgemuth, S.L., Pilgrim, D.B., 2014b. The titin A-band rod domain is dispensable for initial thick filament assembly in zebrafish. Developmental Biology 387, 93-108.

Myhre, J.L., Pilgrim, D., 2014. A titan but not necessarily a ruler: assessing the role of titin during thick filament patterning and assembly. The Anatomical Record 297, 1604-1614.

Natalia, M., J., R.P.W., J., C.J., 2013. Dial M(RF) for myogenesis. The FEBS Journal 280, 3980-3990.

Nishino, I., 2006. Autophagic vacuolar myopathy. Seminars in Pediatric Neurology 13, 90-95.

Nollen, E.A.A., Kabakov, A.E., Brunsting, J.F., Kanon, B., Hohfeld, J., Kampinga, H.H., 2001. Modulation of in vivo Hsp70 chaperone activity by Hip and Bag-1. Journal of Biological Chemistry 276, 4677-4682.

Odunuga, O.O., Longshaw, V.M., Blatch, G.L., 2004. Hop: more than an Hsp70/Hsp90 adaptor protein. BioEssays 26, 1058-1068.

Ortolano, S., Tarrío, R., Blanco-Arias, P., Teijeira, S., Rodríguez-Trelles, F., García-Murias, M., Delague, V., Lévy, N., Fernández, J.M., Quintáns, B., Millán, B.S., Carracedo, Á., Navarro, C., Sobrido, M.-J., 2011. A novel MYH7 mutation links congenital fiber type disproportion and myosin storage myopathy. Neuromuscular Disorders 21, 254-262.

Palmio, J., Udd, B., 2016. Myofibrillar and distal myopathies. Reviews in Neurology 172, 587-593.

Partridge, T.A., 2013. The mdx mouse model as a surrogate for Duchenne muscular dystrophy. The FEBS journal 280, 4177-4186.

Paul, P.K., Bhatnagar, S., Mishra, V., Srivastava, S., Darnay, B.G., Choi, Y., Kumar, A., 2012. The E3 ubiquitin ligase TRAF6 intercedes in starvation-induced skeletal muscle atrophy through multiple mechanisms. Molecular and Cellular Biology 32, 1248-1259.

Paul, P.K., Gupta, S.K., Bhatnagar, S., Panguluri, S.K., Darnay, B.G., Choi, Y., Kumar, A., 2010. Targeted ablation of TRAF6 inhibits skeletal muscle wasting in mice. Journal of Cell Biology 191, 1395-1411.

Peterson, J.M., Bakkar, N., Guttridge, D.C., 2011. NF-κB signaling in skeletal muscle health and disease. Current Topics in Developmental Biology 96, 85-119.

Prill, K., Windsor Reid, P., Wohlgemuth, S.L., Pilgrim, D.B., 2015. Still Heart encodes a structural HMT, SMYD1b, with chaperone-like function during fast muscle sarcomere assembly. PLoS One 10.

Radke, M.H., Polack, C., Methawasin, M., Fink, C., Granzier, H.L., Gotthardt, M., 2019. Deleting Full Length Titin Versus the Titin M-Band Region Leads to Differential Mechanosignaling and Cardiac Phenotypes. Circulation 0.

Raja Rayan, D.L., Hanna, M.G., 2010. Skeletal muscle channelopathies: nondystrophic myotonias and periodic paralysis. Current Opinion in Neurology 23, 466-476.

Ravenscroft, G., Bryson-Richardson, R.J., Nowak, K.J., Laing, N.G., 2018. Recent advances in understanding congenital myopathies. F1000 Research 7.

Rhee, D., Sanger, J.M., Sanger, J.W., 1994. The premyofibril: evidence for its role in myofibrillogenesis. Cell Motility And The Cytoskeleton 28, 1-24.

Richard, P., Charron, P., Carrier, L., Ledeuil, C., Cheav, T., Pichereau, C., Benaiche, A., Isnard, R., Dubourg, O., Burban, M., Gueffet, J.-P., Millaire, A., Desnos, M., Schwartz, K., Hainque, B., Komajda, M., 2003. Hypertrophic Cardiomyopathy. Circulation 107, 2227-2232.

Romero, N.B., 2010. Centronuclear myopathies: A widening concept. Neuromuscular Disorders 20, 223-228.

Romero, N.B., Clarke, N.F., 2013. Chapter 139 - Congenital myopathies, in: Dulac, O., Lassonde, M., Sarnat, H.B. (Eds.), Handbook of Clinical Neurology. Elsevier, pp. 1321-1336.

Sandri, M., Sandri, C., Gilbert, A., Skurk, C., Calabria, E., Picard, A., Walsh, K., Schiaffino, S., Lecker, S.H., Goldberg, A.L., 2004. Foxo transcription factors induce the atrophy-related ubiquitin ligase atrogin-1 and cause skeletal muscle atrophy. Cell 117, 399-412.

Sanger, J.W., Kang, S., Siebrands, C.C., Freeman, N., Du, A., Wang, J., Stout, A.L., Sanger, J.M., 2005. How to build a myofibril. Journal Of Muscle Research And Cell Motility 26, 343-354.

Sanger, J.W., Wang, J., Holloway, B., Du, A., Sanger, J.M., 2009. Myofibrillogenesis in skeletal muscle cells in zebrafish. Cell Motility and the Cytoskeleton 66, 556-566.

Satoh, M., Takahashi, M., Sakamoto, T., Hiroe, M., Marumo, F., Kimura, A., 1999. Structural analysis of the titin gene in hypertrophic cardiomyopathy: identification of a novel disease gene. Biochemical and biophysical research communications 262, 411-417.

Savarese, M., Sarparanta, J., Vihola, A., Udd, B., Hackman, P., 2016. Increasing role of titin mutations in neuromuscular disorders. Journal of Neuromuscular Diseases 3, 293-308.

Sawicki, G., Leon, H., Sawicka, J., Sariahmetoglu, M., Schulze, C.J., Scott, P.G., Szczesna-Cordary, D., Schulz, R., 2005. Degradation of Myosin Light Chain in Isolated Rat Hearts Subjected to Ischemia-Reperfusion Injury. Circulation 112, 544-552.

Scala, M., Accogli, A., De Grandis, E., Allegri, A., Bagowski, C.P., Shoukier, M., Maghnie, M., Capra, V., 2018. A novel pathogenic MYH3 mutation in a child with Sheldon-Hall syndrome and vertebral fusions. American Journal of Medical Genetics 176, 663-667.

Schmittgen, T.D., Livak, K.J., 2008. Analyzing real-time PCR data by the comparative CT method. Nature Protocols 3, 1101-1108.

Schnorrer, F., Schönbauer, C., Langer, C.C.H., Dietzl, G., Novatchkova, M., Schernhuber, K., Fellner, M., Azaryan, A., Radolf, M., Stark, A., Keleman, K., Dickson, B.J., 2010. Systematic genetic analysis of muscle morphogenesis and function in Drosophila. Nature 464, 287-291.

Schultheiss, T., Lin, Z.X., Lu, M.H., Murray, J., Fischman, D.A., Weber, K., Masaki, T., Imamura, M., Holtzer, H., 1990. Differential distribution of subsets of myofibrillar proteins in cardiac nonstriated and striated myofibrils. Journal of Cell Biology 110, 1159-1172.

Seeley, M., Huang, W., Chen, Z., Wolff, W.O., Lin, X., Xu, X., 2007. Depletion of zebrafish titin reduces cardiac contractility by disrupting the assembly of Z-discs and A-bands. Circulation Research 100, 238-245.

Selcen, D., Muntoni, F., Burton, B.K., Md, E.P., Sewry, C., Bite, A.V., Engel, A.G., 2009. Mutation in BAG3 causes severe dominant childhood muscular dystrophy. Annals of Neurology 65, 83-89.

Senf, S.M., 2013. Skeletal muscle heat shock protein 70: diverse functions and therapeutic potential for wasting disorders. Frontiers in Physiology 4, 330-330.

Shieh, P.B., 2013. Muscular dystrophies and other genetic myopathies. Neurologic Clinics 31, 1009-1029.

Shih, Y.-H., Dvornikov, A.V., Zhu, P., Ma, X., Kim, M.J., Ding, Y., Xu, X., 2016. Exon- and contraction-dependent functions of titin in sarcomere assembly. Development 143, 4713-4722.

Shimizu, H., Langenbacher, A.D., Huang, J., Wang, K., Otto, G., Geisler, R., Wang, Y., Chen, J.-N., 2017. The Calcineurin-FoxO-MuRF1 signaling pathway regulates myofibril integrity in cardiomyocytes. eLife 6.

Sieiro-Mosti, D., De La Celle, M., Pelé, M., Marcelle, C., 2014. A dynamic analysis of muscle fusion in the chick embryo. Development 141, 3605-3611.

Smith, D.A., Carland, C.R., Guo, Y., Bernstein, S.I., 2014. Getting folded: chaperone proteins in muscle development, maintenance and disease. The Anatomical Record 297, 1637-1649.

Sorimachi, H., Imajoh-Ohmi, S., Emori, Y., Kawasaki, H., Ohno, S., Minami, Y., Suzuki, K., 1989. Molecular cloning of a novel mammalian calcium-dependent protease distinct from both m- and mu-types. Specific expression of the mRNA in skeletal muscle. The Journal Of Biological Chemistry 264, 20106-20111.

Spencer, J.A., Eliazer, S., Ilaria, R.L., Richardson, J.A., Olson, E.N., 2000. Regulation of microtubule dynamics and myogenic differentiation by MuRF, a striated muscle ring-finger protein. The Journal of Cell Biology 150, 771-784.

Stevenson, D.A., Carey, J.C., Palumbos, J., Rutherford, A., Dolcourt, J., Bamshad, M.J., 2006. Clinical characteristics and natural history of Freeman-Sheldon syndrome. Pediatrics 117, 754-762.

Stibler, H., Edström, L., Ahlbeck, K., Remahl, S., Ansved, T., 2003. Electrophoretic determination of the myosin/actin ratio in the diagnosis of critical illness myopathy. Intensive Care Medicine 29, 1515-1527.

Stickney, H.L., Barresi, M.J.F., Devoto, S.H., 2000. Somite development in zebrafish. Developmental Dynamics 219, 287-303.

Stitt, T.N., Drujan, D., Clarke, B.A., Panaro, F., Timofeyva, Y., Kline, W.O., Gonzalez, M., Yancopoulos, G.D., Glass, D.J., 2004. The IGF-1/PI3K/Akt pathway prevents expression of muscle atrophy-induced ubiquitin ligases by inhibiting FOXO transcription factors. Molecular cell 14, 395-403.

Strach, K., Sommer, T., Grohé, C., Meyer, C., Fischer, D., Walter, M.C., Vorgerd, M., Reilich, P., Bär, H., Reimann, J., Reuner, U., Germing, A., Goebel, H.H., Lochmüller, H., Wintersperger, B., Schröder, R., 2008. Clinical, genetic, and cardiac magnetic resonance imaging findings in primary desminopathies. Neuromuscular Disorders 18, 475-482.

Subhankar, P., 2008. Dysfunction of the ubiquitin–proteasome system in multiple disease conditions: therapeutic approaches. BioEssays 30, 1172-1184.

Tajsharghi, H., Kimber, E., Kroksmark, A.K., Jerre, R., Tulinius, M., Oldfors, A., 2008. Embryonic myosin heavy-chain mutations cause distal arthrogryposis and developmental myosin myopathy that persists postnatally. Archives of neurology 65, 1083-1090.

Tajsharghi, H., Oldfors, A., 2013. Myosinopathies: pathology and mechanisms. Acta Neuropathologica 125, 3-18.

Tajsharghi, H., Thornell, L.-E., Lindberg, C., Lindvall, B., Henriksson, K.-G., Oldfors, A., 2003. Myosin storage myopathy associated with a heterozygous missense mutation in MYH7. Annals of Neurology 54, 494-500.

Takayama, S., Bimston, D.N., Matsuzawa, S., Freeman, B.C., Aime-Sempe, C., Xie, Z., Morimoto, R.I., Reed, J.C., 1997. BAG-1 modulates the chaperone activity of Hsp70/Hsc70. The EMBO Journal 16, 4887-4896.

Tasca, G., Udd, B., 2018. Hereditary myopathy with early respiratory failure (HMERF): Still rare, but common enough. Neuromuscular Disorders 28, 268-276.

Taylor, M., Graw, S., Sinagra, G., Barnes, C., Slavov, D., Brun, F., Pinamonti, B., Salcedo, E.E., Sauer, W., Pyxaras, S., Anderson, B., Simon, B., Bogomolovas, J., Labeit, S., Granzier, H., Mestroni, L., 2011. Genetic variation in titin in arrhythmogenic right ventricular cardiomyopathy-overlap syndromes. Circulation 124, 876-885.

Tokuyasu, K.T., Maher, P.A., 1987. Immunocytochemical studies of cardiac myofibrillogenesis in early chick embryos. II. Generation of alpha-actinin dots within titin spots at the time of the first myofibril formation. The Journal of Cell Biology 105, 2795-2801.

Tonino, P., Kiss, B., Strom, J., Methawasin, M., Smith, J.E., Kolb, J., Labeit, S., Granzier, H., 2017. The giant protein titin regulates the length of the striated muscle thick filament. Nature Communications 8.

Topic Popovic, N., Strunjak-Perovic, I., Coz-Rakovac, R., Barisic, J., Jadan, M., Persin Berakovic, A., Sauerborn Klobucar, R., 2012. Tricaine methane-sulfonate (MS-222) application in fish anaesthesia. Journal of Applied Ichthyology 28, 553-564.

Toydemir, R.M., Bamshad, M.J., 2009. Sheldon-Hall syndrome. Orphanet journal of rare diseases 4.

Toydemir, R.M., Rutherford, A., Whitby, F.G., Jorde, L.B., Carey, J.C., Bamshad, M.J., 2006. Mutations in embryonic myosin heavy chain (MYH3) cause Freeman-Sheldon syndrome and Sheldon-Hall syndrome. Nature Genetics 38, 561-565.

Trybus, K.M., 1994. Role of myosin light chains. Journal of Muscle Research & Cell Motility 15, 587-594.

Tskhovrebova, L., Trinick, J., 2002. Role of titin in vertebrate striated muscle. Philosophical Transactions of the Royal Society of London 357, 199-206.

Tskhovrebova, L., Trinick, J., 2010. Roles of Titin in the Structure and Elasticity of the Sarcomere. Journal of Biomedicine and Biotechnology 2010, 612482.

Tsukamoto, D., Hasegawa, T., Hirose, S.-i., Sakurai, Y., Ito, M., Takamatsu, N., 2019. Circadian transcription factor HSF1 regulates differential HSP70 gene transcription during the arousal-torpor cycle in mammalian hibernation. Scientific Reports 9.

Udd, B., 2013. Titin-related distal myopathies, Muscle Disease.

Udd, B., 2014. Distal myopathies. Current neurology and neuroscience reports 14.

Udd, B., Kaarianen, H., Somer, H., 1991. Muscular dystrophy with separate clinical phenotypes in a large family. Muscle & nerve 14, 1050-1058.

Udd, B., Vihola, A., Sarparanta, J., Richard, I., Hackman, P., 2005. Titinopathies and extension of the M-line mutation phenotype beyond distal myopathy and LGMD2J. Neurology 64, 636-642.

van der Ven, P.F., Bartsch, J.W., Gautel, M., Jockusch, H., Fürst, D.O., 2000. A functional knock-out of titin results in defective myofibril assembly. Journal Of Cell Science 113 (Pt 8), 1405-1414.

van der Ven, P.F.M., Furst, D.O., 1997. Assembly of titin, myomesin and M-protein into the sarcomeric M-band in differentiating human skeletal muscle cells in vitro. Cell Structure and Function 22, 163-171.

Varshavsky, A., 2011. The N-end rule pathway and regulation by proteolysis. Protein Science 20, 1298-1345.

Varshavsky, A., 2017. The ubiquitin system, autophagy, and regulated protein degradation. Annual Review of Biochemistry 86, 123-128.

Vassiliadis, E., Rasmussen, L.M., Byrjalsen, I., Larsen, D.V., Chaturvedi, R., Hosbond, S., Saabye, L., Diederichsen, A.C.P., Genovese, F., Duffin, K.L., Zheng, Q., Chen, X., Leeming, D.J., Christiansen, C., Karsdal, M.A., 2012. Clinical evaluation of a matrix metalloproteinase-12 cleaved fragment of titin as a cardiovascular serological biomarker. J Transl Med 10, 140-140.

Walklate, J., Vera, C., Bloemink, M.J., Geeves, M.A., Leinwand, L., 2016. The most prevalent Freeman-Sheldon syndrome mutations in the embryonic myosin motor share functional defects. Journal of Biological Chemistry 291, 10318-10331.

Walsh, R., Thomson, K.L., Ware, J.S., Funke, B.H., Woodley, J., McGuire, K.J., Mazzarotto, F., Blair, E., Seller, A., Taylor, J.C., Minikel, E.V., Exome Aggregation, C., MacArthur, D.G., Farrall, M., Cook, S.A., Watkins, H., 2017. Reassessment of Mendelian gene pathogenicity using 7,855 cardiomyopathy cases and 60,706 reference samples. Genetics in Medicine 19, 192-203.

Wang, C., Wang, X., 2015. The interplay between autophagy and the ubiquitin-proteasome system in cardiac proteotoxicity. Biochimica et Biophysica Acta 1852, 188-194.

Wang, K., McCarter, R., Wright, J., Beverly, J., Ramirez-Mitchell, R., 1993. Viscoelasticity of the sarcomere matrix of skeletal muscles. The titin-myosin composite filament is a dual-stage molecular spring. Biophysical Journal 64, 1161-1177.

Wang, W., Schulze, C.J., Suarez-Pinzon, W.L., Dyck, J.R., Sawicki, G., Schulz, R., 2002. Intracellular action of matrix metalloproteinase-2 accounts for acute myocardial ischemia and reperfusion injury. Circulation 106, 1543-1549.

Warren, C.M., Jordan, M.C., Roos, K.P., Krzesinski, P.R., Greaser, M.L., 2003. Titin isoform expression in normal and hypertensive myocardium. Cardiovascular Research 59, 86-94.

Weintraub, R.G., Semsarian, C., Macdonald, P., 2017. Dilated cardiomyopathy. The Lancet 390, 400-414.

Westerfield, M., 2007. The zebrafish book : a guide for the laboratory use of zebrafish (Danio rerio), Ed. 5. ed. Printed by the University of Oregon Press ;, Eugene, OR :.

Whiting, A., Wardale, J., Trinick, J., 1989. Does titin regulate the length of muscle thick filaments? Journal of Molecular Biology 205, 263-268.

Wickner, S., Maurizi, M.R., Gottesman, S., 1999. Posttranslational quality control: folding, refolding, and degrading proteins. Science 286, 1888-1893.

Wiederkehr, T., Bukau, B., Buchberger, A., 2002. Protein turnover: a CHIP programmed for proteolysis. Current Biology 12, R26-R28.

Willis, M.S., Schisler, J.C., Portbury, A.L., Patterson, C., 2009. Build it up–tear it down: protein quality control in the cardiac sarcomere. Cardiovascular Research 81, 439-448.

Witt, S.H., Granzier, H., Witt, C.C., Labeit, S., 2005. MURF-1 and MURF-2 target a specific subset of myofibrillar proteins redundantly: towards understanding MURF-dependent muscle ubiquitination. Journal of Molecular Biology 350, 713-722.

Wohlgemuth, S.L., Crawford, B.D., Pilgrim, D.B., 2007. The myosin co-chaperone UNC-45 is required for skeletal and cardiac muscle function in zebrafish. Developmental Biology 303, 483-492.

Wolff, C., Roy, S., Ingham, P.W., 2003. Multiple muscle cell identities induced by distinct levels and timing of hedgehog activity in the zebrafish embryo. Current Biology 13, 1169-1181.

Xolalpa, W., Perez-Galan, P., Rodríguez, M.S., Roue, G., 2013. Targeting the ubiquitin proteasome system: beyond proteasome inhibition. Current Pharmaceutical Design 19, 4053-4093.

Zheng, Q., Su, H., Tian, Z., Wang, X., 2011. Proteasome malfunction activates macroautophagy in the heart. American Journal of Cardiovascular Disease 1, 214-226.

Zhou, J., Ng, B., Ko, N.S.J., Fiedler, L.R., Khin, E., Lim, A., Sahib, N.E., Wu, Y., Chothani, S.P., Schafer, S., Bay, B.-H., Sinha, R.A., Cook, S.A., Yen, P.M., 2019. Titin truncations lead to impaired cardiomyocyte autophagy and mitochondrial function in vivo.

Zou, J., Tran, D., Baalbaki, M., Tang, L.F., Poon, A., Pelonero, A., Titus, E.W., Yuan, C., Shi, C., Patchava, S., Halper, E., Garg, J., Movsesyan, I., Yin, C., Wu, R., Wilsbacher, L.D., Liu, J., Hager, R.L., Coughlin, S.R., Jinek, M., Pullinger, C.R., Kane, J.P., Hart, D.O., Kwok, P.-Y., Deo, R.C., 2015. An internal promoter underlies the difference in disease severity between N- and C-terminal truncation mutations of titin in zebrafish. eLife 4.

APPENDICES

7.1 Sample qPCR Calculation using the $2^{-\Delta\Delta CT}$ Method

Sample values were taken from (Schmittgen and Livak, 2008).

	Treated Mice (Gene of interest)	Untreated Mice (Gene of Interest)	Treated Mice (housekeeping)	Untreated Mice (housekeeping)
Average CT of three technical replicates (N1)	27.2	22.8	24.2	24.8
Average CT of three technical replicates (N2)	28	23	24.7	25
Average CT of three technical replicates (N3)	27.8	22.4	24.9	24.7

ΔCT = average CT(Gene of interest) – average CT (housekeeping)

	ΔCT Treated Mice	ΔCT Untreated Mice
N1	3	-2
N2	3.3	-2
N3	2.9	-2.3

*calculate average and standard deviation for both groups for use below

ΔΔCT = average CT (group of interest) – average CT (wild-type)

	ΔΔCT Treated Mice	ΔΔCT Untreated Mice
N1	5	0
N2	5.3	0
N3	5.2	0

ΔΔCT values are averaged and standard deviation is calculated

Expression = $2^{-AVG\Delta\Delta CT}$

Expression Treated Mice	Expression Untreated Mice
0.027840585	1

To account for linear transformation of a logarithmic equation, upper and lower limits of error must be calculated for error bars. This takes into consideration propagation of error for both the error of the experimental group (Treated Mice) and wild-type group (Untreated Mice; Livak and Schmittgen, 2001).

Propagation of error = square root of (standard deviation ΔCT(treated mice) + standard deviation ΔCT (untreated mice) + standard deviation ΔΔCT (treated mice)).

Upper limit of error = $2^{-(\Delta\Delta CT(\text{treated mice}) - \text{propagation of error})} = 0.0409$

Lower limit of error = $2^{-(\Delta\Delta CT(\text{treated mice}) + \text{propagation of error})} = 0.0189$

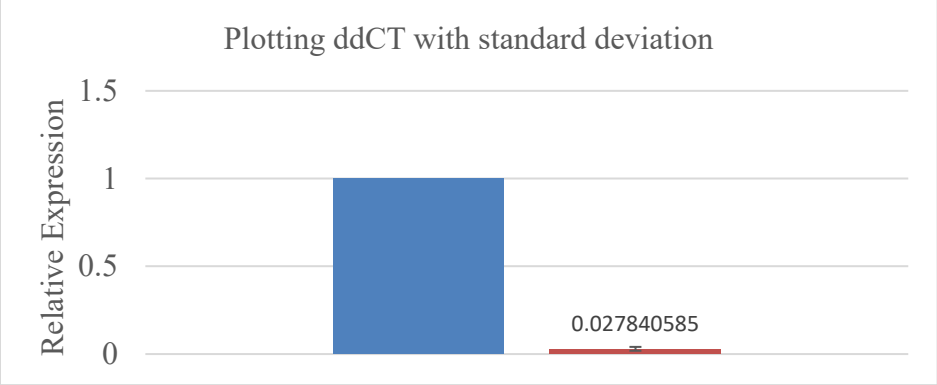

Alternatively, one can plot relative expression calculated from ΔCT with standard deviation:

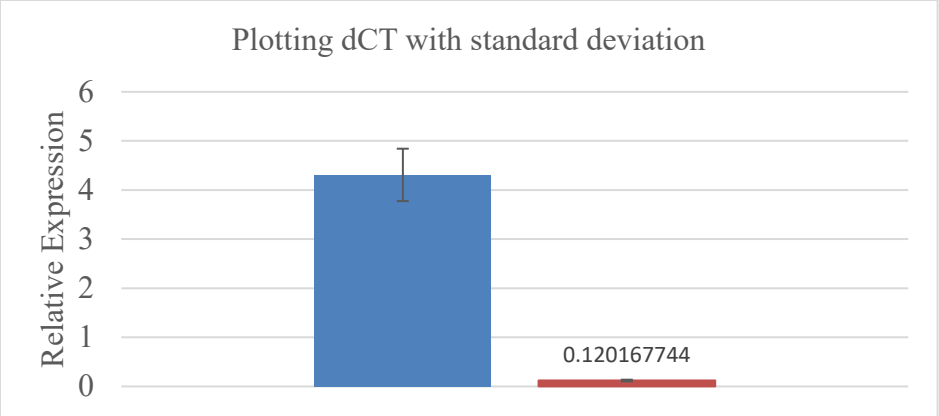

The trends of the graph are the same, and both show a 0.02 fold change in expression. However, it is easier to interpret fold change from the first graph, so we chose to use this format to present our data. Notice the error bars on the orange bar (treated mice) are increased in the first graph to take into consideration the wild-type (blue bar) error on the second graph.

7.2 Supplemental Videos

7.2.1 Supplemental Video 1

https://figshare.com/s/f93b15749a1fb1660c5c

Wild-type (AB) embryo treated with 0.04% tricaine at 17 hpf is unresponsive to tactile stimulus.

7.2.2 Supplemental Video 2

https://figshare.com/s/c43cb4ebb9c1605b1533

The same embryo from supplemental video 1 is now responsive to tactile stimulus after removing the embryo from 0.04% tricaine and allowing it to recover in embryo media.

7.2.3 Supplemental Video 3

https://figshare.com/s/a2f7b66c141edeba0be8

48 hpf *herzschlag* embryo with an unlooped heart showing blood regurgitation from ventricle to atrium.

7.2.4 Supplemental Video 4

https://figshare.com/s/f06ccba166f1a6a9a08d

5 dpf *herzschlag* embryo with severe cardiac consequences.

7.2.5 Supplemental Video 5

https://figshare.com/s/d439e651dfe752b04194

5 dpf *herzschlag* embryo showing blood regurgitation from ventricle to atrium.